Counting Condensation Nuclei in the Antarctic Ozone Mission

NASA Grant NAG 2-458

Final Technical Report Covering the Period from 1 April 1987 to 31 December 1993

Report Submitted by
James Charles Wilson, Principal Investigator
Department of Engineering
University of Denver
Denver, CO 80208-0177

Submitted November 1994

Introduction

This report covers work done in the period from 1 May 1987 through 31 December 1993. The work done on this grant primarily concerns the measurement of aerosol in the stratosphere from NASA ER-2 aircraft. These measurements were made in studies of stratospheric ozone depletion in the northern and southern hemispheres. Measurements were made with several instruments. The ER-2 Condensation Nucleus Counter, ER-2 CNC, measures the number concentration of particles in the diameter range from approximately 0.01 to 1 μm. This instrument was developed under a previous NASA grant, NAG2-31. The Passive Cavity Aerosol Spectrometer measures size distributions in the 0.17 to 3 μm diameter range. This instrument was built by PMS Inc. in Boulder, CO and was upgraded during this grant period to a Focused Cavity Aerosol Spectrometer (FCAS). This upgrade permitted the instrument to measure particles as small as 0.05 μm in diameter. The inlet for the PCAS and FCAS was modified and characterized under this grant so that the modifications to the aerosol due to anisokinetic sampling and heating upon sampling and in transport to the measurement location were accounted for in the data analysis.

These measurements permitted observation of particle production in the southern hemisphere winter polar vortex and observation of the impact of denitrification on the number concentration of the aerosol in the denitrified air. In the northern polar vortex, the measurements provided a characterization of the sulfate aerosol. Following the eruption of Mount Pinatubo in 1991, the measurements permitted an accurate characterization of the sulfate aerosol enhancements resulting from the eruption. This led to studies of the impact of heterogeneous chemistry on the partitioning of the partitioning of the reactive nitrogen species and the partitioning of the chlorine reservoir.

Tasks Funded by this Grant

Some of the tasks listed here were funded entirely by this grant. Others were funded partially by this grant and partially by other grants.

The tasks undertaken for this grant were:

i.) Prepare the ER-2 condensation nucleus counter (ER-2 CNC) for use in the Airborne Antarctic Ozone Experiment (AAOE), and operate the ER-2 CNC in AAOE in 1987.

ii.) Analyze data from AAOE and report the measurements in the refereed literature. The data analyzed included that provided by the ER-2 CNC and data from other instruments on the ER-2. Collaborations with other investigators dealt with studies of polar stratospheric clouds as well as with condensation nuclei.

iii.) Calibrate the PMS Passive Cavity Aerosol Spectrometer (PCAS) and provide an inlet for the instrument which permits representative sampling at air speeds of Mach 0.7.

iv.) Operate the ER-2 CNC in the Airborne Arctic Stratospheric Expedition of 1988-1989 (AASE), calibrate the PCAS in the field.

v.) Analyze the ER-2 CNC and PCAS data from AASE, submit the data to the data archive and report on the results in the scientific literature

vi.) Upgrade the PCAS to a Focused Cavity Aerosol Spectrometer (FCAS). Check the alignment of the FCAS probe on the ER-2 aircraft with a Rosemont 858 wind vector probe.

vii.) Operate and calibrate the FCAS and the ER-2 CNC in the Airborne Arctic Stratospheric Expedition II of 1991-1992 (AASEII).

viii.) Analyze the data produced by the FCAS, submit it to the data archive and report the results and conclusions in the scientific literature.

Accomplishments

i.) The ER-2 Condensation Nucleus Counter was flown in AAOE in 1987. New particle formation in the descending air of the polar vortex was observed and reported (Wilson, et al., 1989). The impact of denitrification on the aerosol concentration was noted in the same paper.

ii.) Contributions were made to the analysis of the data which demonstrated that polar stratospheric clouds (PSCs) contain reactive nitrogen species (Fahey et al., 1989).

iii.) The inlet of the PCAS was instrumented and data analysis techniques were developed to permit the sampling artifacts to be taken into consideration. The FCAS was calibrated prior to AASE , during AASE and after AASE. The ER-2 CNC was operated in AASE.

iv) The data from AASE were reported to the data archive and were analyzed. Publications describing the formation of new particles in the descending air of the polar vortex, and the impact of denitrification on the size distribution of the aerosol in denitrified air were published (Wilson, et al., 1990, Wilson et al., 1992).

v.) The PCAS was converted to a Focused Cavity Aerosol Spectrometer (FCAS) and this instrument was calibrated with monodisperse aerosol prior to, during and after AASE II (Jonsson et al., in press).

vi.) The aerosol size distribution data acquired in AASEII permitted the evolution of the Mt. Pinatubo aerosol and its optical properties to be tracked (Wilson et al., 1993, Brock et al., 1993) and permitted the impact of heterogeneous chemistry on the nitrogen (Fahey et al., 1993, Kawa et al., 1993) and chlorine reservoirs (Wilson et al., 1993) to be studied. These measurements were helpful in determining the impact of sulfate aerosol heterogeneous chemistry on ozone loss (Weaver et al., 1993, Salawitch et al., 1993).

References and Publications

The refereed publications listed here include those authored or co-authored by an investigator supported by this grant (i.e. C. A. Brock, W. E. Clark, H. H. Jonsson, M. R. Stolzenburg, J. C. Wilson). Since the data sets acquired on this grant are of continuing interest in the atmospheric science community, it is certain that more contributions will appear using these data. Therefore this list cannot be considered to be complete. Copies of the whose first author was supported on NAG2-458 are found in Appendix A.

Borrmann, S., Dye, J. E., Baumgardner, D., Wilson, J. C., Jonsson, H. H., Brock, C. A., Loewenstein, M., Podolske, J. R., Ferry, G. V., Barr, K. S., "In situ measurements of changes in stratospheric aerosol and the N_2O-aerosol relationship inside and outside of the polar vortex", *Geophysical Research Letters, 22, 2559-2562,* 1993.

Brock, C. A. Jonsson, H. H., Wilson, J. C., Dye, J. E., Baumgardner, D., Borrmann, S., Pitts, M. C., Osborn, M. T., DeCoursey, R. J., Woods, D. C., "Relationships between optical extinction, backscatter and aerosol surface and volume in the stratosphere following the eruption of Mt. Pinatubo", *Geophysical Research Letters, 20, 2555-2558,* 1993.

Dye, J. E., Gandrud, D. B., Baumgardner, D., Chan, K. R., Ferry, G. V., Loewenstein, M., Kelly, K. K., Wilson, J. C. "Observed particle evolution in the polar stratospheric cloud of January 24, 1989", *Geophysical Res. Lett., 17: 413-416,* 1990.

Fahey, D.W., Kelly, K. K., Ferry, G. V., Poole, L. R., Wilson, J. C., Murphy, D. M., Loewenstein, M., Chan, K. R. "In Situ measurements of total reactive nitrogen, total water and aerosol in a polar stratospheric cloud in the Antarctic", *Journal of Geophysical Research, 94:11299-11316,* 1989.

Fahey, D. W., Kawa, S. R., Woodbridge, E. L., Tin, P., Wilson, J. C., Jonsson, H. H., Dye, J. E., Baumgardner, D., Borrmann, S., Toohey, D. W., Avalone, L. M., Proffitt, M. H., Margitan, J., Loewenstein, M., Podolske, J. R., Salawitch, R. J., Wofsy, S. C., Ko, M. K. W., Anderson, D. E., Schoeberl, M. R., Chan, K. K. "In situ measurements constraining the role of sulphate aerosols in mid-latitude ozone depletion", *Nature, 363, 509-514,* 1993.

Jonsson, H. H., J. C. Wilson, C. A. Brock, R. G. Knollenberg, R. Newton, J. E. Dye, D. Baumgardner, S. Borrmann, G. V. Ferry, R. Pueschel, D. C. Woods, M. C. Pitts, "Performance of a focused cavity aerosol

spectrometer for measurements in the stratosphere of particle size in the 0.062 -2.0 μm diameter range", *Journal of Atmospheric and Oceanic Technology*, in press.

Kawa, S. R., Fahey, D. W., Wilson, J. C., Schoeberl, M. R., Douglass, A. R., Stolarski, R. S., Woodbridge, E. L., Jonsson, H., Lait, L. R., Newman, P. A., Profitt, M. H., Anderson, D. E., Loewenstein, M., Chan, K. R., Webster, C. R., May, R. D., Kelly, K. K., Interpretation of NOx/NOy observations from AASE-II using a model of chemistry along trajectories, *Geophys. Res. Lett., 20, 2507-2550,* 1993.

Salawitch, R. J., Wofsy, S. C., Gottlieb, E. W., Lait, L. R., Newman, P. A., Schoeberl, M. R., Loewenstein, M., Podolske, J. R., Strahan, S. E., Proffitt, M. H., Webster, C. R., May, R. D., Fahey, D. W., Baumgardner, D., Dye, J. E., Wilson, J. C., Kelly, K. K., Elkins, J. W., Chan, K. R., Anderson, J. G., "Chemical loss of ozone in the Arctic polar vortex in the winter of 1991-1992", *Science, 261, 1146-1149,* 1993.

Weaver, A., Loewenstein, M., Podolske, J. R., Strahan, S. E., Proffitt, M. H., Aikin, K., Margitan, J., Jonsson, H. H., Brock, C. A., Wilson, J. C., Toon, O. B., "Effects of Pinatubo aerosol on stratospheric ozone at mid-latitudes", *Geophysical Research Letters, 20, 2515-2518,* 1993.

Wilson, J.C., Loewenstein, M.,. Fahey, D. W, Gary, B., Smith, S. D., Kelly, K. K.,. Ferry, G. V, Chan, K. R. "Observations of condensation nuclei in the airborne Antarctic ozone experiment: implications for new particle formation and stratospheric cloud formation", *Journal of Geophysical Research, 94:16437-16448*, 1989.

Wilson, J. C.,. Stolzenburg, M. R, Clark, W. E., Loewenstein, M., Ferry, G. V., Chan, K. R. "Measurements of Condensation Nuclei in the Airborne Arctic Stratospheric Expedition: Observations of Particle Production in the Polar Vortex", *Geophysical Res. Lett., 17:361-364*, 1990.

Wilson, J. C., Stolzenberg, M. R., Clark, W. E., Loewenstein, M., Ferry, G. V., Chan, K. R., Kawa, S. R., Kelly, K. K., "Stratospheric sulfate aerosol in and near the northern hemisphere polar vortex: The morphology of the sulfate layer, multimodal size distributions and the effect of denitrification", *Journal of Geophysical Research, 97:8,7997-8013,* 1992.

Wilson, J. C., Jonsson, H. H., Brock, C. A., Toohey, D. W., Avalone, L. M., Baumgardner, D., Dye, J., E., Poole, L. R., Woods, D. C., DeCoursey, R. J., Osborne, M., Pitts, M. C., Kelly, K. K., Chan, K. R., Ferry, G. V., Loewenstein, M., Podolske, J. R., Weaver, S., "In situ observations of aerosol and chlorine monoxide after the 1991 eruption of Mount Pinatubo: effect of reactions on sulfate aerosol", *Science, 271, 1140-1143,* 1993.

Appendix A

Copies of papers whose first authors were supported in part by grant NAG2-458.

GEOPHYSICAL RESEARCH LETTERS, VOL. 20, NO.22, PAGES 2555-2558, NOVEMBER 19, 1993

RELATIONSHIPS BETWEEN OPTICAL EXTINCTION, BACKSCATTER AND AEROSOL SURFACE AND VOLUME IN THE STRATOSPHERE FOLLOWING THE ERUPTION OF MT. PINATUBO

Charles A. Brock[1], Haflidi H. Jonsson[1], James C. Wilson[1], James E. Dye[2], Darrel Baumgardner[2], Stephan Borrmann[2], Mike C. Pitts[3], Mary T. Osborn[3], Robert J. DeCoursey[3], and David C. Woods[4]

Abstract. The eruption of the Mt. Pinatubo volcano in the Philippines in June 1991 has resulted in increases in the surface and mass concentrations of aerosol particles in the lower stratosphere. Airborne measurements made at midlatitudes between 15 and 21 km from August 1991 to March 1992 show that, prior to December 1991, the Pinatubo aerosol cloud varied widely in microphysical properties such as size distribution, number, surface and volume concentrations and was also spatially variable. Aerosol surface area concentration was found to be highly correlated to extinction at visible and near-infrared wavelengths throughout the measurement period. Similarly, backscatter at common lidar wavelengths was a good predictor of aerosol volume concentrations. These results support the use of satellite extinction measurements to estimate aerosol surface and of lidar measurements to estimate aerosol volume or mass if temporal changes in the relationships between the variables are considered.

Introduction

The changes in stratospheric aerosol properties following the eruption of Mt. Pinatubo have been substantial. Stratospheric aerosol surface and volume concentrations measured nine months after the eruption show enhancements of factors exceeding 30 and 100, respectively, and mean aerosol diameters showed similar increases from ~0.15 μm to ~1.1 μm [Wilson et al., 1993]. These particles are mostly liquid sulfuric acid produced by the oxidation and subsequent condensation of sulfur gases. Optical depth and its wavelength dependence have also changed significantly from pre-Pinatubo values [Russell et al., 1993, Valero and Pilewskie, 1992].

Remote sensing instruments, such as the satellite-borne Stratospheric Aerosol and Gas Experiment II (SAGE II) and ground-based lidars measure variations in the optical backscatter or extinction over large regions and/or long periods of time. If extinction can be related to aerosol surface or volume concentrations, satellite observations can map the global distributions and temporal evolution of these parameters [Jäger et al., 1988; Pinnick et al., 1980; Russell et al., 1981]. Similarly, to extract extinction, optical depth and aerosol surface and volume concentrations from profiles of lidar backscatter, parameterizations must be used to relate backscatter to these parameters [Gobbi et al., 1989; Salemink et al., 1984; Vaughan et al., 1988].

Jäger and Hofmann [1991] related lidar backscatter to extinction and to in situ measurements of aerosol mass and surface area concentrations for the stratosphere from the period from 1980 to 1987. Their data include periods when the stratospheric aerosol was modified by the eruption of the El Chichón volcano. Thomason and Osborn [1992] provided similar parameterizations based solely on satellite measurements of extinction in the first five months after the eruption of Mt. Pinatubo. The purpose of this work is to use in situ aerosol size distribution measurements measured in the stratosphere in the first nine months after the eruption of Mt. Pinatubo to calculate the relationships between extinction and backscatter and between these optical properties and aerosol surface and volume concentrations.

Measurement Methods

The measurements discussed in this paper were obtained with two aerosol particle sizing spectrometers, the Forward Scattering Spectrometer Probe (FSSP-300) and the Focused Cavity Aerosol Spectrometer (FCAS), both manufactured by Particle Measuring Systems, Inc., Boulder, Colorado. The FSSP measures particles with diameters between about 0.4 μm and 20 μm in 18 grouped size bins [Baumgardner et al. 1992]. The sensing volume of the FSSP is external to the aircraft and particles are not substantially modified before measurement. The FCAS [Wilson et al., 1993] sizes particles with diameters greater than about 0.068 μm to 3.3 μm within a pod on the aircraft. During sampling and transport, the particles measured by the FCAS undergo substantial heating, leading to volatilization of water from the particles. Ambient particle size distributions are reconstructed by accounting for this volatization assuming that the particles are liquid sulfuric acid in equilibrium with the ambient temperature and humidity and by correcting for anisokinetic sampling [Wilson et al., 1993]. Calibration procedures are also described in Wilson et al. [1993].

The data discussed here were acquired on the NASA ER-2 high-altitude research aircraft during AASE-II at pressure altitudes between 15 and 21 km and may be divided into two discrete periods based on aerosol microphysical and optical characteristics. The first period, from 91/08/22 to 91/10/14, included the latitude range from 21.9 to 90.0 °N. The second period, from 91/12/08 to 92/03/26 spanned the latitude range from 21.9 to 70.3 °N.

Data measured within the polar vortex, where the aerosol is substantially different from lower latitudes at similar altitudes [Wilson et al., 1992, 1993] have not been included in this analysis. For the data considered here, the FSSP and FCAS generally show good agreement in both integrated

[1]Department of Engineering, University of Denver
[2]National Center for Atmospheric Research
[3]Science Applications International Corporation
[4]National Aeronautics and Space Administration, Langley Research Center

Paper number 93GL01691
0094-8534/93/93GL-01691$03.00

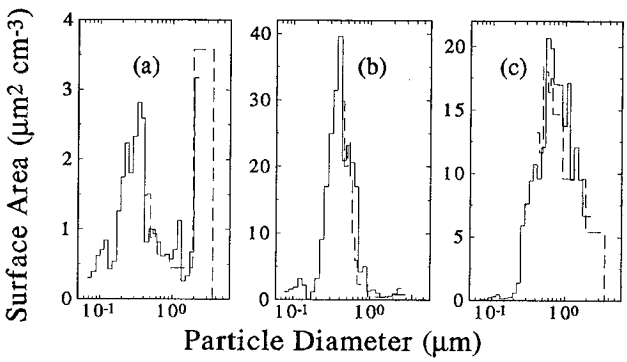

Fig. 1. Particle surface area as a function of particle diameter. Solid lines are data from the FCAS; dashed lines from the FSSP. Data obtained onboard the ER-2 at: a) 30.2 °N, 19.2 km , 91/08/22; b) 36.5 °N, 16.4 km, 91/08/22; c) 65.8 °N, 15.9 km, 92/03/15.

aerosol properties (surface and volume concentrations) and in particle size distributions in their overlapping range. Further results from the aerosol measurements made during AASE-II may be found in Wilson et al. [1993] and Borrmann et al. [1993].

Results

Aerosol Size Distributions

The size distribution of the stratospheric aerosol in the absence of major volcanic eruptions can be described as approximately unimodal, with a typically lognormal distribution [e.g., Turco et al., 1982]. In contrast, from August to December 1991, the particle size distributions measured during the ER-2 flights were highly variable. On 22 August 1991, substantial portions of the total surface area were sometimes found in particles with diameters (D_p) > 1 μm (Figure 1a). These "coarse mode" particles were presumably the fallout of volcanic material from higher layers and contributed significantly to total surface area about 34% of the time at altitudes above 15 km. Figure 1b shows a size distribution also measured on 22 August 1991. Total aerosol surface concentration was much greater than in Figure 1b, and the coarse particle mode did not contribute significantly to total surface.

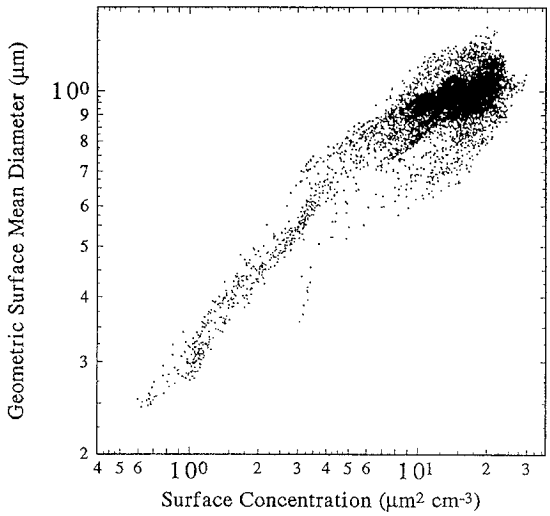

Fig. 2. Surface-weighted geometric mean particle diameter as a function of aerosol surface area concentration measured from December 1991 to March 1992.

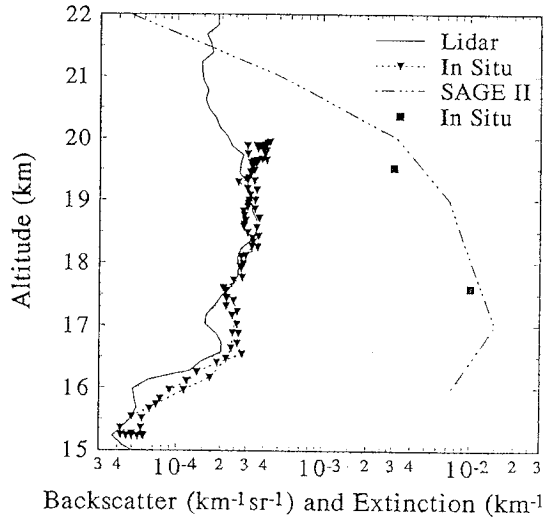

Fig. 3. SAGE-II profile of extinction at 453 nm (dashed-dotted line) measured on 92/01/20 at 49.4 °N, 293 °E, at 75538 UT seconds. Squares are the same parameter calculated from ER-2 size distribution measurements at 49.4 °N, 292 °E, at 49489 UT seconds (lower point) and 70499 UT seconds (upper point). Also shown is a 694 nm lidar profile measured NASA/Langley on 92/01/12 (solid line). The dashed line and triangles are backscatter calculated from measurements during an ER-2 descent and ascent on 92/01/12 at a point projected to be in the same airmass.

Figures 1a and 1b represent the variability present in the particle size distributions measured prior to December 1991. Significant contributions to the total particle surface area came from particles with diameters from about 0.1 to almost 10 μm at various times and locations in this period. From December 1991 to March 1992, in contrast, aerosol size distributions were predominately monomodal (Figure 1c), and the aerosol was much more spatially uniform than in the period prior to December 1991. The geometric surface mean diameter was found to increase with surface concentration from December 1991 to March 1992 (Figure 2). Thus, the Pinatubo aerosol cannot be described adequately by a single lognormal function with fixed mean diameter and geometric standard deviation.

Calculations of Optical Properties

Extinction and backscattering coefficients were calculated from the measured particle size distributions using Mie theory. To estimate the refractive index of the particles, the mass fraction of sulfuric acid was calculated from Steele and Hamill [1981] using measured temperatures. The refractive index for each flight segment then was interpolated from the data of Palmer and Williams [1975] for the appropriate wavelength and sulfuric acid mass fraction, and corrected for

[1] Supplement Tables is available with entire article on microfiche. Order from American Geophysical Union, 2000 Florida Avenue, N.W., Washington, DC 20009. Document L93-003; $2.50. Payment must accompany order.

temperature [Steele and Hamill, 1981]. Mie efficiency curves were smoothed by averaging 100 geometric steps for each measured size interval. The FCAS measurements were used for diameters less than 1.98 μm and the FSSP data were used for diameters greater than 1.93 μm. No correction was made for the small overlap. Extinction coefficients were calculated at the SAGE II wavelengths of 380, 453, 525 and 1020 nm, while backscattering coefficients were calculated at the common lidar wavelengths of 532, 694 and 1064 nm.

The extinctions calculated with the above procedure were compared with profiles of extinction measured by SAGE II [Osborn et al., 1989]. Figure 3 shows comparisons between a SAGE II profile and extinctions calculated from the measured particle size distributions at approximately the same location but ~7 and ~ 1 hrs apart. The agreement between the two techniques was good.

On 12 January 1992, the ER-2 performed a dip at a location calculated by trajectory analysis [P. Newmann, pers. comm., 1992] to be in the same air column recently measured by the ruby lidar (694 nm) operated by NASA Langley Research Center. Figure 3 also shows the results of this comparison. These comparisons show that the optical calculations obtained from the ER-2 data are consistent with independent, remote optical measurements.

Relationships Between Extinction, Backscatter, Aerosol Surface and Aerosol Volume

Regressions relating extinction and backscatter to aerosol surface and volume concentrations are available in tables in a microform supplement (and from C. Brock). The results are briefly described here.

Plots of aerosol optical properties against aerosol surface and volume showed that most of the data were heteroscedastic (i.e., variance was not constant with changing values of x). Therefore, the data were logarithmically transformed before performing least-squares regressions. Despite this transformation, most of the data from the period prior to December 1991 remained substantially heteroscedastic, and least squares fits to these parameters are of limited predictive value. Exceptions were the relationships between aerosol surface and extinction at visible wavelengths, and aerosol volume and backscatter at visible wavelengths. There was little scatter in the data in both of these relationships throughout AASE-II.

Table 1 shows the ratios between extinction, aerosol surface and aerosol mass to backscatter for the lidar wavelengths from the present work and from Jäger and Hofmann [1991] after El Chichón and from Thomason and Osborn [1992] following Pinatubo. Because of the nonlinear fit between variables in the present work, we have used median values of the x parameter to calculate the ratios. The ratio between aerosol surface and backscatter calculated from our work for the period prior December 1991 differs from the period from December 1991 onward. (When the regression between these two parameters is calculated for all of the data, aerosol surface and backscatter are poorly correlated [Brock et al., 1992].) Ratios from this latter period are consistent with the data of Jäger and Hofmann following El Chichón. The ratio of mass to backscatter did not change significantly between the two periods; both show ratios slightly below those of Jäger and Hofmann [1991] and Thomason and Osborn [1992]. The ratios of extinction to backscatter also changed substantially between the pre-December and post-December periods. The changes were particularly pronounced for the 532 and 1064 nm wavelengths.

TABLE 1. Ratios between aerosol surface, mass, extinction and backscatter from this work and from Jäger and Hofmann [1991] and Thomason and Osborn [1992]. Variable y is backscatter.

			Ratio x/y		
Period	x	λ (nm)	This work	Jäger & Hofmann	Thomason & Osborn
91/08-91/10	Sfc	532	[a,b]6.18-6.79	[b]3.9-5.9	
91/12-92/03	Sfc	532	[b,c]3.69-4.05	[b]3.9-5.9	
91/08-91/10	Sfc	694	[a,b]8.32-9.30	[b]4.7-7.8	
91/12-92/03	Sfc	694	[b,c]4.93-5.45	[b]4.7-7.8	
91/08-91/10	Sfc	1064	[a,b]12.6-14.1	[b]9.7-15	
91/12-92/03	Sfc	1064	[b,c]9.66-10.6	[b]9.7-15	
91/08-91/10	Mass	532	[d,e]9.81-10.3	[e]12-14	[e]14-16
91/12-92/03	Mass	532	[e,f]9.87-10.2	[e]12-14	[e]14-16
91/08-91/10	Mass	694	[d,e]13.5-14.5	[e]14-18	[e]16-18
91/12-92/03	Mass	694	[e,f]13.2-13.5	[e]14-18	[e]16-18
91/08-91/10	Mass	1064	[d,e]34.9-45.7	[e]25-33	
91/12-92/03	Mass	1064	[e,f]27.5-29.5	[e]25-33	
91/08-91/10	Ext	532	[g]34.9-45.7 sr	19-39 sr	35-55 sr
91/12-92/03	Ext	532	[h]27.5-29.5 sr	19-39 sr	35-55 sr
91/08-91/10	Ext	694	[i]37.7-52.7 sr	27-50 sr	
91/12-92/03	Ext	694	[j]36.3-40.7 sr	27-50 sr	
91/08-91/10	Ext	1064	[k]47.6-60.9sr	54-66 sr	
91/12-92/03	Ext	1064	[m]72.9sr	54-66 sr	

[a]Sfc. conc.=1.5 $\mu m^2 cm^{-3}$. [b]In units of 10^{13} $\mu m^2 m^{-3} sr$ m. [c]Sfc. conc.=15 $\mu m^2 cm^{-3}$. [d]Vol. conc.=0.3 $\mu m^3 cm^{-3}$, density=1.427 (70% H_2SO_4). [e]In units of g $m^{-3} sr$ m. [f]Vol. conc.=3.5 $\mu m^3 cm^{-3}$. [g]Ext. Coef.= 0.001. [h]Ext. Coef.=0.012. [i]Ext. Coef.=0.001. [j]Ext.Coef=0.011. [k]Ext. Coef.=0.0005. [m]Ext. Coef.=0.01.

The data presented here provide independent in situ evidence that satellite extinction and lidar backscatter measurements can be used from August 1991 to March 1992 to estimate stratospheric aerosol surface and volume concentrations between 15 and 21 km and southward of the Arctic polar vortex. However, the relationships between the optical parameters and aerosol surface and volume differ between the period prior to December 1991. Regressions between extinction and aerosol volume and between backscatter and aerosol surface are particularly less robust in this period due to highly variable aerosol size distributions which led to wide scatter in the relationships.

Acknowledgements. This work was supported by the Upper Atmosphere Research Program of the U. S. National Aeronautics and Space Administration under grant NAG 2-458. We would like to thank P. B. Russell for valuable suggestions regarding the optical calculations.

References

Baumgardner, D., J. E. Dye, B. W. Gandrud and R. G. Knollenberg, Interpretation of measurements made by the

forward scattering spectrometer probe (FSSP-300) during the airborne arctic stratospheric expedition, J. Geophys. Res., 97, 80305-80406, 1992.

Borrmann, S., D. Baumgardner, J. E. Dye, J. C. Wilson, H. H. Jonsson, C. A. Brock, M. Loewenstein, J. R. Podolske and G. V. Ferry, In Situ measurements of changes in stratospheric aerosol and the N_2O-aerosol relationship inside and outside of the polar vortex. Submitted to Geophys. Res. Letts., 1993).

Brock, C. A., J. C. Wilson, H. J. Jonsson, J. E. Dye and D Baumgardner, Optical Properties of the Pinatubo Aerosc Calculated from Airborne Aerosol Size Distribution Meas urements, Paper presented at the Fall Meeting of the AGU San Francisco, CA, December 7-11, 1992.

Gobbi, G. P., A. Adriani and F. Congeduti, Stratospheric aerosol mass content estimated by lidar after El Chichón eruptions, J. Geophys. Res., 94, 9909-9916, 1989.

Jäger, H. and D. Hofmann, Midlatitude lidar backscatter to mass, area, and extinction conversion model based on in situ aerosol measurements from 1980 to 1987, Appl. Optics, 30, 127-138, 1991.

Jäger, H., M. Littfass, D. J. Hofmann and J. M. Rosen, Stratospheric extinction and mass variations after a major volcanic eruption, derived from lidar measuements at northern midlatitudes, in Aerosols and Climate, edited by P. V. Hobbs and M. P. McCormick, 215-222, A. Deepak, Hampton, VA, 1988.

Osborn, M. T., J. M. Rosen, M. P. McCormick, P.-H. Wang,J. M. Livingston and T. J. Swissler, SAGE II aerosol correlative observations: profile measurements, J. Geophys. Res., 94, 8353-8366, 1989.

Palmer, K. F. and D. Williams, Optical constants of sulfuric acid; application to the cloud of Venus?, Appl. Optics, 14, 208-219, 1975.

Pinnick, R. G., S. G. Jennings and P. Chylek, Relationships between extinction, absorption, backscattering, and mass content of sulfuric acid aerosols, J. Geophys. Res., 85, 4059-4066, 1980.

Russell, P. B., M. P. McCormick, T. J. Swissler, W. P. Chu, J. M. Livingston, W. H. Fuller, J. M. Rosen, D. J. Hofmann, L. R. McMaster, D. C. Woods and T. J. Pepin, Satellite and correlative measurements of the stratospheric aerosol. II: Comparison of measurements mad by SAM II, dustsondes and an airborne lidar, J. Atmos. Sci., 38, 1295-1312, 1981.

Russell, P. B., J. M. Livingston, E. G. Dutton, R. F. Pueschel, J. A. Reagan, T. E. DeFoor, M. A. Box, D. Allen, P. Pilewskie, B. M. Herman, S. A. Kinne and D. J. Hofmann, Pinatubo and pre-Pinatubo optical depth spectra: Mauna Loa measurements, comparisons, inferred particle size distributions, radiative effects, and relationship to lidar data, J. Geophys. Res., in press, 1993.

Salemink, H. W. M., P. Schotanus and J. B. Bergwerff, Quantitative lidar at 532 nm for vertical extinction profiles and the effect of relative humidity, Appl. Phys., B34, 187-189, 1984.

Steele, H. M., and P. Hamill, Effects of temperature and humidity on the growth and optical properties of sulfuric acid-water droplets in the stratosphere, J. Aerosol Sci., 12, 517-528, 1981.

Thomason, L. W. and M. T. Osborn, Lidar conversion parameters derived from SAGE II extinction measurements, Geophys. Res. Letts., 19, 1655-1658, 1992.

Turco, R. P., R. C. Whitten and O. B. Toon, Stratospheric aerosols: observation and theory, Rev. Geophys., 20, 233-279, 1982.

Valero, F. P. J. and P. Pilewskie, Latitudinal survey of spectral optical depths of the Pinatubo volcanic cloud--derived particle sizes, columnar mass loadings and effects on planetary albedo, Geophys. Res. Letts., 19, 163-166, 1992.

Vaughan, J. M., D. W. brown, P. H. Davies, C. Nash, G. Kent and M. P. McCormick, Comparison of SAGE II solar extinction data with airborne measurements of atmospheric backscattering in the troposphere and lower stratosphere, Nature, 332, 709-711, 1988.

Wilson, J. C., M. R. Stolzenburg, W. E. Clark, M. Loewenstein, G. V. Ferry, K. R. Chan and K. K. Kelly, Stratospheric sulfate aerosol in and near the northern hemisphere polar vortex: The morphology of the sulfate layer, multimodal size distributions, and the effect of denitrification, J. Geophys. Res., 97, 7997-8013, 1992.

Wilson, J. C, H. H. Jonsson, C. A. Brock, D. W. Toohey, L. M. Avallone, D. Baumgardner, J. E. Dye, L. R. Poole, D. C. Woods, R. J. DeCoursey, M. Osborn, M. C. Pitts, K. K. Kelly, K. R. Chan, G. V. Ferry, M. Loewenstein, J. R. Podolske, and A. Weaver, In Situ observations aerosol and ClO after the 1991 eruption of Mt. Pinatubo: effect of reactions on sulfate aerosol, in press, Science, 1993.

Charles A. Brock, Haflidi H. Jonsson and James C. Wilson, Department of Engineering, University of Denver, Denver, CO 80208.

James E. Dye, Darrel Baumgardner and Stephan Borrmann, National Center for Atmospheric Research, PO Box 3000, Boulder, CO 80307.

Mike C. Pitts, Mary T. Osborn and Robert J. Decoursey, Science Applications International Corporation, Hampton VA, 23665.

David C. Woods, National Aeronautics and Space Administration, Langley Research Center, Hampton VA 23665.

(Received: March 11, 1993;
accepted: June 11, 1993)

JOURNAL OF GEOPHYSICAL RESEARCH, VOL. 94, NO. D14, PAGES 16,437–16,448, NOVEMBER 30, 1989

Observations of Condensation Nuclei in the Airborne Antarctic Ozone Experiment: Implications for New Particle Formation and Polar Stratospheric Cloud Formation

J. C. WILSON,[1] M. LOEWENSTEIN,[2] D. W. FAHEY,[3] B. GARY,[4] S. D. SMITH,[5] K. K. KELLY,[3] G. V. FERRY,[2] AND K. R. CHAN[2]

The ER-2 Condensation Nucleus Counter (ER-2 CNC) was operated in the Airborne Antarctic Ozone Experiment in August, September, and October 1987. The ER-2 CNC measures the mixing ratio of particles, CN, with diameters from approximately 0.02 μm to approximately 1 μm. Comparisons of CN and other aerosol measurements with N_2O show that the vertical profile of the sulfate aerosol was probably displaced downward by the subsidence and mixing processes that determined the inclination of the N_2O isopleths. At altitudes above the minimum in the CN mixing ratio profile, CN mixing ratios correlated negatively with that of N_2O, demonstrating new particle production. The region of particle production was above and south of the 160 ppbv N_2O isopleth. The relationship between CN and N_2O did not change noticeably when moving from air containing normal levels of reactive nitrogen compounds (NO_y) to air depleted in those compounds. This suggests that the removal of NO_y was accompanied by the removal of a small minority of the CN. Concentrations of CN are compared with those of larger particles to study cloud formation mechanisms. In some cases condensation of water or nitric acid trihydrate following rapid cooling caused most of the CN to grow to diameters larger than 0.81 μm. Models published elsewhere predict that these conditions should result in a large fraction of particles growing to these sizes. Episodes of this type probably did not remove reactive nitrogen compounds through particle sedimentation from the chemically perturbed region. Small numbers of large particles were observed in other instances. The composition of the particles and their origins are unclear.

INTRODUCTION

Three interrelated populations dominate the stratospheric aerosol in the Antarctic winter and spring. These populations are the submicron sulfate particles, nitric acid trihydrate particles, and particles consisting mostly of water ice and, presumably, some nitric acid. These aerosols and their interactions are important in the processes which deplete ozone.

Satellite observations show that polar stratospheric clouds (PSCs) form in this region at low temperatures [*McCormick et al.*, 1989]. Models of aerosol growth [*Poole and McCormick*, 1988] show that the formation of nitric acid trihydrate ($HNO_3 \cdot 3H_2O$) particles and ice particles at low temperatures can explain important features observed in remote, optical measurements of PSCs. Nitric acid trihydrate particles with diameters near 1 μm, as well as larger particles, presumed to be mostly ice, have been observed in situ [*Fahey et al.*, 1989].

Reactions occurring on the surface of the predominantly ice particles may release chlorine [*Molina et al.*, 1987; *Tolbert et al.*, 1987], which destroys ozone. Removal of nitric acid from the gas phase is necessary for the maintenance of high concentrations of active chlorine and the catalytic destruction of ozone [*Solomon*, 1988]. It is widely thought that gravitational sedimentation of large particles containing nitric acid is responsible for its removal.

The sulfate particles are always present and serve as nuclei for PSC formation. Their size distribution depends upon altitude and likely affects the properties of the PSCs [*Poole and McCormick*, 1988; *Toon et al.*, 1989]. At midlatitudes the sulfate volume mixing ratio has a maximum near 20-km altitude, and the number mixing ratio profile has a minimum near the same location (D. J. Hofmann, Stratospheric sulfuric acid aersol background increase 1960–1988, submitted to *Nature*, 1988). In the spring, at high latitudes in the southern hemisphere, the maximum in volume and minimum in number occur at lower altitudes, and a particle production mechanism is observed at higher altitudes [*Hofmann et al.*, 1988].

The aerosol and gas measurements made from the ER-2 in the Airborne Antarctic Ozone Experiment (AAOE) of 1987 permit physical characteristics of the aerosol to be compared with dynamical and chemical tracers. This permits study of the processes affecting these populations and their interactions. This paper focuses on the results of the Er-2 Condensation Nucleus Counter (ER-2 CNC) which provides a measure of aerosol number mixing ratio. The aerosol number mixing ratio in an air parcel can be changed by new particle formation, by mixing with air having a different mixing ratio, by coagulation, or by cloud processes. If these processes are negligible, the mixing ratio remains constant under changes in pressure or temperature.

In this paper, the effect of subsidence in the polar region on the profile of aerosol number mixing ratio and on the sulfate aerosol is discussed. Evidence for new sulfate particle formation is presented and related to the amount of

[1]Department of Engineering, University of Denver, Colorado.
[2]NASA Ames Research Center, Moffett Field, California.
[3]Aeronomy Laboratory, National Oceanic and Atmospheric Administration, Boulder, Colorado.
[4]Jet Propulsion Laboratory, Pasadena, California.
[5]Dillon Smith Engineering, Inc., St. Louis Park, Minnesota.

Paper number 89JD01186.
0148-0227/89/89JD-01186$05.00

subsidence experienced by air parcels in the formation of the polar vortex. Measurements in air from which nitric acid has been removed are compared with measurements in air from which nitric acid has not been removed to determine the effect of this process on the sulfate aerosol number. The fraction of nuclei which have participated in clouds is determined and compared with existing theories.

DESCRIPTION OF INSTRUMENTS AND KEY MEASUREMENTS

ER-2 Condensation Nucleus Counter

The ER-2 CNC [*Wilson et al.*, 1983*a*] consists of a thermal growth chamber in which nuclei are grown to sizes which permit optical detection and an optical counter in which grown particles are individually counted. Sampling and transport systems bring the sample from the outside of the aircraft to the growth chamber and control the sample flow. The critical temperatures and flows are continuously monitored in flight so that correct instrument function is verified.

The continuous flow, thermal growth chamber in the ER-2 CNC consists of a saturator in which the aerosol sample is saturated with butyl alcohol vapor at 28°C followed by a condenser tube cooled to 5°C. In the condenser, the vapor becomes supersaturated, and the nuclei in the sample grow by condensation. Modeling of continuous flow growth chambers shows that the supersaturation for a given streamline in the flow depends upon the radial position of the streamline in the condenser [*Stolzenburg and McMurry*, 1986]. In the ER-2 CNC the aerosol sample is confined near the center streamline of the condenser so that all particles experience the same supersaturation. If the particle surface is wetted by the vapor, then this supersaturation determines the smallest particle which will grow. Experiments performed on the ER-2 CNC with particles of known size and concentration showed that at pressures between 53 and 187 mbar, more than 90% of all particles larger than 0.01 μm in diameter reaching the growth chamber are counted [*Wilson et al.*, 1983*a*].

The overall performance of the ER-2 CNC depends upon the characteristics of the sampling and transport system as well as those of the growth chamber and detector. Estimates of sampling efficiency were made based on assumptions concerning the fluid mechanics of the inlet. Transport efficiency was calculated from measured housekeeping variables.

Losses by diffusion were calculated using the results of Gormley and Kennedy [*Fuchs*, 1964]. Inertial losses of particles in the bends and losses by turbulent deposition were estimated using the results of *Chen and Wang* [1981] and *Pui et al.* [1987]. Effects of anisokinetic sampling were evaluated using the results of *Rader and Marple* [1988] for the three locations in the sampling and transport system where the sample is extracted from a larger flow. The analysis shows that the sampling efficiency should vary from 0.7 to 1.3 for particles in the 0.02- to 1-μm diameter range. However, comparisons with other aerosol sensors suggest that the ER-2 CNC lost particles having diameters near to and larger than 1 μm and that the upper size cutoff of the instrument is not well understood. It is likely that the CN measurements in some clouds in the AAOE underestimated the total number of particles present.

Definition of Condensation Nuclei

Condensation nuclei (CN) are the particles which are grown by condensation after creating a supersaturation in some working fluid, then counted. Usually these methods, reviewed by *Wilson et al.* [1983*a*], succeed in accurately measuring the aerosol number mixing ratio in the stratosphere, since the size range accurately counted by the instruments usually covers the size range present. The emphasis in CN counting has often been on the smallest particles detected by the instruments, since they are usually appreciably smaller than those typically detected by optical techniques. Therefore CN are often defined as the particles larger than the minimum size detected by the CNC. In the present case, the upper size cutoff of the instrument becomes important due to the occurrence of PSCs with mean diameters near 1 μm. Therefore, CN are defined here as particles in the 0.02- to 1-μm range. When the aerosol number distribution is dominated by particles outside of this range, the CN count provided by the ER-2 CNC may not accurately represent the total number of particles.

Potential Temperature

Potential temperature (θ) is defined in (1), where P is the ambient pressure in millibars and T is the temperature in degrees Kelvin.

$$\theta = T\left[\frac{1000}{P}\right]^{0.286} \tag{1}$$

Theta increases with altitude and is the vertical coordinate used most often in this discussion. Isentropic motion is along surfaces of constant θ. At high latitudes in winter, air cools diabatically by radiation. The sinking air parcels are said to be subsiding and cross surfaces of constant θ.

The FSSP

The FSSP is a laser aerosol spectrometer built by PMS, Inc., of Boulder, Colorado, and is operated by the NASA Ames Research Center [*Ferry et al.*, this issue]. The instrument sizes particles in the approximate diameter range from 0.81 to 9.74 μm.

The smallest size range in the FSSP data was found to be noisy, and 100 counts were subtracted from each 10-s FSSP count in this range. This correction was developed by *Fahey et al.* [1989] and corresponds to a subtraction of about 0.5 particles/cm^3. The uncertainty associated with this correction is of the same order of magnitude as the correction. A postmission calibration of the FSSP was done by *Baumgardner et al.* [1989], who also provide corrected channel boundaries. The corrections account for the differences between the refractive index of the calibration aerosol and of water and for the velocity dependence of the instrument response. Use of these boundaries is based on the assumption that the refractive index of the measured aerosol does not differ much from water. *Baumgardner et al.* [1989] also determined the size of the FSSP viewing volume and found the uncertainty in viewing volume to be ±45%.

The NO_y Instrument

The NO_y instrument measures reactive nitrogen compounds in both the aerosol and gas phase [*Fahey et al.*,

1989]. Gas phase species include NO, NO_2, NO_3, N_2O_5, HNO_3, $ClONO_2$, and HO_2NO_2. NO_y species on particles entering the instrument are released by evaporation and detected as equivalent gas phase NO_y. The instrument response to aerosol nitrate depends strongly on particle size because the inlet of the NO_y instrument is subisokinetic. Therefore the concentration of particles entering the inlet exceeds the population just upstream of the inlet. An external flow, inertial separator upstream of the NO_y inlet is designed to separate particles larger than about 5 μm from the air stream that impinges on the inlet of the NO_y instrument. The details of the separation efficiency as a function of particle size for the device are not certain. Nonetheless, NO_y on particles larger than the inertial cutoff size are not sampled.

Other Instruments

N_2O was measured with the ATLAS system described by *Loewenstein et al.* [1989]. The microwave temperature profiler (MTP), described by *Denning et al.* [this issue], permits mapping of the isentropic surfaces in the vicinity of the ER-2. When the plane is traveling parallel to the wind vector, the local temperature history of air parcels can be determined from the MTP data [*Gary*, 1989].

The ASAS-X is a laser aerosol spectrometer built by PMS in Boulder, Colorado, and operated by the NASA Ames Research Center. It is designed to measure the size and concentration of particles in the diameter range from 0.1 to 3 μm. During the transport of particles from the free stream to the laser cavity where the measurement is made, the aerosol is heated to temperatures well above ambient. It is likely that most of the nitric acid trihydrate or ice evaporates before the measurement. Thus the ASAS-X data are used here to describe the sulfate aerosol rather than PSC particles. Due to an instrument malfunction, a significant fraction of each sample was systematically undersized. Corrections for this systematic error have not been made; therefore the measured size distributions and magnitudes of derived quantities are not cited here. It is possible to account for these errors when making comparisons between ASAS-X measurements. In the uses of the ASAS-X data which follow, these errors have been taken into account. The output of the mass flow meter in the ASAS-X was used when calculating mixing ratios.

The total water instrument is described by *Kelly et al.* [1989]. The measurements of pressure, temperature, and location are described by *Chan et al.* [1989].

Units

The mixing ratio of CN is expressed as number of particles per milligram of air. Aerosol volume mixing ratios are expressed as μm^3 per milligram of air. Mixing ratios of gases are expressed as pptv, ppbv, or ppmv. These units represent one molecule of the species for every 10^{12}, 10^9, or 10^6 molecules of air, respectively.

Description of the Experiment

The AAOE is described in detail elsewhere [*Tuck et al.*, 1989]. Those features of AAOE relevant to this paper are highlighted here. The NASA ER-2 aircraft flew to Punta Arenas, Chile (latitude −53°), from NASA Ames Research Center (latitude 37°), via Panama and Puerto Montt, Chile (latitude −41°). Twelve missions were flown from Punta Arenas south toward Antarctica near the Palmer Peninsula between August 17 and September 22, 1987. Data were also taken on the ferry legs as the aircraft returned to Moffett Field. Figure 1 shows the potential temperature encountered along typical flight paths as a function of latitude. Most of the flights south from Punta Arenas were flown on surfaces of nearly constant potential temperature. The θ surfaces at about 425 and 455 K were frequently flown. At the south end of the flight path, a vertical profile was often flown.

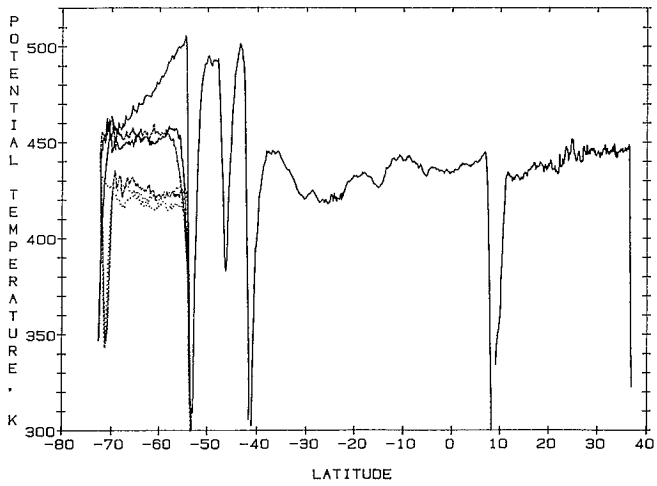

Fig. 1. Potential temperature as a function of latitude for return AAOE ferry flights and selected science flights: August 28 (dotted line), September 20 (solid line), and September 28 (dashed line).

Figure 2 shows the relationship between pressure altitude and θ for several flights south from Punta Arenas. In the southern portion of the flights, the geometric altitude may be as much as 2 km less than the pressure altitude, since the actual temperature profiles differ from those in the Standard Atmosphere.

A chemically perturbed region was encountered on flights

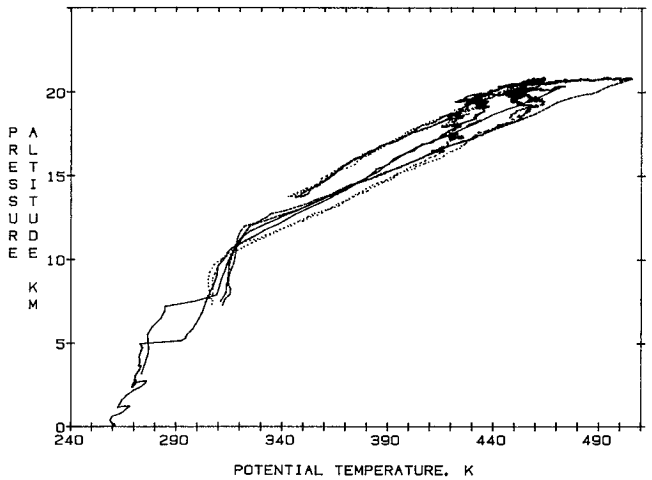

Fig. 2. Pressure altitude as a function of potential temperature for three flights. The pressure altitudes do not accurately represent geometric altitudes due to the temperature structure of the atmosphere. August 28 (dotted line), September 20 (solid line), and September 28 (dashed line).

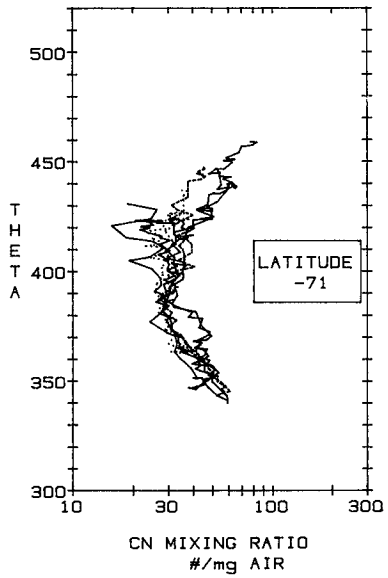

Fig. 3. Mixing ratio profiles measured at −71° latitude on four days: August 28 (solid line), August 30 (dotted line), September 9 (dashed line), and September 20 (solid line). The September 20 profiles reach highest potential temperatures.

south from Punta Arenas [*Proffitt et al.*, 1989]. At latitudes which varied from flight to flight, but averaged −65.6°, an abrupt increase in chlorine monoxide, ClO, was noted. This was often accompanied by decreases in water and NO_y. It is generally believed that water and NO_y were removed from the sampled air parcels through the sedimentation of large aerosol particles consisting mainly of ice and nitrates. Increasingly with time, ozone was seen to decrease in the chemically perturbed region (CPR). For the purposes of the discussion which follows, the edge of this region is arbitrarily defined as that point at which the ClO mixing ratio reaches 130 pptv. This point is referred to below as the ClO wall. Due to the paths flown, this feature was encountered within two potential temperature ranges: from about 415 K to about 430 K and from about 445 K to about 460 K.

The ER-2 CNC acquired data on 11 of the 12 flights south from Punta Arenas, failing on August 23. The instrument acquired data on four of the ferry legs, including all three of the return legs. On September 21 the ER-2 CNC measured mixing ratios which were a factor of 2 smaller than values seen on September 20 and 22. The exclusion of the September 21 data from the figures below is based on subjective judgment.

Features of the N_2O Measurement and Definition of NO_y^*

N_2O is a long-lived tracer for tropospheric air, since its source is in the troposphere and it is destroyed in the stratosphere. The mixing ratio of N_2O generally decreases with increasing altitude and θ. Since the lifetime of N_2O is long compared with the processes which perturb the chemistry in the polar vortex, it serves as a dynamical tracer which indicates origins of air parcels. When comparing air parcels, the ones with smaller mixing ratios of N_2O are likely to have come from higher in the stratosphere or to have been there longer. Parcels with larger mixing ratios of N_2O show more influence of the troposphere. In AAOE, N_2O was observed to decrease on surfaces of constant θ while moving south from Punta Arenas. *Podolske et al.* [this issue] draw several conclusions from these observations: that the air in the region was not well mixed meridionally, that a gradient in subsidence occurred during the winter, with greater subsidence occurring poleward, and that the air sampled at the south end of the flights subsided by 3–5 km more than that over Punta Arenas. Although north-south mixing was not complete, *Podolske et al.* [this issue] conclude that the location of the N_2O isopleths was determined by a combination of mixing along θ surfaces and subsidence.

Fahey et al. [1989, this issue] developed a means of estimating the amount of NO_y which was originally in an air parcel from the N_2O mixing ratio. This expected amount of NO_y is referred to as NO_y^*. When the mixing ratio of NO_y^* exceeds the measured NO_y, NO_y has been removed from the parcel or is on particles which were separated from the NO_y instrument inlet by the inertial separator. When NO_y exceeds NO_y^*, the NO_y signal includes aerosols being sampled and enhanced in the NO_y inlet. The term denitrification denotes either partial or total removal of NO_y from an air parcel.

GEOGRAPHICAL DISTRIBUTION OF CN AND RELATION TO N_2O

Observations of Geographical Distribution of CN

Figure 3 shows vertical profiles measured at latitudes near −71. These profiles were located from 1° to 10° latitude south of the ClO wall and are all in the CPR. Most of the profiles measured in this region show a mixing ratio minimum at a value of θ between 380 and 420 K. The ASAS-X data indicate that the sulfate aerosol volume mixing ratio profile has a maximum at the same θ as the CN minimum.

Figure 4 shows typical vertical profiles of CN mixing ratio

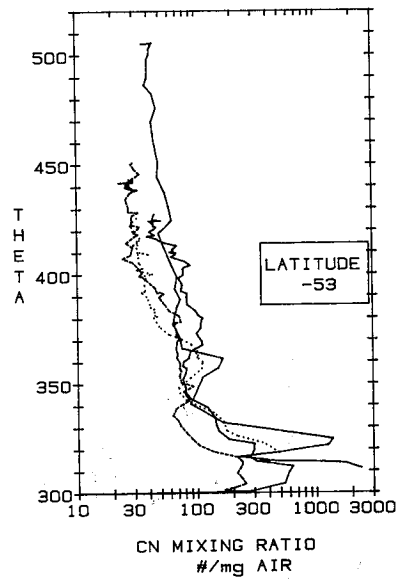

Fig. 4. Mixing ratio profiles measured at −53° latitude on four days: August 28 (solid line), August 30 (dotted line), September 9 (dashed line), and September 20 (solid line). The September 20 profiles reach highest potential temperatures.

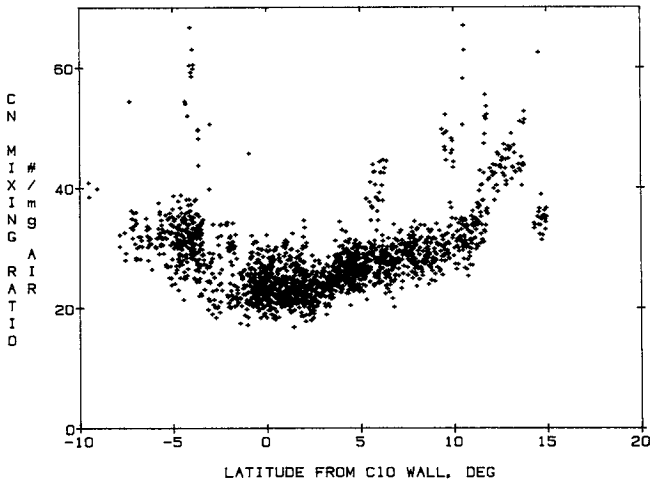

Fig. 5. CN mixing ratio as a function of latitude from the ClO wall for θ between 422 and 427 K. All flights except September 21 are plotted.

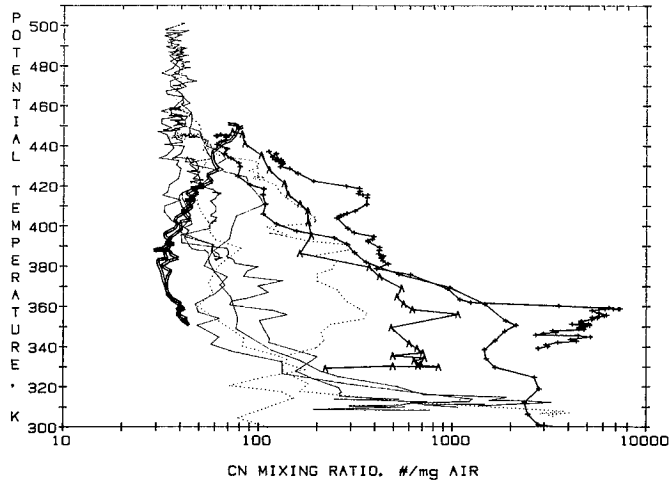

Fig. 7. Mixing ratio as a function of potential temperature. Panama (plus signs), Moffett Field, California (A), Puerto Montt, Chile (dotted line), Punta Arenas, Chile (solid line), and latitude −72° (double solid line).

measured near −53° latitude. Mixing ratios generally decrease as θ increases above 300 K. Those profiles reaching $\theta > 450$ K usually have a region of nearly constant CN mixing ratio extending from the top end of the decreasing segment to the top of the profile. On average, the lower edge of this CN plateau is found at $\theta = 440$ K. The highest θ reached in these profiles was about 505 K. The ASAS-X shows that the sulfate aerosol volume mixing ratio tends to correlate negatively with CN on these profiles. Sulfate volume generally increases as CN decreases above θ of 300 K and shows a plateau with a maximum value where CN has a plateau with a minimum.

Figure 5 shows mixing ratios measured between 422 and 427 K as a function of latitude from the ClO wall. The range of θ has been restricted to emphasize the latitudinal dependence. The mixing ratio increases to the south of the ClO wall and decreases south from Punta Arenas to a minimum just north of the ClO wall. Figure 6 shows a similar plot for values of $\theta \sim 455$ K. In this plot the mixing ratio increases south of the ClO wall.

CN mixing ratio profiles in the CPR, near Punta Arenas, and at various locations in the ferry flights are shown in Figure 7. For the most part, smaller mixing ratios were observed near Punta Arenas and in the CPR than in the tropics and northern hemisphere mid-latitudes.

Relation Between CN and N_2O Mixing Ratios

CN mixing ratios showed both positive and negative correlations with N_2O during the AAOE study. Figure 8 shows a scatter plot of CN mixing ratio against N_2O for 11 flights between August 28 and October 3. All the available data from −71° to about 35° are plotted. CN tend to be positively correlated with N_2O for N_2O values larger than about 160 ppbv. For mixing ratios of N_2O less than 150 ppbv, CN mixing ratios tend to correlate negatively with the N_2O mixing ratios. Most locations where N_2O mixing ratios exceeded 240 ppbv were north of Punta Arenas, and those where N_2O was less than 130 ppbv were south of Punta

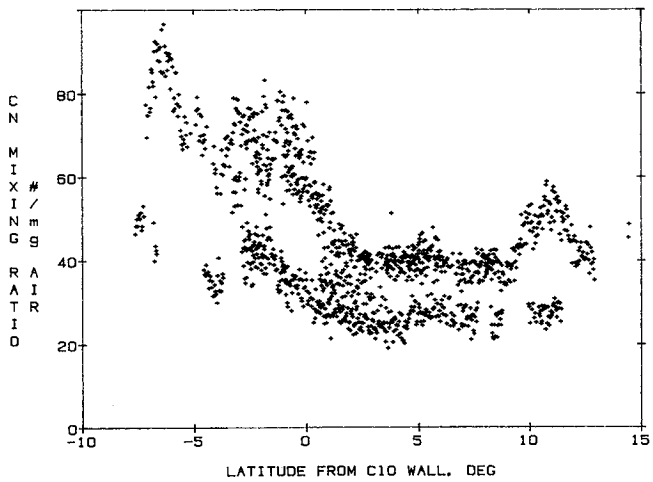

Fig. 6. CN mixing ratio as a function of latitude from the ClO wall for θ between 450 and 460 K. All flights except September 21 are plotted.

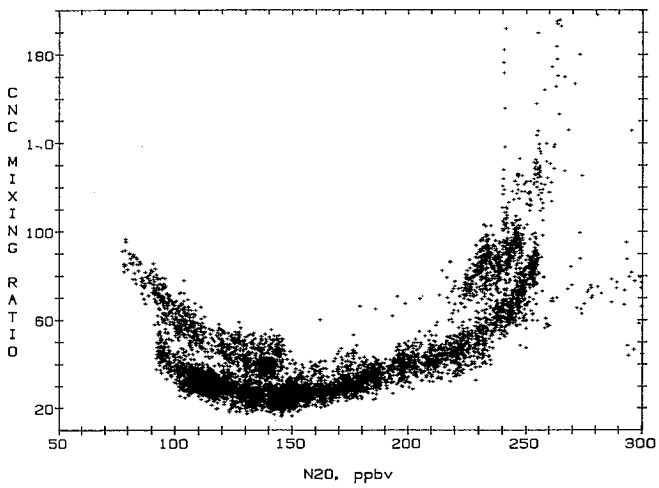

Fig. 8. CN mixing ratio plotted as a function of N_2O mixing ratios. All flights included except September 21.

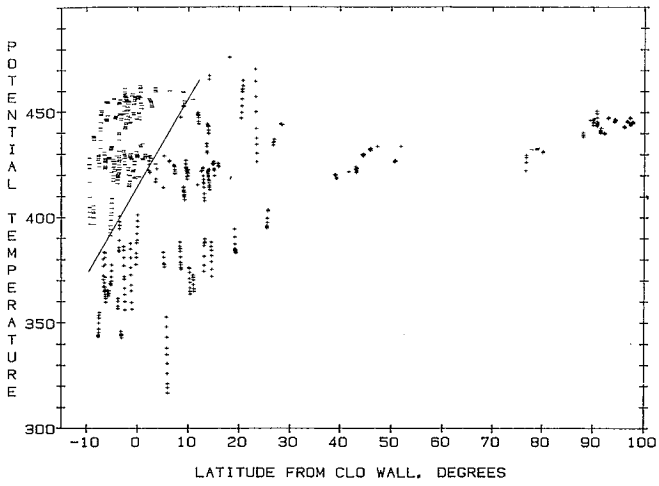

Fig. 9. Locations where correlations between CN and N_2O exceed +0.5 or are less than −0.5. Correlations were calculated over 400-s intervals using 20 data points. Each data point used in the correlation was an average over 20 s. The solid line indicates a boundary between positive and negative correlations. The horizontal axis is latitude from the ClO wall as determined for each flight.

Arenas. Sorting into narrow bins in θ or temperature did not reduce the scatter in the CN-N_2O data.

Figure 9 shows the geographical distribution of the sign of the CN-N_2O correlation. Each correlation was calculated with 20 pairs of points measured along approximately 80 km of flight path. Each of the 20 points is an average over twenty 1-Hz measurements. A moving correlation was done. Locations where the CN-N_2O correlation exceeds 0.5 are indicated with a plus sign, and locations where it is less than −0.5 are indicated with a minus sign. Most of the points above the sloped dividing line are negative, and most below and to the right are positive. *Podolske et al.* [this issue] present a contour plot of the N_2O mixing ratio on potential temperature-latitude coordinates. The dividing line in Figure 9 falls very near the 160 ppbv isopleth in their contour plot. Air above and south of the dividing line has N_2O mixing ratios less than 160 ppbv, and air to the north and below it has N_2O mixing ratios greater than 160 ppbv.

Discussion of CN Distribution

For N_2O mixing ratios in excess of about 160 ppbv, CN and N_2O correlate positively. The vertical CN mixing ratio profiles in Figures 3 and 4 show this effect where CN is increasing as θ decreases. This is likely due to the increasing influence of tropospheric air as N_2O increases. The troposphere is a source of both CN and N_2O.

For N_2O mixing ratios less than about 150 ppbv, CN and N_2O correlate negatively. Since decreasing N_2O indicates increasing influence of stratospheric air, this negative correlation shows the effect of a high-altitude source of CN. Increasing CN mixing ratios with increasing θ illustrate a region where this occurs in Figure 3.

The dividing line in Figure 9 was drawn to separate regions of positive and negative correlation between CN and N_2O. Figure 8 shows that the minimum in CN mixing ratio falls between these regions of positive and negative correlation. Therefore the dividing line also indicates the approximate location of the minimum in the CN mixing ratio vertical profiles.

Since the dividing line in Figure 9 falls very near the 160-ppbv N_2O isopleth, Figure 9 associates the location of the minimum in the CN mixing ratio profile with a narrow range of N_2O mixing ratios, as does Figure 8. In the absence of subsidence, isopleths of N_2O should be parallel to surfaces of constant θ [*Loewenstein et al.*, 1989]. Therefore in the early months of 1987 prior to the setup of the polar vortex and CPR, it is likely that the CN vertical profiles were similar in the −53°–−71° region. That is, the mixing ratios of CN probably decreased as θ increased to values above 440 K and were nearly constant above that to $\theta > 500$ K. Later in the season, subsidence and mixing on θ surfaces established the slope of the N_2O isopleths. The CN profile subsided with the air. The line connecting the points where CN mixing ratio profiles stopped decreasing with θ acquired the same inclination as the N_2O isopleths. Above this line, particle production (discussed below) occurred, and the line became the locus of the minima in the CN profiles.

The flight segments at nearly constant θ showed structure which is consistent with differential subsidence of a fairly uniform profile. Figure 5 shows that the CN mixing ratio was often observed to decrease south of Punta Arenas at $\theta \sim 425$ K. The profiles at −53° often continued to decrease at $\theta >$ 425 K. Increasing subsidence poleward brought those lower values of CN mixing ratio to the 425 K surface south of Punta Arenas. The increase in CN mixing ratio south of the ClO wall resulted from the increased subsidence experienced at those locations, causing the high-altitude source to exert more influence.

The number and volume mixing ratios indicated by the ASAS-X are consistent with the interpretation of the CN data. The maximum in sulfate aerosol volume mixing ratio is found at the same θ as the minimum in CN, as would be expected following subsidence. Sulfate filter sulfate measurements [*Gandrud et al.*, 1989] also show decreasing mass mixing ratios as the ER-2 proceeded south on surfaces of constant θ. Differential subsidence turned a gradient in altitude into one in latitude with the result that the filter samples were taken at altitudes increasingly above the maximum in mass mixing ratio in the sulfate layer. At −71° the filter sulfate mass mixing ratios often increased as the ER-2 descended to lower altitudes and toward the maximum in the sulfate mass mixing ratio profile.

Loewenstein et al. [1989] argue that the subsidence occurred prior to the start of AAOE. The effect of the subsidence on the sulfate aerosol size distribution at any fixed geometric altitude can be inferred from the CN and ASAS-X profile data. At altitudes above the CN minimum, the sinking air likely brought smaller volume mixing ratios and constant or increasing CN mixing ratios to a given geometric altitude. Thus the size distribution shifted toward smaller sizes. This shift affected the optical properties of the aerosol observed in the absence of clouds. The ER-2 aerosol data suggest that the scattering ratio at a given geometric altitude should have decreased with time as the CN minimum sank below it. The scattering ratio data [*McCormick et al.*, 1989] do show a decrease at the appropriate altitudes during the time of the subsidence. It is also likely that during the subsidence the size distribution of the PSC nuclei and the microphysics of PSC formation changed with time at fixed geometric altitudes.

CN profiles were measured at −78° with the balloon-borne University of Wyoming CNC [*Hofmann et al.*, 1989] and show minima in mixing ratios at potential temperatures near 385 K. The mixing ratios reported at −78° on August 29 were roughly twice the values reported for the minima measured by the ER-2 CNC at −71°. It is expected that the CN mixing ratio minimum would occur at smaller values of θ at higher latitudes than it does at −71°, since more subsidence should have occurred at higher latitudes. The increase in the minimum CN mixing ratio observed at −78° may be partially due to the increased effect of the upper altitude source due to increased subsidence.

NEW PARTICLE FORMATION

Background

Observations of new particle formation in the stratosphere have been attributed to either chemical or thermal mechanisms. The first involves gas phase reactions between sulfur-bearing gases and free radicals producing sulfuric acid vapor, which can condense to produce particles [*Turco et al.*, 1982; *McKeen et al.*, 1984]. Examples of chemical production of new particles in the presence of preexisting aerosol were observed following volcanic eruptions when large amounts of SO_2 were injected into the stratosphere [*Hofmann and Rosen*, 1981; *Wilson et al.*, 1983*b*].

The thermal mechanism involves the evaporation and recondensation of sulfuric acid and was observed at mid-latitudes following sudden warmings in polar regions which presumably vaporize sulfuric acid particles. Subsequent transport of the vapor to cooler regions led to high levels of supersaturation, and nucleation resulted [*Hofmann et al.*, 1985]. These events enhanced mixing ratios by orders of magnitude in the 25- to 30-km altitude range following warmings. *Hofmann et al.* [1985] suggest that this mechanism causes an apparently global layer of CN in this altitude range. This layer appears in balloon soundings, which reveal a minimum in the CN mixing ratio at altitudes of 18–22 km (D. J. Hofmann, Stratospheric sulfuric acid aerosol background increase 1960–1988, submitted to *Nature*, 1988) and an increase in mixing ratio at higher altitudes. This thermal source may also explain the observed reversals of correlation between CN and O_3 in mid-latitudes at pressure altitudes of 20 km near the jet stream (J. C. Wilson et al., Measurements of condensation nuclei above the jet stream: Evidence for cross jet transport by waves and new particle formation at high altitudes, submitted to *Journal of Geophysical Research*, 1989.) At lower altitudes, a negative correlation between CN and O_3 indicates a tropospheric source for the CN.

Balloon-borne CN measurements in the Antarctic spring of 1986 revealed a layer of greatly enhanced CN above the region of ozone depletion [*Hofmann et al.*, 1988]. Both thermal and chemical mechanisms have been suggested to explain this CN layer.

Oppenheimer [1987] suggested that the CN layer might have been formed from the products of oxidation of OCS by OH. His calculations show that typical stratospheric concentrations of OCS and the enhanced concentrations of OH suggested by *Crutzen and Arnold* [1986] would produce the required particles in 1–2 months. These workers argue that enhanced OH concentration is a likely result of denitrification and is another way in which the Antarctic vortex is chemically perturbed.

Hofmann et al. [1988] suggest that subsiding air and radiative cooling could result in high sulfuric acid vapor supersaturations. The sulfuric acid vapor concentration increases with altitude, and subsidence is likely to increase the saturation. This could be followed by homogeneous and/or ion nucleation and the creation of new particles without requiring additional sulfuric acid production via chemical mechanisms.

New Particle Formation Observations in AAOE

The negative correlation between mixing ratios of CN and N_2O shown in Figures 8 and 9 demonstrates the effects of a source of CN at altitudes above the minimum in the CN vertical profile. Due to the lifetime of CN, it is not possible to know whether the production occurred during or before AAOE. The negative correlations were observed in AAOE whenever sufficiently low N_2O mixing ratios were encountered. Thus a starting date for this particle production cannot be inferred from the AAOE data.

Increases in CN at low mixing ratios of N_2O are not matched by increases in the ASAS-X signal. Since the ASAS-X detects particles larger than about 0.1 μm, it is likely that the newly produced particles are smaller than 0.1 μm. It is also likely that these new particles are not volatile, since they survive heating to 28°C in the saturator of the ER-2 CNC. Thus the counted particles probably consist of $H_2SO_4 \cdot nH_2O$, since both pure $HNO_3 \cdot 3H_2O$ and H_2O should evaporate in the ER-2 CNC saturator.

Discussion of New Particle Formation

The observations of new particle formation discussed here do not rule out either chemical production of sulfuric acid vapor or an increase in the saturation of existing vapor due to subsidence.

Support for thermal formation of new particles in subsiding air parcels comes from the correlation between observed new particles and N_2O mixing ratios. Air parcels with the low N_2O mixing ratios probably subsided more than parcels with high mixing ratios and generally have more particles. The thermal explanation for the particles suggests that greater subsidence would cause greater increase in the saturation of sulfuric acid vapor and would make a greater quantity of vapor available.

The new particles correlate more closely with the dynamical tracer, N_2O, than with any of the chemical tracers associated with the CPR, such as ClO or denitrification. For example on September 22, CN was negatively correlated with N_2O north of the ClO wall at $\theta \sim 450$ K, where denitrification had not occurred. Figure 9 shows a number of occurrences this type north of the ClO wall. Also, the boundary of the region in which new particles were observed is parallel to isopleths of N_2O and is inclined with respect to the boundary of the chemically perturbed region. The boundary of the chemically perturbed region was only located and defined for values of θ near 425 and 455 K.

It is not known if there is sufficient sulfuric acid vapor at the appropriate altitudes to form the particles observed after subsidence of 3–5 km. However, if the new particles are

assumed to have diameters near the low end of the detectable size range and little vapor is assumed to condense on preexisting particles, the sulfuric acid vapor vertical profiles measured by *Arnold et al.* [1981] provide just enough sulfuric acid to account for the new particles.

The production of CN observed outside of the chemically perturbed region does not rule out a chemical origin for the new particles. CN usually have long lifetimes compared with ClO. Therefore it is possible that particles could have been formed in parcels containing elevated OH and ClO and that the ClO disappeared later. This could happen if NO_y were deposited on PSC particles which were too small to sediment significantly. Then the perturbed chemistry would disappear after the evaporation of the PSC. New particles made while the chemistry was perturbed would exist longer than the indications of the perturbed chemistry which caused them.

A second chemical mechanism can be suggested in addition to that of *Oppenheimer* [1987]. Rates and products of reactions between ClO and OCS are not known. However, the upper limits for these reactions [*DeMore et al.*, 1987] and reasonable concentrations for OCS [*Oppenheimer*, 1987] together with the measured values of ClO concentration do not preclude the possibility that the new particles were formed from products of oxidation of OCS by ClO. In such an instance, the formation of the new particles would not serve as a significant sink for ClO, since the numbers of reacting molecules would be small compared with the measured ClO concentrations.

The number of particles produced is affected by the quantity of preexisting aerosol as well as the saturation and properties of the condensing vapor. Preexisting aerosol provides a surface on which the vapor condenses, and this condensation competes with new particle formation. The dividing line in Figure 9 identifies the approximate location of the minimum in the CN mixing ratio profiles and the maximum in aerosol volume mixing ratio. It is likely that the quantity of preexisting aerosol surface also decreases to the south and above the dividing line. If so, this would facilitate the increased formation of new particles which is observed when moving to the south and above the line. The aerosol size distribution in this region is likely to be bimodal. The new particles will probably form a mode with a diameter small compared with that of the preexisting aerosol.

The relationship between the increases in CN reported here and the layer of CN reported at −78° [*Hofmann et al.*, 1989] is unknown. It is worth noting that this layer seems to be formed in a region having very little preexisting aerosol.

CN Mixing Ratios in and out of Denitrified Air

Observations

Figure 10 is a plot of CN versus N_2O for denitrified and nondenitrified air on September 22. Nitrate aerosols are not present on this day. Therefore air in which NO_y is significantly less than NO_y^* has been denitrified. Data in the figure are sorted into two groups: those points for which $NO_y/NO_y^* < 0.25$ represent denitrified air, and points for which $NO_y/NO_y^* > 0.75$ represents air which is not significantly denitrified. The points with $N_2O > 120$ ppbv and $NO_y/NO_y^* < 0.25$ were encountered in the profile near −71°. For values of N_2O between 140 and 190 ppbv, the CN mixing ratio is

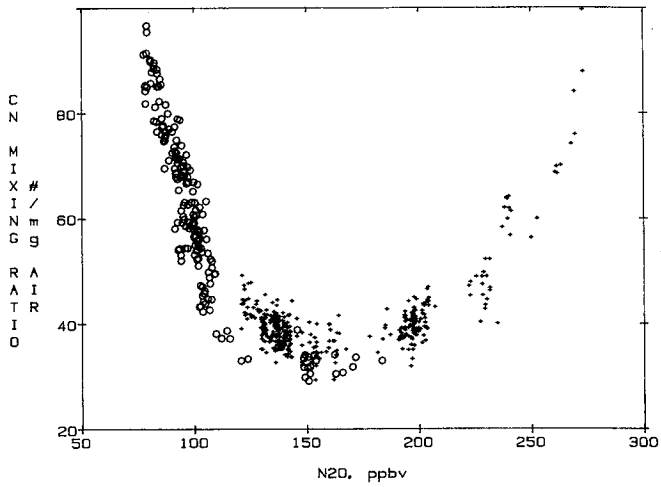

Fig. 10. CN mixing ratio plotted as a function of N_2O for September 22, 1987. Data are segregated into two classes. For the data indicated with plus signs, NO_y/NO_y^* exceeds 0.75. These points represent air which is not significantly denitrified. The points marked with open circles have values of NOy/NO_y^* less than 0.25 and represent denitrified air.

approximately 15% less in denitrified air than in nondenitrified air. On September 16 the denitrified air holds slightly more CN. So within approximately ±20%, CN mixing ratios are the same in denitrified and nondenitrified air having the same N_2O mixing ratios.

Implications for Removal of NO_y

Comparison of these different air parcels requires some justification. The nondenitrified air parcels with $N_2O \sim 150$ ppbv were found north of the ClO wall at $\theta > 415$ K. The denitrified parcels with similar N_2O mixing ratios were found south of the ClO wall at $\theta < 400$ K. If the differential subsidence scenario described above is correct, then it is reasonable to assume that the parcels were at similar potential temperatures and contained similar aerosols before the chemically perturbed region was established.

The comparison of denitrified and nondenitrified air suggests that the removal of NO_y was accompanied by removal of only 0–20% of the CN. If a significantly greater fraction of CN were removed, the comparison requires that the particle production process replaced most of them. It is likely that the larger particles in the sulfate distribution would serve as nuclei for PSCs and hence be removed. If a significant fraction of them were removed and were replaced by smaller, newly formed ones, the size distribution of the aerosol would shift to smaller sizes. Signs of this shift are not seen in the ASAS-X data. Thus, if the replacement occurred, the new small particles had to grow by condensation of gas phase sulfuric acid, so that the final distribution resembled the initial one. A significant amount of sulfate would have been required. At these altitudes there is probably not enough sulfuric acid vapor in the air mass to replace a significant fraction of the sulfate aerosol [*Arnold et al.*, 1981], and the conversion of OCS to sulfuric acid vapor is probably too slow to provide the required sulfate [*Oppenheimer*, 1987].

The limitations of the ASAS-X data and the uncertainties concerning available sulfate weaken the argument against the removal of a significant fraction of the CN. But the

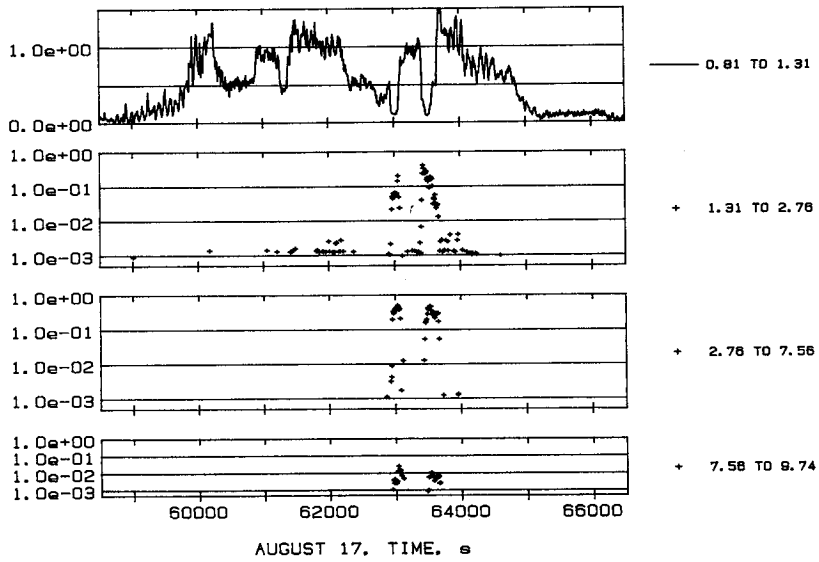

Fig. 11. Fraction of total particles measured in each size range on August 17. The bottom three curves are shown with a log scale. From top to bottom the diameter ranges are 0.81–1.31, 1.31–2.76, 2.76–7.56, and 7.56–9.74 μm.

comparison constrains the aerosol processes, requiring removed aerosol to be replaced.

Comparison of CN and Larger Particles in PSC Formation

Background

The formation of aerosols containing nitric acid was predicted by *Crutzen and Arnold* [1986], *Toon et al.* [1986], and *McElroy et al.* [1986] and confirmed by *Fahey et al.* [1989], *Gandrud et al.* [1989], and *Pueschel et al.* [1989]. The measurements of *Hanson and Mauersberger* [1988] show that nitric acid trihydrate ($HNO_3 \cdot 3H_2O$) will form at temperatures and water and nitric acid concentrations frequently occurring in the polar vortex. The temperatures are above those needed to form ice particles. The $HNO_3 \cdot 3H_2O$ particles can serve as a removal mechanism if they are large enough. Small particles settle too slowly to be removed and may sublimate, releasing nitric acid. Removal of nitric acid from the gas phase is necessary for the maintenance of high concentrations of active chlorine and consequent destruction of ozone [*Solomon*, 1988]. *Fahey et al.* [this issue] show that up to 90% or ~ 10 ppbv of NO_y has been removed from the CPR.

It is known that PSC particles which are predominantly ice can serve as sites for heterogeneous reactions necessary for the release of active chlorine [*Molina et al.*, 1987]. Although removal of water by sedimenting ice particles may not be necessary for ozone depletion, measurements of water vapor in the chemically disturbed region shows that it does occur [*Kelly et al.*, 1989].

Observations

Comparisons of concentrations of CN with concentrations of particles having diameters between 0.81 and 9.75 μm show that a variety of size distributions was observed in AAOE. In most cases when large particles were observed at operating altitudes, measured NO_y exceeded the mixing ratio of HNO_3 required to achieve saturation over $HNO_3 \cdot 3H_2O$. The mixing ratio of HNO_3 required to achieve saturation over $HNO_3 \cdot 3H_2O$ was calculated from the results of *Hanson and Mauersberger* [1988], the temperature, and water vapor concentration. At these times, it was possible that particles of $HNO_3 \cdot 3H_2O$ were in equilibrium with water and nitric acid vapor. But saturation is not assured, since NO_y includes more than nitric acid. Occasions when water vapor was found to be saturated with respect to ice were also examined.

Plots of the fraction of particles having grown into specific size ranges are presented in Figures 11–13 for August 17, 18, and 30. The plotted data contain most of the episodes encountered at operating altitudes during which the FSSP indicated significant aerosol volume and for which CN and NO_y data are available. These observations are typical of those made on other days for which the data set was not complete.

The total mixing ratio of particles present is determined by adding the CN mixing ratio to the mixing ratio of particles with diameters larger than 1.06 μm measured by the FSSP. The FSSP data provide the mixing ratio in each size range. The uncertainty in the upper size limit of the ER-2 CNC and the uncertainty in the FSSP viewing volume may account for the occurrence of fractions as large as 1.5.

On August 17, water mixing ratios exceed that necessary for saturation over ice at times near 63,000 and 63,500 s. The resulting size distribution (referred to as SD1) is characterized by a large fraction of the particles having grown to diameters larger than 1.31 μm. While fewer than 10% grew to diameters between 7.56 and 9.47 μm, the majority of the particles grew to larger than 2.76 μm in diameter.

A second type of size distribution (SD2) has a significant fraction of the total aerosol number in the 0.81- to 1.31-μm range. When SD2 was present, the FSSP signal in this size range correlated with the NO_y signal, indicating that these particles contained NO_y. The population of larger particles in SD2 is less than a few per thousand. SD2 occurred over much of the interval between 60,000 and 65,000 s on August 17, except during the ice events. On August 18, SD2 was

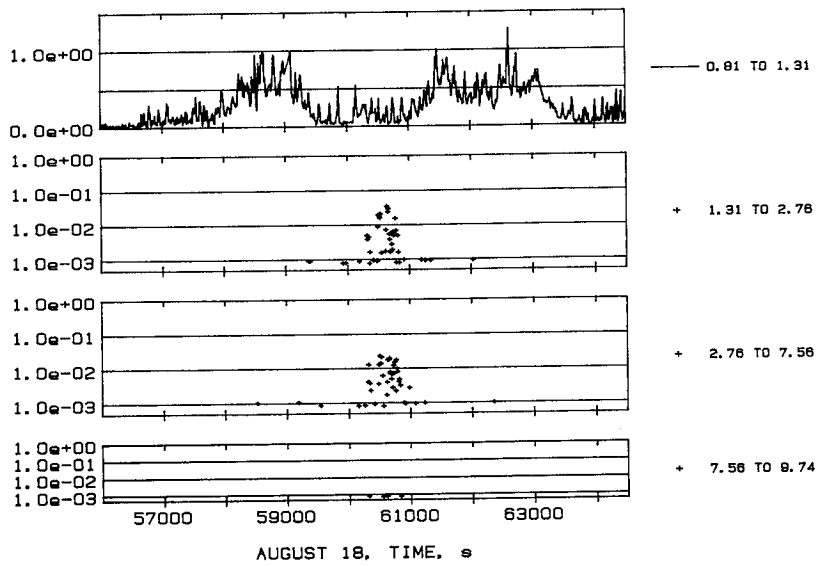

Fig. 12. Fraction of total particles measured in each size range on August 18. The bottom three curves are shown with a log scale. From top to bottom the diameter ranges are 0.81–1.31, 1.31–2.76, 2.76–7.56, and 7.56–9.74 μm.

observed from about 58,200 to 59,200 s and from about 61,300 to 63,100 s. On August 30, time intervals from 57,500 to 58,000 s, from about 59,700 to 60,200 s, and around 61,500 and 62,500 s all show positive correlations between NO_y and the fraction of particles in the range 0.81–1.31 μm. For the most part, these intervals on August 30 show evidence of denitrification. That is, NO_y is less than NO_y^*. Yet there appear to be particles in the 0.81- to 1.31-μm range containing NO_y.

A third type of size distribution (SD3) is seen between 60,000 and 61,000 s on August 18 and around 57,000 and 63,000 s on August 30. In these cases, large particles appear when there is minimal activity in the 0.81- to 1.31-μm range. These particles are not positively correlated with the NO_y signal. So either they did not contain significant quantities of NO_y or they did not reach the NO_y inlet. They occurred when mixing ratios of water vapor were less than required for saturation over ice, so they were not pure ice particles in equilibrium with ambient water vapor. These particles did occur when NO_y was less than NO_y^*. So they could have contained NO_y without causing the air parcel to contain more NO_y than would be predicted from the N_2O-NO_y correlation.

Discussion

The occurrence of ice particles observed on August 17 in the SD1 episodes seems to be well understood. Analysis of the Microwave Temperature Profiler and wind data shows that these events followed cooling in mountain waves and that a cooling rate of 0.011 K s^{-1} would be achieved in an air parcel following the isentropic surfaces through the mountain wave. This event was modeled by *Toon et al.* [1989], who used a cooling rate of 0.003 K s^{-1}. Toon et al.'s model

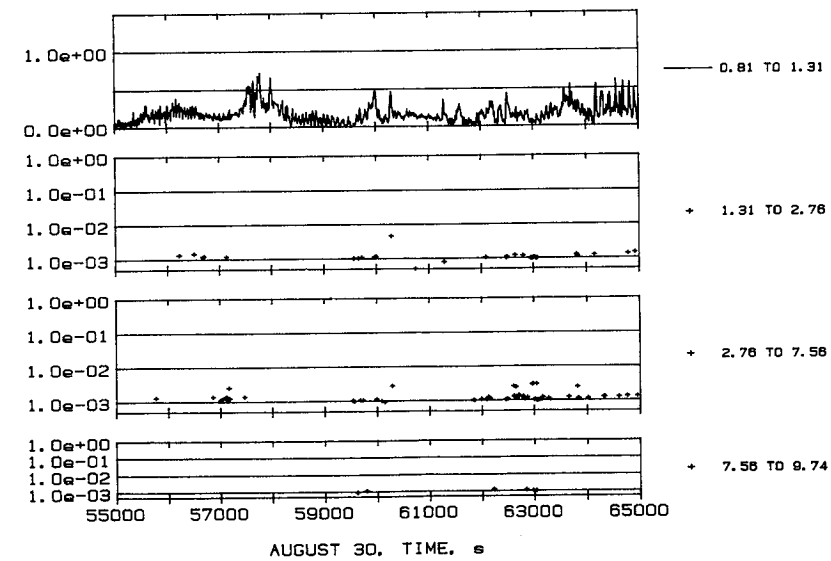

Fig. 13. Fraction of total particles measured in each size range on August 30. The bottom three curves are shown with a log scale. From top to bottom the diameter ranges are 0.81–1.31, 1.31–2.76, 2.76–7.56, and 7.56–9.74 μm.

produced ice crystals from every nucleus when observed FSSP concentrations were used.

Isentropic back trajectories calculated for the 420 K theta surface for August 17 show cooling rates between 10 and 20 K d^{-1} [*McKenna et al.*, this issue]. This cooling occurred as the air moved around the vortex and does not include the effects of mountain waves. Results of calculations modeling the formation of $HNO_3 \cdot 3H_2O$ particles in the Antarctic stratosphere [*Poole and McCormick*, 1988] are applicable to the examples of SD2 observed on August 17. These results show that cooling rates in excess of 2.5 K d^{-1} should cause a large fraction of the nuclei in the background size distribution to nucleate and grow. The model assumed that the growth of particles is limited by mass transfer in the gas phase of the condensing vapor. The air parcel trajectories and aerosol growth models are consistent with these observations of type SD2 distributions.

On August 18 the SD2 type distributions occurred in a region frequently influenced by waves. The fraction grown, however, was less than in the episodes on August 17. On August 30 an even smaller fraction of the nuclei grew in the 0.81- to 1.31-μm-diameter range in the SD2 distributions. Since this air showed evidence of denitrification, less NO_y was available.

The third type of size distribution, SD3, contained particles larger than 2.76 μm. The composition of these particles is unknown.

The model of *Poole and McCormick* [1988] was able to produce large $HNO_3 \cdot 3H_2O$ particles by nucleating less than 5% of the available nuclei with cooling rates of the order of tenths of degrees per day. At those rates, diffusion of vapor to the growing particles depletes the vapor fast enough to keep the supersaturation from reaching levels required to activate the small particles. The model probably requires a nucleation barrier in order to simulate situations in which the fraction of particles growing to large sizes was much smaller than 5% (L. Poole, personal communication, 1989). The observations of SD3 on August 18 were made while encountering mountain waves. Rapid oscillations in temperatures are expected in this region. Parcels of air following θ surfaces probably experienced temperature swings of ± 2°C with a period of about 5 min. The response of these aerosol systems to this type of forcing is unknown. Monotonic, slow cooling does not seem likely. So both the composition and formation mechanism of the large particles in the SD3 size distributions are unknown.

In the cases of SD1 and SD2, large fractions of the sulfate aerosol were involved in cloud formation. The SD1 particles probably did not settle significantly under gravity, since they probably evaporated upon exiting the mountain wave in which they were formed. If they were to settle significantly under gravity, they would remove a significant fraction of the CN with them. Similarly, if the nitric acid trihydrate particles in SD2 were to be incorporated into large ice particles which could settle significantly, the removal of a significant fraction of the NO_y would remove a significant fraction of the sulfate nuclei. Comparisons of the CN-N_2O relationship in and out of denitrified air suggest that this did not routinely happen.

In order to remove NO_y and water from the chemically perturbed region without destroying the CN-N_2O relationship, a mechanism for getting these species onto a few large particles is needed. The observations considered here fail to reveal a clear microphysical path by which this can occur.

CONCLUSIONS

The vertical profile of the CN mixing ratio was found to be closely related to that of N_2O. The location of the minima in the CN mixing ratio profile between $-71°$ and $-53°$ latitude was near the 160 ppbv N_2O isopleth. This observation and others suggest that the processes of mixing and subsidence which determine the inclination of that isopleth also strongly affected the spatial distribution of the sulfate aerosol.

New particle production was observed in air above and south of the 160 ppbv N_2O isopleth. This close relationship between the region of particle production and the dynamic tracer N_2O suggests that the production mechanism may be related to the amount of subsidence but does not exclude a chemical origin.

Similar CN mixing ratios were found in denitrified air and nondenitrified air with similar N_2O mixing ratios. This suggests that a minority of the nuclei were removed in denitrification events or that they were replaced by aerosol production processes.

Comparison of CN concentration with concentrations of particles larger than 0.81 μm provides a means of comparing observations of polar stratospheric cloud events with models of PSC formation. Known events of rapid cooling produced clouds with compositions and properties in agreement with published theories. But these types of clouds may not have contributed to removal of NO_y and water from the CPR. Size distributions were observed in which a few particles reached a large enough size to sediment but their composition was unknown.

Acknowledgments. In support of this work, J. M. Piasecki did computer programming in the field, and Wei Xu did data analysis after the AAOE missions. The spirit of cooperation among participants in AAOE was splendid and inspiring. Gathering of these data required dedication and courage on the part of the people who maintain and fly the ER-2 aircraft. Particularly useful conversations were held with Lamont Poole, Mark Stolzenburg, and Susan Solomon. This work was funded by NASA grant NAG 2-458 through the Atmospheric Experiments Branch, NASA Ames Research Center.

REFERENCES

Arnold, F. A., R. Fabian, and W. Joos, Measurements of the height variation of sulfuric acid vapor concentration in the stratosphere, *Geophys. Res. Lett.*, *8*, 293–296, 1981.

Baumgardner, D., J. E. Dye, and B. W. Gandrud, Calibration of the forward scattering spectrometer probe used on the ER-2 during the AAOE, *J. Geophys. Res.*, this issue.

Chan, K. R., S. G. Scott, T. P. Bui, S. W. Bowen, and J. Day, Temperature and horizontal wind measurements on the ER-2 aircraft during the 1987 Airborne Antarctic Ozone Experiment, *J. Geophys. Res.*, *94*, 11,573–11,587, 1989.

Chen, Y. S., and C. S. Wang, Motion of particles in bends in circular pipes, *Atmos. Environ.*, *15*, 301, 1981.

Crutzen, P. J., and F. Arnold, Nitric acid cloud formation in the cold Antarctic stratosphere: A major cause for the springtime "ozone hole," *Nature*, *324*, 651, 1986.

DeMore, W. B., M. J. Molina, S. P. Sander, D. M. Golden, R. F. Hampson, J. J. Kurylo, C. J. Howard, and A. R. Ravishankara, Chemical kinetics and photochemical data for use in stratospheric modeling, Evaluation number 8, *JPL Publ.*, *87-41*, 1987.

Denning, R. F., S. L. Guidero, G. S. Parks, and B. L. Gary,

Instrument description of the airborne microwave temperature profiler, *J. Geophys. Res.*, this issue.

Fahey, D. W., K. K. Kelly, G. V. Ferry, L. R. Poole, J. C. Wilson, D. M. Murphy, M. Loewenstein, and K. R. Chan, In situ measurements of total reactive nitrogen, total water, and aerosols in a polar stratospheric cloud in the Antarctic, *J. Geophys. Res.*, *94*, 11,299–11,315, 1989.

Fahey, D. W., D. M. Murphy, C. S. Eubank, K. Kelly, M. H. Proffitt, G. V. Ferry, M. K. W. Ko, M. Loewenstein, and K. R. Chan, Measurements of nitric oxide and total reactive nitrogen in the Antarctic stratosphere: observations and chemical implications, *J. Geophys. Res.*, this issue.

Ferry, G. V., E. Neish, M. Schultz, and R. F. Pueschel, Concentrations and size distributions of Antarctic stratospheric aerosols, *J. Geophys. Res.*, this issue.

Fuchs, N. A., *The Mechanics of Aerosols*, p. 204, Pergamon, New York, 1964.

Gandrud, B. W., P. D. Sperry, L. Sanford, K. K. Kelly, G. V. Ferry, and K. R. Chan, Filter measurement results from the Airborne Antarctic Ozone Experiment, *J. Geophys. Res.*, *94*, 11,285–11,297, 1989.

Gary, B. L., Observational results using the microwave temperature profiler during the Airborne Antarctic Ozone Experiment, *J. Geophys. Res.*, *94*, 11,223–11,231, 1989.

Hanson, D., and K. Mauersberger, Laboratory studies of the nitric acid trihydrate: Implications for the south polar stratosphere, *Geophys. Res. Lett.*, *15*, 855–858, 1988.

Hofmann, D. J., and J. M. Rosen, Stratospheric aerosols and condensation nuclei enhancements following the eruption of Alaid in April 1981, *Geophys. Res. Lett.*, *8*, 1231, 1981.

Hofmann, D. J., J. M. Rosen, and W. Gringel, Delayed production of sulfuric acid condensation nuclei in the polar stratosphere from El Chichon volcanic vapors, *J. Geophys. Res.*, *90*, 2341, 1985.

Hofmann, D. J., J. M. Rosen, and J. W. Harder, Aerosol measurements in the winter/spring Antarctic stratosphere, 1, Correlative measurements with ozone, *J. Geophys. Res.*, *93*, 665, 1988.

Hofmann, D. J., J. M. Rosen, J. W. Harder, and J. V. Hereford, Balloon-borne measurements of aerosol, condensation nuclei, and cloud particles in the stratosphere at McMurdo station, Antarctica, during the spring of 1987, *J. Geophys. Res.*, *94*, 11,253–11,269, 1989.

Kelly, K. K., et al., Dehydration in the lower Antarctic stratosphere during late winter and early spring 1987, *J. Geophys. Res.*, *94*, 11,317–11,357, 1989.

Loewenstein, M., J. R. Podolske, K. R. Chan, and S. E. Strahan, Nitrous oxide as a dynamical tracer in the 1987 Airborne Antarctic Ozone Experiment, *J. Geophys. Res.*, *94*, 11,589–11,598, 1989.

McCormick, M. P., C. R. Trepte, and M. C. Pitts, Persistence of polar stratospheric clouds in the southern polar region, *J. Geophys. Res.*, *94*, 11,241–11,251, 1989.

McElroy, M. B., R. J. Salawitch, and S. C. Wofsy, Antarctic O_3: Chemical mechanisms for the spring decrease, *Geophys. Res. Lett.*, *13*, 1296, 1986.

McKeen, S. A., S. C. Liu, and C. S. Kiang, On the chemistry of stratospheric SO_2 from volcanic eruptions, *J. Geophys. Res.*, *89*, 4873, 1984.

McKenna, D. S., R. L. Jones, A. T. Buckland, J. Austin, A. F. Tuck, R. H. Winkler, and K. R. Chan, The southern hemisphere lower stratosphere during August and September 1987: Analyses based on the United Kingdom Meteorological Office Global Model, *J. Geophys. Res.*, this issue.

Molina, M. J., T. L. Tso, L. T. Molina, and F. C. Y. Wang, Antarctic stratospheric chemistry of chlorine nitrate, hydrogen chloride, and ice: Release of active chlorine, *Science*, *238*, 1253, 1987.

Oppenheimer, M., Stratospheric sulfate production and the photochemistry of the Antarctic circumpolar vortex, *Nature*, *328*, 702, 1987.

Podolske, J. R., M. Loewenstein, S. E. Strahan, and K. R. Chan, Stratospheric nitrous oxide in the southern hemisphere, *J. Geophys. Res.*, this issue.

Poole, L. R., and M. P. McCormick, Polar stratospheric clouds and the Antarctic ozone hole, *J. Geophys. Res.*, *93*, 8423–8430, 1988.

Proffitt, M. H., et al., A chemical definition of the boundary of the Antarctic ozone hole, *J. Geophys. Res.*, *94*, 11,437–11,448, 1989.

Pueschel, R. F., K. G. Snetsinger, J. K. Goodman, O. B. Toon, G. V. Ferry, V. R. Oberbeck, J. M. Livingston, S. Verma, W. Fong, W. L. Starr, and R. K. Chan, Condensed nitrate, sulfate, and chloride in Antarctic stratospheric aerosols, *J. Geophys. Res.*, *94*, 11,271–11,284, 1989.

Pui, D. Y. H., F. Romay-Novas, and B. Y. H. Liu, Experimental study of particle deposition in bends of circular cross section, *Aerosol Sci. Technol.*, *7*, 301, 1987.

Rader, D. J., and V. A. Marple, The effects of anisokinetic sampling, *Aerosol Sci. Technol.*, *8*, 283–299, 1988.

Solomon, S., The mystery of the Antarctic ozone hole, *Rev. Geophys.*, *26*, 131, 1988.

Stolzenburg, M. R., and P. H. McMurry, Counting efficiency of an ultrafine aerosol condensation nucleus counter: Theory and experiment, in *Aerosols: Formation and Reactivity*, p. 786, Pergamon, New York, 1986.

Tolbert, M. A., M. J. Rossi, R. Malhotra, and D. M. Golden, Reaction of chlorine nitrate with hydrogen chloride and water at Antarctic stratospheric temperatures, *Science*, *238*, 1258, 1987.

Toon, O. B., P. Hamill, R. P. Turco, and J. Pinto, Condensation of HNO_3 and HCl in the winter polar stratosphere, *Geophys. Res. Lett.*, *13*, 1284, 1986.

Toon, O. B., R. P. Turco, J. Jordan, J. Goodman, and G. V. Ferry, Physical processes in polar stratospheric ice clouds, *J. Geophys. Res.*, *94*, 11,359–11,380, 1989.

Tuck, A. F., R. T. Watson, E. P. Condon, J. J. Margitan, and O. B. Toon, The planning and execution of ER-2 and DC-8 aircraft flights over Antarctica, August and September 1987, *J. Geophys. Res.*, *94*, 11,181–11,222, 1989.

Turco, R. P., R. C. Whitten, and O. B. Toon, Stratospheric aerosols: Observation and theory, *Rev. Geophys.*, *20*, 233–279, 1982.

Wilson, J. C., J. H. Hyun, and E. D. Blackshear, The function and response of an improved stratospheric condensation nucleus counter, *J. Geophys. Res.*, *88*, 6781, 1983*a*.

Wilson, J. C., E. D. Blackshear, and J. H. Hyun, Changes in the sub-2.5 micron diameter aerosol observed at 20 km altitude after the eruption of El Chichon, *Geophys. Res. Lett.*, *10*, 1029, 1983*b*.

K. R. Chan, G. V. Ferry, and M. Loewenstein, NASA Ames Research Center, Moffett Field, CA 94035.

D. W. Fahey and K. K. Kelly, Aeronomy Laboratory, National Oceanic and Atmospheric Administration, 325 Broadway, Boulder, CO 80303.

B. Gary, Jet Propulsion Laboratory, 4800 Oak Grove Drive, Pasadena, CA 91109.

S. D. Smith, Dillon Smith Engineering, Inc., 1457 Idaho Avenue S., St. Louis Park, MN 55426.

J. C. Wilson, Department of Engineering, University of Denver, Denver CO 80208.

(Received August 10, 1988;
revised June 2, 1989;
accepted June 2, 1989.)

GEOPHYSICAL RESEARCH LETTERS, VOL. 17, NO. 4, PAGES 361-364, MARCH SUPPLEMENT 1990

MEASUREMENTS OF CONDENSATION NUCLEI IN THE AIRBORNE ARCTIC STRATOSPHERIC EXPEDITION: OBSERVATIONS OF PARTICLE PRODUCTION IN THE POLAR VORTEX

J. C. Wilson, M. R. Stolzenburg

Department of Engineering, University of Denver

W. E. Clark

Department of Mechanical Engineering, California Polytechnic State University, San Luis Obispo, CA

M. Loewenstein, G. V. Ferry, K. R. Chan

NASA Ames Research Center, Moffett Field, CA

Abstract. The ER–2 Condensation Nucleus Counter (ER–2 CNC) was operated in the Airborne Arctic Stratospheric Expedition (AASE) in January and February 1989. The ER–2 CNC measures the mixing ratio of particles, CN, with diameters from approximately 0.02 μm to approximately 1 μm. The spatial distribution of CN in the Arctic polar vortex was found to resemble that measured in the Antarctic in the Spring of 1987. The vertical profile of CN in the vortex was lowered by subsidence. At altitudes above the minimum in the CN mixing ratio profile, CN mixing ratios correlated negatively with that of N_2O, demonstrating new particle production. CN serve as nuclei in the formation of Polar Stratospheric Clouds (PSC's) and the concentration of CN can affect PSC properties.

Introduction

Definition and role of CN

It is believed that sulfate aerosol provides nuclei for polar stratospheric cloud (PSC) formation and that the number of these particles and their size affect the properties of the PSC's formed in the polar winter. The PSC's probably participate in the removal of nitric acid and provide sites for heterogeneous chemistry. Characterization of the nucleus population aids in understanding these aerosol processes.

The ER–2 Condensation Nucleus Counter (ER–2 CNC) [Wilson et al., 1983, Wilson et al., 1989] measures the mixing ratio (number of particles per milligram of air) of particles. The ambient concentration (number of particles per cm^3) equals the mixing ratio times the ambient air density (mg per cm^3) calculated from the pressure and temperature. The aerosol is sampled from the free stream and then saturated with butyl alcohol vapor at 28C. The sample is then cooled to 8C and the vapor condenses on the particles which then grow to sizes permitting convenient optical detection. The resulting droplets are counted individually. Particles detected in this way are called condensation nuclei (CN). Since the aerosol is heated to 28C in this process only particles with a nonvolatile core will be detected. Comparison with another aerosol sensor, the FSSP [Dye et al., 1990], suggests that the ER–2 CNC may not have efficiently counted larger, volatile particles in PSC's. Therefore, measurements made in PSC's when the FSSP indicated more particles than the ER–2 CNC are not reported here. So in this work, CN are defined as particles initially smaller than 1μm in diameter and having a nonvolatile core larger than 0.02μm.

Paper number 90GL00185.
0094-8276/90/90GL-00185$03.00

Other Instrumentation and Experiment Procedure

The NASA ER–2 aircraft was flown from Stavanger, Norway (59N, 6E) fourteen times between January 3 and February 10, 1989. The aircraft usually operated in the approximate altitude range from 13.5 to 19.5km. The northern most latitude varied from 73N to 82N. The flight tracks often followed surfaces of constant potential temperature, theta, which is used as the principal vertical coordinate in this paper. On most flights, the ER–2 executed a descent and/or ascent north of Stavanger permitting vertical profiles to be measured.

Also used in this analysis are measurements of N_2O made with the ATLAS spectrometer [Loewenstein et al., 1989] and size distributions of nonvolatile particles larger than 0.1 μm in diameter measured with the Passive Cavity Aerosol Spectrometer (PCAS).

The Polar Vortex

In flights north, the ER–2 encountered steep gradients in trace species along surfaces of constant theta. N_2O was observed to decrease and chlorine monoxide, ClO, [Brune, et al. 1989] was often found to increase. The wind speed was near its maximum at this location. These gradients in trace species were created by gradients in diabatic descent. The poleward end of the gradients consisted of air which had been brought down farther from aloft. (Tuck [1989] describes the Antarctic vortex which resembles that of the Arctic.) The most striking observations of nitric acid removal occur in the vortex [Kawa, et al. 1989] along with the strongest chemical perturbations associated with ozone depletion [Solomon, 1988]. The vortex is also perturbed with respect to CN.

Proffitt et al. [1989] developed a consistent set of criteria for locating the vortex edge and applied the approach to the AASE data [Proffitt, personal communication]. Proffitt's locations are used in this paper. The average latitude of the vortex edges is 68.4N.

Observations

CN Mixing Ratios in and out of the Vortex

Average CN mixing ratio profiles inside and outside the vortex are plotted against potential temperature in Figure 1. Also shown are the minimum and maximum CN mixing ratios. Outside of the vortex, approximately

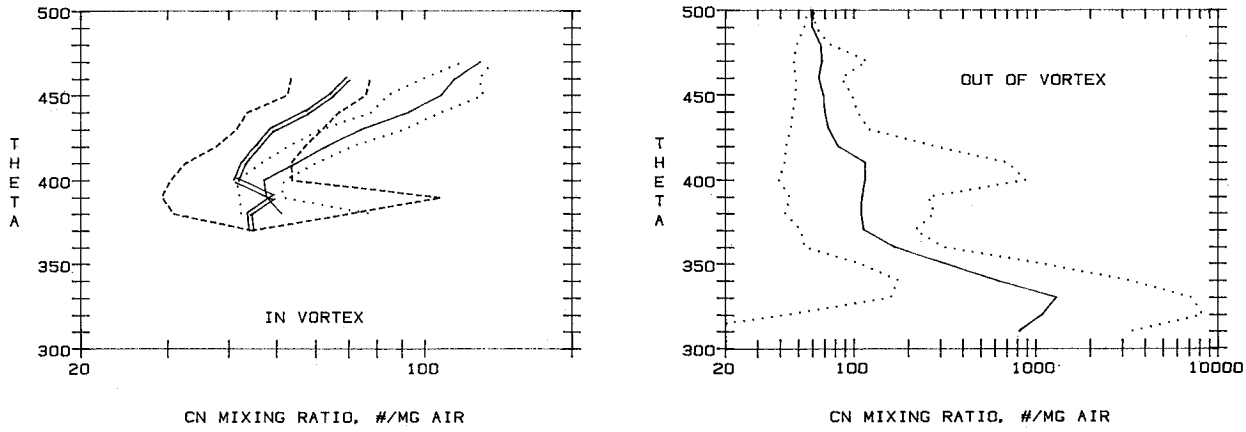

Fig. 1. Average CN mixing ratio profiles and maximum and minimum values. In vortex: double line is average for January and dashed lines are extremes; single line is average for February and dotted lines indicate extremes. Out of vortex: single line is average for January and February and dotted lines indicate extremes.

27 profiles were measured near 59N where the tropopause typically occurred between 320 and 340K (near 10–12 km altitude). The average latitude of the 11 profiles measured in the vortex was 73.7N. The January profiles measured in the vortex differed from those seen in February. However, for both months, at thetas above 400K, mixing ratio increased with potential temperature in the vortex. Outside of the vortex, the CN mixing ratio did not increase with theta above 400K.

CN concentration profiles are plotted against pressure altitude in Figure 2. The pressure altitude is derived from the standard atmosphere and overestimates the geometrical altitude by around 1.5km at altitudes above 15km due to the low temperatures at these latitudes and season. The average of the January profiles measured in the vortex has a minimum at 19km pressure altitude. The average of the February profiles has a minimum at 17km. The average of the profiles measured outside the vortex decreases with altitude above 11km.

Measurements of mixing ratio sorted into intervals of potential temperature and latitude from the vortex boundary are shown in Figure 3 for the January and February flights. Around 420K (approximately 16km altitude), CN mixing ratios are higher outside the vortex than inside. Near 470K (around 18km altitude) this relationship is reversed. Near 450K, the January flights show little change on entering the vortex and the February flights show increasing mixing ratios on entering.

Relationship of CN and N_2O

CN mixing ratios are plotted as a function of the N_2O mixing ratio in Figure 4 for January and February flights. The data from all flights in the respective months falling in 10ppbv N_2O intervals were grouped and averaged. The error bars include +– one standard deviation. For mixing ratios of N_2O in excess of about 220ppbv, CN mixing ratios correlate positively with N_2O and show large scatter. For mixing ratios of N_2O less than about 180ppbv, CN correlate negatively with N_2O.

Figure 5 shows the location of positive and negative correlations with respect to the vortex boundary. One hertz data were averaged over 20s. Then correlations between CN and N_2O were calculated over 400s intervals. Thus 20 points are included in each correlation. The locations of correlations greater than .5 or less than –.5 are shown.

Discussion

Spatial Distribution of CN

The average of the CN mixing ratio profiles measured outside the vortex decreases as theta increases from the tropopause (Figure 1). Throughout this region, CN tended to correlate positively with N_2O (Figure 5). Since the troposphere is the source for N_2O, the positive correl-

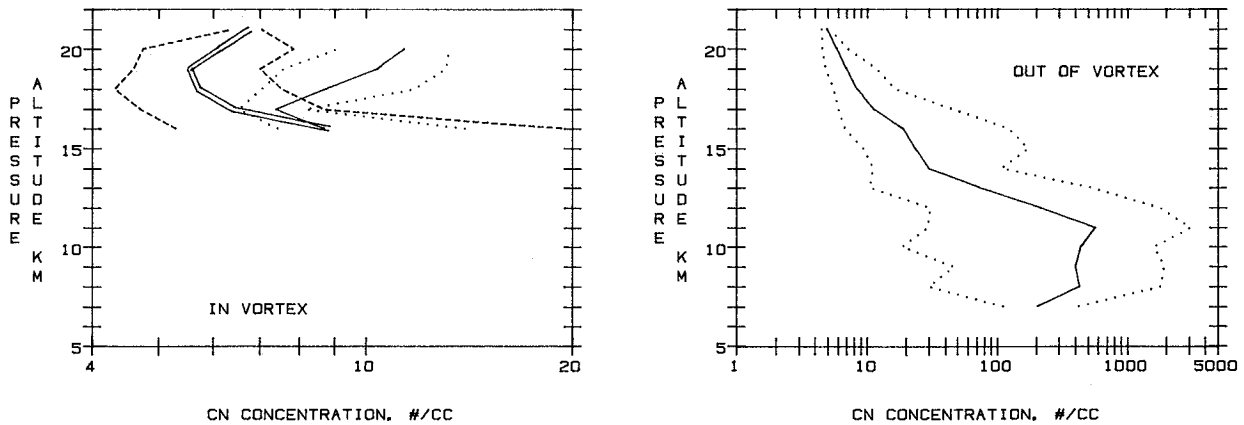

Fig. 2. Average CN concentration profiles as a function of pressure altitude in and out of the vortex. In vortex: double line is average for January and dashed lines are extremes; single line is average for February and dotted lines indicate extremes. Out of vortex: single line is average for January and February and dotted lines indicate extremes.

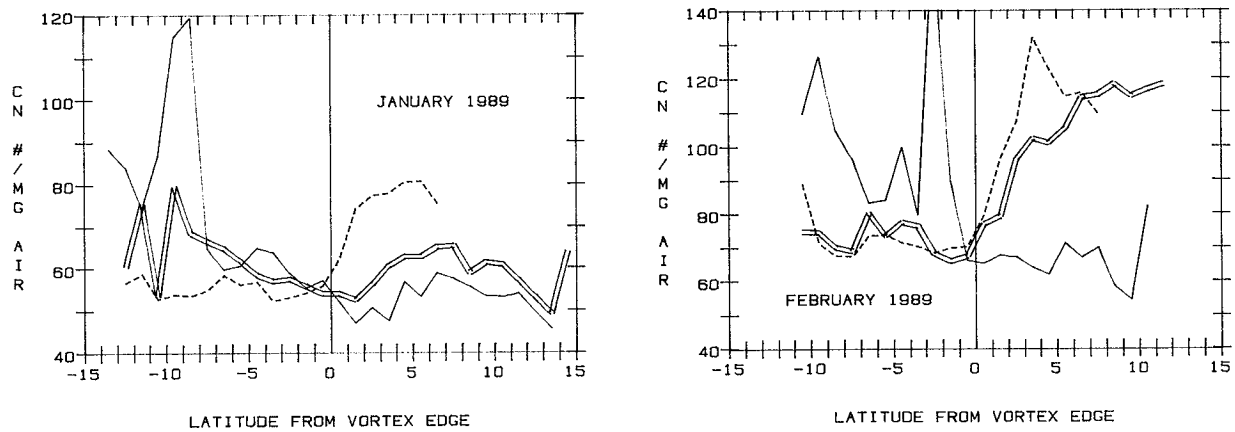

Fig. 3. CN mixing ratio as a function of theta and latitude from the vortex edge in January and February. Single line: 400K < THETA < 440K. Double line: 440K < THETA < 460K. Dashed line: 460K < THETA < 480K.

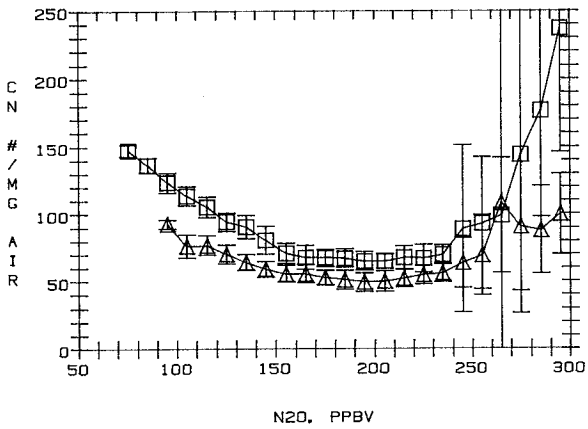

Fig. 4. CN mixing ratio as a function of N2O. Squares are February and Triangles are January data.

ation suggests that the troposphere is the dominant source for CN in this region.

In the vortex, the CN mixing ratio minimum of about 30 to 50mg^{-1} occurred at around 400K or near 15km geometric altitude (Figures 1 and 2). When flying into the vortex at potential temperatures of 400 to 440K (Figure 3), CN often decreased near the boundary. This suggests that the minimum in the CN mixing ratio profile was above this potential temperature outside of the vortex and had subsided inside the vortex to this potential temperature.

At high latitudes in the winter, CN mixing ratios are seen to increase above the minimum [Wilson et al. 1989, Hofmann et al. 1989]. This increase is also shown in Figure 1 for measurements in the vortex and caused the increase in CN noted at the vortex boundary when entering the vortex at theta near 470K. This increase is due to particle production as discussed below.

Measurements of CN from balloons in the polar winter regions have shown a dramatic increase in CN at altitudes above 20km [Hofmann et al. 1989], but this layer is not within reach of the ER–2.

Particle Production

The increase in CN with potential temperature in the vortex and the negative correlation with N_2O both suggest particle production in this or higher regions. In the vortex, the air with low N_2O has descended from higher altitudes. Increasing CN as N_2O decreases suggests a high altitude source for CN. The distribution of negative correlations between CN and N_2O (Figure 5), shows that this source affects most of the region above theta of 400K inside the vortex and just outside of the vortex at theta above 450K. These new particles are very likely to contain at least some sulfuric acid. Particles consisting of

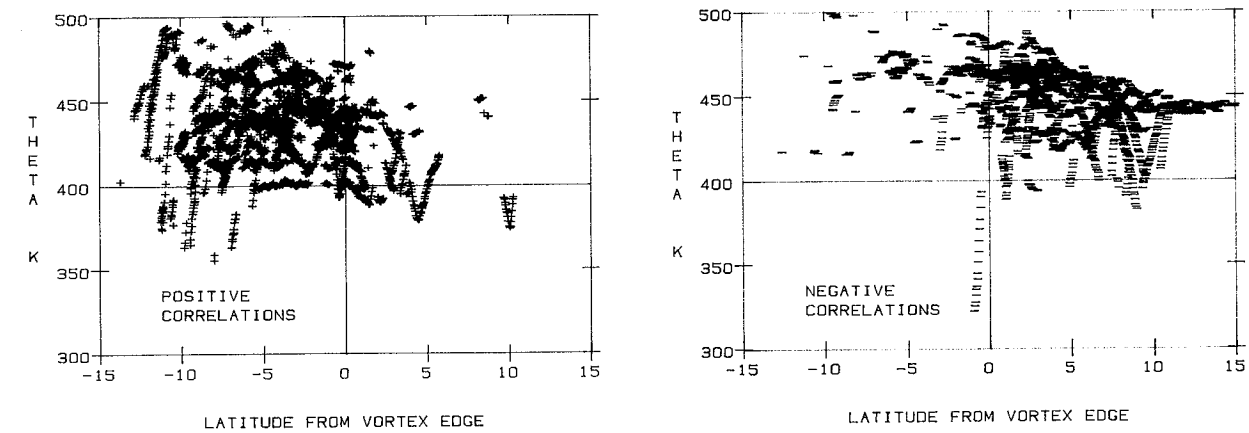

Figure 5. Location of correlations between CN and N2O in excess of 0.5 (+) and less than –.5 (–).

only nitric acid trihydrate or water ice would completely evaporate in the ER–2 CNC saturator.

Outside of the region of particle formation, a positive correlation is observed between CN and PCAS number mixing ratios. This correlation is reduced or disappears in the regions of new particle production which shows that the new particles are, for the most part, smaller than 0.1μm in diameter.

These new particles exhibit a strong negative correlation with N_2O which suggests that CN production is greatest in air which has subsided most. This is consistent with a thermal origin for these particles in which existing H_2SO_4 vapor increases in supersaturation as the air subsides and condenses to form new particles. Hofmann et al. [1989] suggested such a source for for the layer of CN observed in the polar region at altitudes above 20km.

Photochemical sources have also been suggested for new particle formation in the polar regions [Oppenheimer, 1987, Hofmann et al., 1989]. In this scenario, additional H_2SO_4 is formed from a precursor sulfur gas by free radicals whose concentrations are enhanced due to the perturbed chemical state of the vortex.

The CN mixing ratio correlates negatively with the PCAS aerosol volume. Either of the above mechanisms is expected to produce this result, since the preexisting aerosol suppresses the production of new particles by serving as a competing sink for condensing vapor.

The new particles were observed in air masses which did not have elevated ClO concentrations or evidence of HNO_3 removal. And they were seen in air masses which were sampled in the dark and as early in the mission as January 3. So evident markers for perturbed photochemistry did not always accompany evidence of CN production. But these markers may be short lived compared to CN and the trajectory of the parcels sampled in the dark may have included sunlit segments prior to the sampling. Thus perturbed photochemistry may have occurred prior to the observations of elevated CN and may not have left other markers. Thus, the current data do not preclude either possible source.

Comparison with Antarctic Measurements

The features described above are in substantial agreement with results from the Airborne Antarctic Ozone Experiment [Wilson, et al., 1989].

Conclusions

Observations of condensation nuclei in the Arctic winter revealed patterns very similar to those in the Antarctic winter. The CN profile was shifted downward due to the large scale subsidence in the region. New particles were produced. These particles correlated very strongly with the region of subsidence, were mostly smaller than 0.1 μm in diameter and were likely to contain sulfuric acid and water. The particle production was observed at altitudes above 400K (approximately 15km geometric altitude) inside the vortex and at altitudes above 450K just north of the vortex boundary.

These data do not require a choice between the photochemical and thermal production mechanisms.

In the vortex, concentrations increased with altitude at geometric altitudes above about 17km in January and 15km in February. In the Antarctic, rapid cooling rates produced PSC's in which all or nearly all available nuclei grew to diameters near or larger than 1μm [Wilson, et al 1989]. In such cases, the mixing ratios of nuclei and nitric acid will control the resulting particle size, optical effects and sedimentation velocity of the PSC particles. The observed increase in nucleus concentration with altitude doubtless affected PSC properties.

Acknowledgements. This work was funded by the NASA Upper Atmosphere Research Program.

References

Brune, W.H., J.G. Anderson,D.W. Toohey, et al., ClO measurements from AASE, Geophys. Res. Lett., this issue, 1989.

Dye, J.E., B. W. Gandrud, D. Baumgardner, L. Sanford, G. V. Ferry, A Survey of particle measurements in the Arctic from the Forward Scattering Spectrometer Probe Model 300, Geophys. Res. Lett., this issue, 1989.

Hofmann, D. J., J. M.Rosen, W. Gringel, Delayed production of sulfuric acid condensation nuclei in the polar stratosphere from El Chichon volcanic vapors, J.Geophys. Res., 90, 2341, 1985.

Hofmann, D. J., J .M. Rosen, J. W. Harder, J. V. Hereford, Balloonborne measurements of aerosol, condensation nuclei, and cloud particles in the stratosphere at McMurdo station Antarctica during the spring of 1987, J. Geophys. Res., 94:11235, 1989.

Kawa, S. R., D. W. Fahey, L.C. Anderson, M. Loewenstein, K. R. Chan, Measurements of total reactive nitrogen during the airborne arctic stratospheric expedition, Geophys. Res. Lett.,this issue, 1989.

Loewenstein, M., J. R. Podolske, R. K. Chan, S. E. Strahan, Nitrous oxide as a dynamical tracer in the 1987 airborne Antarctic ozone experiment, J. Geophys. Res., 94:11589, 1989.

Oppenheimer, M., Stratospheric sulfate production and the photochemistry of the Antarctic circumpolar vortex, Nature, 328:702, 1987.

Proffitt, M. H., J. A. Powell, A. F. Tuck, D. W.Fahey, K. K. Kelly, K. R.Chan,et al., A chemical definition of the boundary of the Antarctic ozone hole, J. Geophys. Res. 94: 11437, 1989.

Solomon, S., The mystery of the Antarctic ozone hole, Reviews of Geophysics, 26, 131, 1988.

Tuck, A.F., Synoptic and chemical evolution of the Antarctic vortex in late winter and early spring 1987, J. Geophys. Res. 94:11687, 1989.

Wilson, J. C., J. H. Hyun, E. D. Blackshear, The function and response of an improved stratospheric condensation nucleus counter, Journal of Geophysical Research, 88, 6781, 1983.

Wilson, J.C., M. Loewenstein, D. W. Fahey, B. Gary, S. D. Smith, K. K. Kelly, G. V.Ferry, K. R. Chan, Observations of condensation nuclei in the airborne antarctic ozone experiment: implications for new particle formation and polar stratospheric cloud formation, J. Geophys. Res.,94, 16437, 1989.

K. R. Chan, G. V. Ferry, M. Loewenstein, NASA Ames Research Center, SGG:254–5, Moffett Field, CA 94035.

W. E. Clark, Department of Mechanical Engineering, California Polytechnic State University, San Luis Obispo, CA, 93041.

M. R. Stolzenburg and J. C. Wilson, Department of Engineering, University of Denver, Denver, CO 80208.

(Received December 1, 1989;
revised January 8, 1990;
accepted January 10, 1990)

JOURNAL OF GEOPHYSICAL RESEARCH, VOL. 97, NO. D8, PAGES 7997–8013, MAY 30, 1992

STRATOSPHERIC SULFATE AEROSOL IN AND NEAR THE NORTHERN HEMISPHERE POLAR VORTEX: THE MORPHOLOGY OF THE SULFATE LAYER, MULTIMODAL SIZE DISTRIBUTIONS, AND THE EFFECT OF DENITRIFICATION

J. C. Wilson,[1] M.R. Stolzenburg,[2] W. E. Clark,[3] M. Loewenstein,[4]
G. V. Ferry,[4] K. R. Chan,[4] and K. K. Kelly[5]

Abstract. Measurements were made of stratospheric sulfate aerosols using a passive cavity aerosol spectrometer and a condensation nucleus counter on a NASA ER–2 aircraft in the Airborne Arctic Stratospheric Experiment of 1989. The problems of representative and accurate sampling and particle evaporation were explicitly addressed in the design of the inlets and reduction of the data. The measurements suggest that the sulfate aerosol is bimodal in the polar vortex above the mass mixing ratio maximum in the sulfate layer. It appears that a nuclei mode of small, newly formed particles exists in this region. A stronger case is made for a nuclei mode in the upper few kilometers of the troposphere and in the lower few kilometers of the stratosphere. This mode is probably a global phenomenon occurring in all seasons. Comparison of denitrified and nondenitrified air suggests that denitrification removes some of the larger sulfate particles.

Introduction

The stratospheric sulfate aerosol layer consists primarily of sulfuric acid and water and is found all over the world [Junge et al., 1961; Turco et al., 1982; McCormick et al., 1981; Hofmann, 1990]. These particles are typically around 0.1μm in diameter and have mixing ratios of around 50 particles/mg air in the heart of the aerosol layer. Their size distribution is often described as being lognormal during periods of volcanic inactivity [Pinnick et al., 1976; Hofmann, 1990] and multimodal sulfate aerosols have been observed after eruptions [Oberbeck et al., 1983]. Production of sulfate particles has been observed following volcanic eruptions [Hofmann and Rosen, 1981; Wilson et al., 1983a], in the air transported from the polar winter vortex [Rosen and Hofmann, 1983; Hofmann et al., 1985] and in the polar winter vortex [Hofmann et al., 1988; Wilson et al., 1989]. Sulfate aerosols apparently serve as nuclei for the formation of polar stratospheric clouds [Steele et al., 1983; Hofmann et al., 1989; Wilson et al., 1989; Dye et al., 1990a].

Processes affecting the sulfate aerosol in the polar regions include subsidence, new particle formation, nucleation of polar stratospheric clouds, and denitrification [Hofmann et al., 1989, Wilson et al., 1989]. Significant questions concerning these processes remain.

[1]Department of Engineering, University of Denver, Colorado.
[2]Aerosol Dynamics Inc., Berkeley, California.
[3]Department of Mechanical Engineering, California Polytechnic State University, San Luis Obispo.
[4]NASA Ames Research Center, Moffett Field, California.
[5]NOAA Aeronomy Laboratory, Boulder, Colorado.

Paper number 92JD00065.
0148–0227/92/92JD–00065$05.00

The effects of subsidence, new particle formation and denitrification on the morphology and size distribution of the north polar sulfate aerosol layer are described in this paper. Although the stratospheric aerosol is approaching a background level after a considerable period of volcanic quiescence [Hofmann, 1990], the present observations suggest that the polar aerosol is multimodal. A nuclei mode is needed to accommodate new particles and a mode with diameter near 0.6μm is present both in and out of the vortex. In the Antarctic, the effect of denitrification on the number mixing ratio of sulfate aerosol was found to be small [Wilson et al., 1989]. The present measurements suggest that denitrification removes a few of the larger sulfate aerosols.

Measurement of the sulfate aerosol was made with a Passive Cavity Aerosol Spectrometer (PCAS) on a NASA ER–2. The measurements were designed to account for the effects of anisokinetic sampling, of particle evaporation in sampling and transport, and of refractive index on optical sizing. Comparisons with a number of aerosol measurements suggest that the PCAS may be underestimating aerosol number concentration in the 0.5 to 1 μm diameter range, but none of the comparisons are definitive.

Measurements

The Passive Cavity Aerosol Spectrometer (PCAS)

Size distributions of stratospheric aerosols were measured with a Passive Cavity Aerosol Spectrometer built by Particle Measuring Systems Inc., Boulder, Colorado. The optical system consists of a passive cavity containing a high-order, multimode He-Ne laser beam, detection optics and a photodetector. The passive cavity is formed by an output coupler mirror mounted on the laser and an opposing mirror which oscillates at 180 kHz. Light exiting the laser is reflected back and forth in the cavity a few hundred times and, due to the vibrating mirror, is incoherent over the time required for particles to traverse the beam. The collection optics consist of opposing Mangian mirrors with apertures having colinear axes perpendicular to the laser beam. Thus, light scattered into co-axial cones with half angles of 45 degrees and with axes at right angles to the laser beam is collected. Light scattered by individual particles is measured using a photodiode. Each particle generates a pulse whose height is analyzed by a multichannel analyzer. Pulse height distributions are recorded over contiguous 10 second intervals throughout the flight. The PCAS sizes particles in the approximate diameter range from 0.1 to 3μm.

Optical calibration of the PCAS. The instrument was calibrated with monodisperse polymer microspheres obtained from Duke Scientific, Palo Alto, California. These certified particle size standards are NBS/BCR traceable. Eleven calibration aerosols with diameters between 0.220 and 1.63μm were used. The refractive index of these particles is 1.59. Figure 1 shows the mean voltage pulse height indicated by the PCAS for each of the eleven calibration aerosols. The horizontal lines on Figure 1 show the voltage boundaries of the channels in which the multichannel analyzer accumulates pulses.

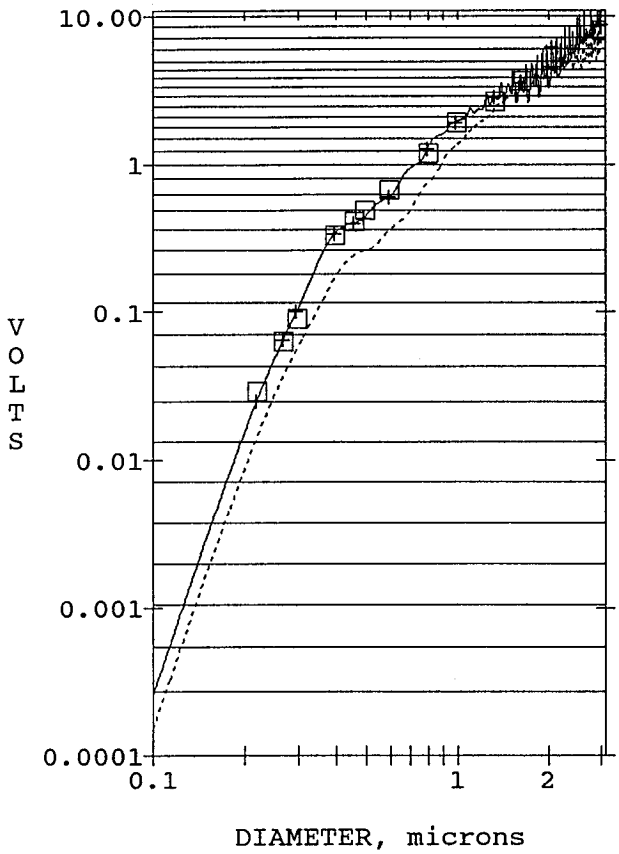

Fig. 1. Calibration curves for PCAS. Solid line shows refractive index of 1.59, pluses show theory for polymer microspheres, squares show measurement for polymer microspheres and dotted line shows refractive index of 1.44.

Also shown are expected pulse heights derived from theory as follows. The scattering cross sections for the calibration aerosols were calculated using Mie theory for light scattered into the collecting optics of the PCAS. It was assumed that incoherent beams impinge on the particles from opposite directions with random incident polarizations in the active cavity. The calculated scattering cross section for each standard size was divided by the mean measured voltage pulse height observed for the corresponding monodisperse polymer microspheres. If the theory correctly describes the instrument, this calibration ratio should be independent of particle size and refractive index and should depend upon laser intensity, optical collection efficiency and gain of the electronics. The calibration ratio for the eleven particles was found to lie within ±10% of the mean of the eleven ratios. The mean of the eleven calibration ratios was divided into the scattering cross section to produce the theoretical pulse height expected for each calibration aerosol. In Figure 1, the observed pulse heights are seen to lie within one channel of the expected pulse heights, justifying use of the theory to describe the instrument.

It was necessary to calibrate the PCAS for the refractive index of the sulfate aerosol reaching the laser beam in the stratosphere. The refractive index of sulfuric acid and water aerosols is 1.44 over a broad range of compositions [Steele and Hamill, 1981]. Calculation of evaporation of water from particles in sampling and transport showed that particles could be reasonably characterized with this refractive index when they reached the beam.

The calibration curve for refractive index 1.44 was determined as follows. The scattering cross sections for six hundred particle sizes were calculated for scattering into the collection optics of the PCAS. These cross sections were divided by the mean calibration ratio determined for the standard polymer particles. The horizontal grids on Figure 1 locate the channel boundaries of the multichannel analyzer. The intersections of these lines with the curve showing the expected pulse heights for aerosols of refractive index 1.44 define the diameters assigned to each channel.

The thirty one channels are distributed over the diameter range from 0.11 to 4.0μm in nearly even logarithmic steps. Thus the width of each channel is nearly 10% of the channel mean. The smallest relative channel width is about 5% and the largest is near 20%.

Spatial and temporal variability in the intensity of the multimode laser introduces some dispersion into the instrument response for monodisperse test aerosols. The standard deviation for the test aerosol size distributions equaled approximately 10% of the diameter. The mean discrepancy between the theoretical and measured calibration points is 7% in voltage. Due to the slope of the calibration curve, this discrepancy corresponds to a few percent in diameter. These uncertainties appear to be random.

Evaporation in sampling and transport. The inlet of the PCAS was designed to sample aerosol from the free stream and to slow the sample stream so that the aerosol could be efficiently transported to the laser cavity. Particles entering the PCAS aircraft inlet experience a nearly instantaneous 20 K increase in temperature due to adiabatic heating caused by slowing the Mach 0.7 sample flow. This heating is referred to as ram heating. The particles remain at ram temperature for tenths of a second until they reach the inlet to the passive cavity itself where they experience an even greater temperature jump to nearly 273 K. This second heating is by heat transfer from the cavity walls and lasts only a hundredth of a second. This history of heating causes evaporation of water and other volatile material from the particles which changes their composition, diameter and refractive index. This effect was theoretically modeled and the model results were used to correct the measured data to provide a description of the ambient aerosol size distribution.

The model assumes that the ambient aerosol consists of a supercooled solution of sulfuric acid and water. Since this assumption is not met in polar stratospheric clouds, PSCs, the data presented here exclude measurements made in PSCs.

In the case of supercooled solutions of sulfuric acid and water where water vapor is in equilibrium with the water in solution, the fraction of the solution mass which is acid, f_a, can be calculated from the temperature and water vapor concentration. The refractive index of the solution and its density can be calculated from f_a and temperature. The determination of these relations at stratospheric temperatures involves extrapolation from measured values at much warmer temperatures [Steele and Hamill, 1981; Gmitro and Vermeulen, 1963, 1964].

The model calculations utilized transition regime heat and mass transfer formulas which account for the fact that the mean free path of the gas molecules is significant compared to the particle diameter. The Fuchs and Sutugin [1970] transition regime flux interpolation scheme was used for the mass transfer. A similar interpolation scheme was adapted for heat transfer. A number of transition regime schemes were tried, and the results were not found to be very sensitive to the choice of scheme. Heat and mass transfer were coupled.

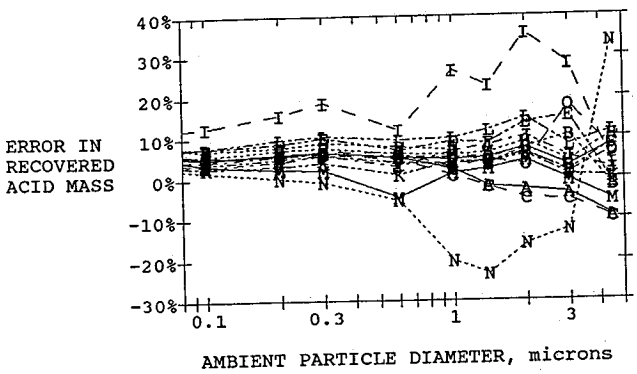

Fig. 2. Error in the mass of sulfuric acid in a particle obtained with the simplified data reduction scheme. The full evaporation model is used as the standard. Case N, 400 mbar ambient pressure and 900 ppmv of water vapor, and case I, 200 mbar ambient pressure and 4 ppmv of water vapor, represent extreme values rarely encountered in the data set.

Combinations of aircraft Mach number, sample flow rates, water vapor mixing ratios, ambient temperatures and pressures representative of those encountered in flight were chosen as test cases and particle density, temperature, refractive index and solution strength were calculated along the particle trajectories from the ambient air to the laser beam. All relevant particle properties where then determined at the laser beam.

In order to reduce the computational tasks to manageable proportions, the flight data were analyzed with a scheme which used the results of the test cases as follows. It was found that the final droplet solution concentration, f_a, could be predicted with a correlation equation based on final droplet diameter obtained from the PCAS measurement and the equilibrium solution concentrations at ambient and laser cavity conditions. In this analysis, a refractive index of 1.44 was assumed for the sizing. The final droplet temperature was assumed to equal the cavity temperature, and particle properties were calculated at the laser beam. This simplified method was used to calculate the mass of sulfuric acid in the particles reaching the laser beam for the test cases. Figure 2 shows the results of the comparison between the detailed analysis and the simplified scheme. In all the test cases except two, the mass of acid retrieved from the simplified scheme was within 10% of that calculated with the full analysis for submicron particles. Since the mass of sulfuric acid reaching the beam is the desired variable and since particles larger than one micron were only occasionally encountered, the simplified scheme was determined to be adequately accurate.

The flight data were reduced using the simplified scheme. For each size distribution measured, the ambient equilibrium sizes, composition, density and refractive index were determined. Figures 3a and 3b show the ratio of diameter at the laser to the diameter at ambient conditions for two conditions. In Figure 3a, ambient temperature of 197 K and water vapor mixing ratio of 5.3 ppmv result in water vapor saturation over ice of 0.254. This is fairly representative of cold yet noncloudy conditions encountered in the vortex. In Figure 3b, the ambient temperature was 217 K and the water vapor mixing ratio was 4.6 ppm which is more characteristic of mid-latitude water vapor saturations of 0.016. The higher humidity in the first case results in more water on the particle and a lower value of f_a.

Sampling and transport efficiency. The inlet of the PCAS was designed to sample aerosol from the free stream with known efficiency and to slow the sample stream to permit efficient transport to the laser cavity. Two diffusers were used (Figure 4). The first diffuser has a sharp edged inlet and an included angle of 6.7 degrees.

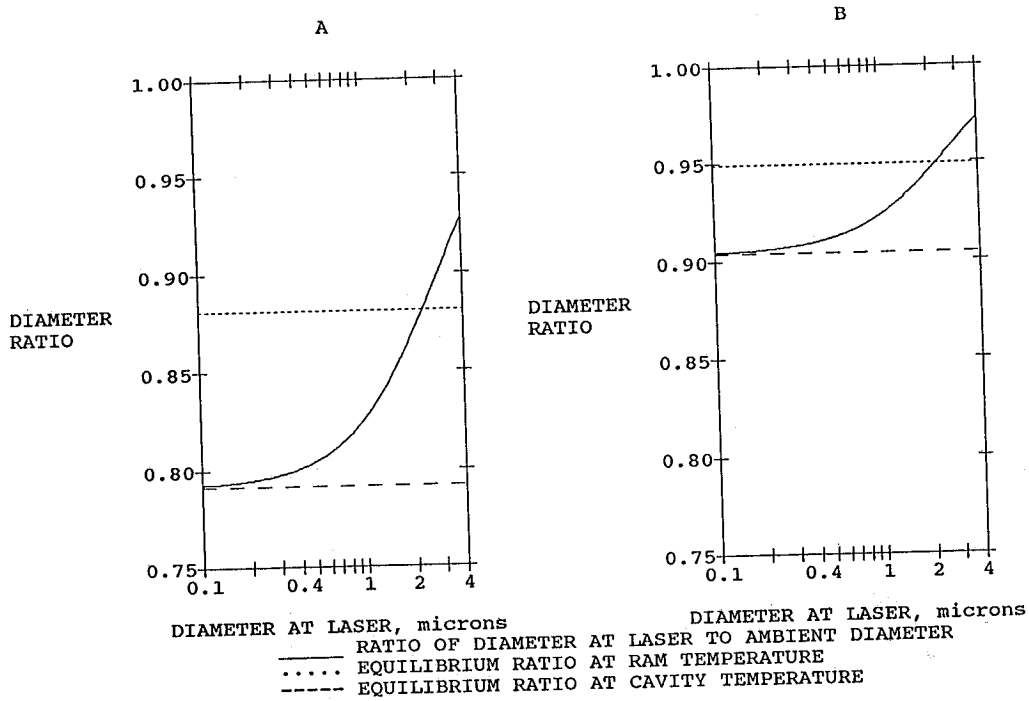

Fig. 3. Ratios of diameter at the laser to equilibrium diameter in the ambient as a function of the diameter at the laser. (a) Saturation of water vapor over ice is 0.254; acid mass fraction is 0.54. (b) Saturation of water vapor over ice is 0.016; acid mass fraction is 0.77.

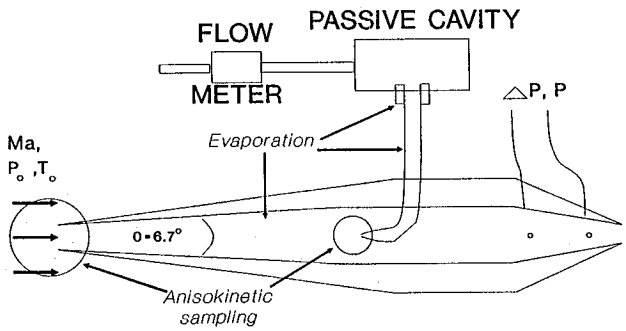

Fig. 4. PCAS ER-2 inlet. The exit flow meter is indicated by the pressure taps in the converging section on the right end of the inlet.

Inside this diffuser there is a second sampling tube with its own diffuser. If the mass flow velocity in the inlet of these diffusers does not match that in their respective free streams, then a sampling artifact, referred to as anisokinetic sampling, will occur [Belyaev and Levin, 1974; Rader and Marple, 1988]. If the velocity mismatch is small, the resulting error can be estimated.

To estimate the sampling artifact, the mass flow velocity in the free stream and into the first diffuser, the velocity profile and gas density in the inlet at the point of the second diffuser, and the mass flow in the second diffuser must all be known. The mass flow out the exit flow meter nearly equals the flow into the first diffuser and is calculated from the ambient stagnation temperature, the ambient stagnation pressure, the aircraft Mach number, the diffuser efficiency, the exit flow meter discharge coefficient and the pressure drop across the exit flow meter. This pressure drop is measured in flight. The exit flow meter discharge coefficient, the flow profile in the inlet and the diffuser efficiency were determined experimentally in the laboratory at the Reynolds numbers and Mach numbers encountered in flight.

The sample flow into the second diffuser is transported to the PCAS for measurement. This mass flow was measured in flight with a Tylan, model FM 360, mass flow meter at the exit of the PCAS. This meter was calibrated at the pressures experienced in flight. The volumetric sample flow was nearly constant with pressure up to about 100 mbar. It decreased from approximately 14 $cm^3\ s^{-1}$ to about 6 $cm^3\ s^{-1}$ as pressure decreased from 100 to 50 mbar.

The ratio of the particle mixing ratio in the diffuser to that in the free stream is called the aspiration coefficient. It was calculated for each of the two diffusers using the empirical correlation of Belyaev and Levin [1974] modified for compressible flow. The aspiration coefficient varies with particle size and is used to correct the measured data.

The net aspiration coefficient accounting for both sampling points for 1 μm diameter particles was typically around two. That is, the ambient mixing ratios for 1 μm particles were calculated to be about one half that seen by the PCAS. The aspiration coefficients for 0.1 μm diameter particles approached 1. The major source of the enhancement was the second diffuser where the velocity ratio often approached two. The velocities at the first diffuser were matched to within 25% over a wide range of ER-2 Mach numbers.

The inertial losses in the bend between the second diffuser and the PCAS were evaluated by comparing the conditions encountered in flight with the analysis performed by Tsai and Pui [1990]. Their numerical analysis included calculation of the secondary flows in the bend. For the tube, curvature and flows in the inlet to the PCAS, the analysis predicts that fewer than 2.5% of the one micron particles will be lost at the highest altitude. Losses will be less for smaller particles and higher pressures.

Comparison of PCAS measurements with those of other instruments. A number of uncertainties remain concerning the performance of the PCAS. For example, it is not known if the inlet is correctly aligned with the flow around the wing tank holding the PCAS. If not, turbulence induced by a large angle of attack could induce particle loss in the inlet. Assumptions concerning the ambient state of the sulfate aerosol have not been confirmed. Thus the response of the PCAS is not sufficiently well understood to permit assignment of measurement uncertainties from first principles. Therefore, it is informative to compare the measurements made with the PCAS with those made by other sensors.

Figures 5a and 5b show number distributions from the PCAS and Ames Wire Impactor (AWI) samples (R. Pueschel, personal communication) acquired simultaneously on February 7. Distribution A was acquired at a potential temperature, referred to here as theta, of 458 K and 8 degrees inside the vortex. Distribution B was acquired on the vortex edge at a theta of 458 K. For both methods, the ambient size distribution was constructed from the raw data by assuming that the ambient aerosol is a supercooled solution of sulfuric acid and water in equilibrium with the ambient water vapor at ambient temperature. In one case the PCAS shows more small particles than the Ames Wire Impactor, in the other case the impactor shows more small particles. These distributions illustrate the variability seen in several similar comparisons. In both size distributions, the PCAS shows fewer particles between 0.5 and 1 micron than does the impactor. This is also typical of the other comparisons. The error bars on the Ames Wire Impactor indicate the statistical uncertainties associated with the sample size. These two methods produce agreement to within about a factor of two.

It is interesting to note that the Ames Wire Impactor and PCAS showed similar agreement for measurements made in PSC's. Figure 5c shows a sample collected in a PSC on January 16 at a theta of 444 K and 14 degrees inside the vortex. The impactor samples were analyzed in a Scanning Electron Microscope at NASA Ames. All the nitric acid trihydrate which struck the impactor has evaporated before the samples reached the microscope. The agreement between the PCAS and AWI suggests that the PCAS succeeds in evaporating the volatile PSC material before it reaches the laser. In this PSC, the volatile material often constituted well over ninety percent of the total volume.

As is described above, the PCAS data analysis provides the composition and density of the ambient aerosol as well as the size. This permits calculation of sulfate mixing ratio from the PCAS output. PCAS sulfate mixing ratios were compared with filter measurements of sulfate mass mixing ratio made on the ER-2 and provided by B. Gandrud (personal communication, 1990). The average ratio of PCAS sulfate mass mixing ratio to the filter values was 0.52. The regression coefficient, r^2, equaled 0.52. The filter values spanned 0.35 to 0.70 ppbm, parts per billion by mass. Eleven filters were available for comparison and two PCAS data points were discarded because they contained unbelieved large particles as is discussed below.

Since the PCAS data analysis provided a value for the ambient refractive index, it was also possible to

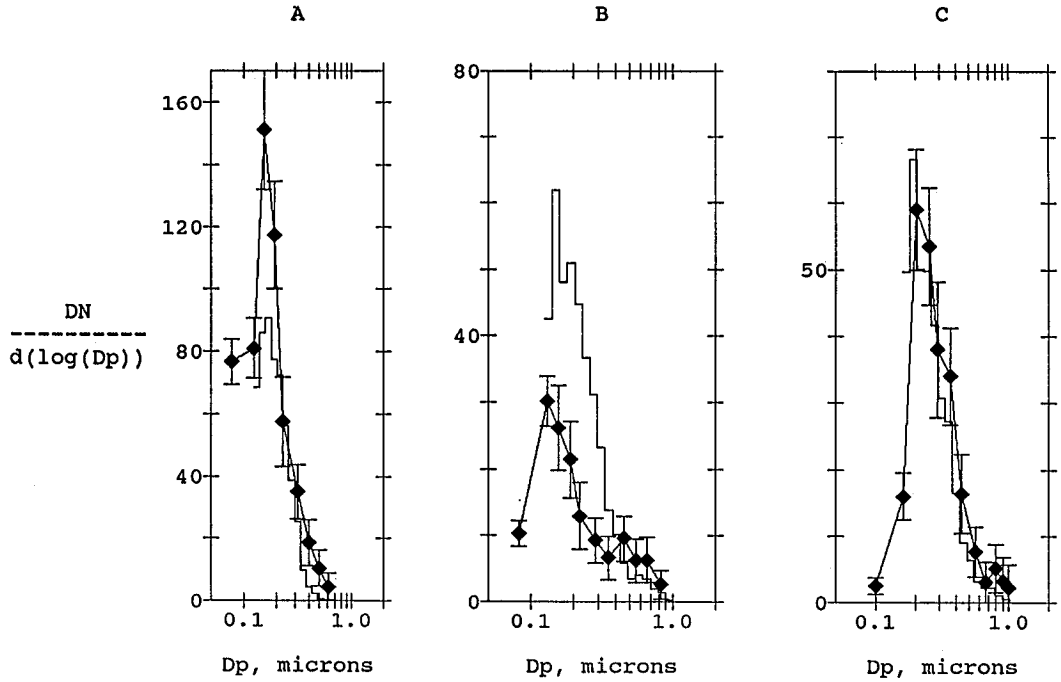

Fig. 5. Comparisons of PCAS and AWI. Units on the vertical axis are particles/mg air. (a) Distribution A was acquired in clear air in the vortex at a pressure altitude of 19.9 km and a latitude of 77N on February 7. (b) Distribution B was acquired in clear air on the edge of the vortex at a pressure altitude of 18.9 km and a latitude of 69N on February 7. (c) Distribution C was acquired in a PSC at a pressure altitude of 20.3 km and a latitude of 78.2N on January 16.

calculate the extinction at wavelengths of 1 μm that the ambient aerosol would cause and to compare it with that measured by the SAM II instrument on the Nimbus7 spacecraft. Data from the SAM II measurements [Osborn et al., 1990] are plotted with extinctions calculated from PCAS size distributions in Figures 6a, 6b, and 6c. The potential temperatures for the SAM II measurements were determined from the reported geometric altitudes and the meteorological analyses of Rood et al.[1990]. It was not often possible to find a satellite measurement at the latitude and longitude of an ER-2 vertical profile. In the cases shown in Figure 6, the the ER-2 passed the latitude of the the SAM II measurement point at two altitudes and made its profile maneuver several degrees latitude to the north. The PCAS points measured at the same latitude as the SAM II profiles are indicated with a square symbol. The PCAS profiles are indicated with asterisks. In Figures 6a and 6b, the data suggest that the extinction profiles did vary with latitude and that the square symbols should be used for the the comparison. In the case shown in Figure 6c, comparing the PCAS profile with the the square points suggests that the profile shows appropriate values at the upper end. In these cases, the PCAS seems to underestimate the scattering by less than a factor of two at smaller thetas and by a factor as large as four at the higher altitudes. The uncertainties in the satellite measurement approach 30% at 19 km altitude and are less at lower altitudes.

A Forward Scattering Spectrometer Probe Model 300 (FSSP-300) was also flown on the ER-2 in AASE. The FSSP–300 measures aerosol larger than 0.4μm without heating the particles [Dye et al., 1990b]. The FSSP–300 shows more particles in the diameter range from 0.4μm to 1μm than does the the PCAS. This discrepancy is about a factor of two in air that is clearly of mid-latitude origins but increases to values as high as eight near the edge of the vortex and often exceeds fifteen in the vortex. The discrepancy is greatest at the highest altitudes and deepest penetrations in the vortex.

Conclusions concerning accuracy of PCAS measurements. Due to questions concerning aerosol sampling from aircraft traveling at Mach 0.7, it is not possible to assign absolute uncertainties to either the AWI or the filter sampler. However, the comparisons between the PCAS and AWI and the PCAS and the filters suggest that the PCAS may be underestimating the aerosol population in the diameter range from 0.5μm to 1μm. This would cause underestimation of the scattering at wavelengths of 1 μm and of the mass as well. If true, this might result from ignoring particle loss by turbulent deposition in the PCAS inlet. Losses by turbulent deposition in the diffuser are not presently calculable and may be significant.

Cautioned by the comparisons, we use the PCAS data to quantitatively describe the integral and differential parameters of the sulfate aerosol, but we do not claim accuracy of better than a factor of two. Therefore, for the present, we will not interpret differences between the PCAS and other instruments unless they are larger than this factor. We will also limit ourselves to conclusions which are robust in the face of errors of this magnitude. The data suggest that the precision of the measurements are better than the factor of two and so comparisons of PCAS data in various circumstances will be interpreted even if differences are smaller than a factor of two.

The discrepancy between the PCAS and FSSP–300 may indicate that the sulfate aerosol is not supercooled liquid everywhere. One possible scenario is that the number of frozen particles may increase with altitude and latitude. Such particles are likely to carry more water than supercooled ones at a given water vapor pressure. If, as seems likely, the PCAS is able to remove most of

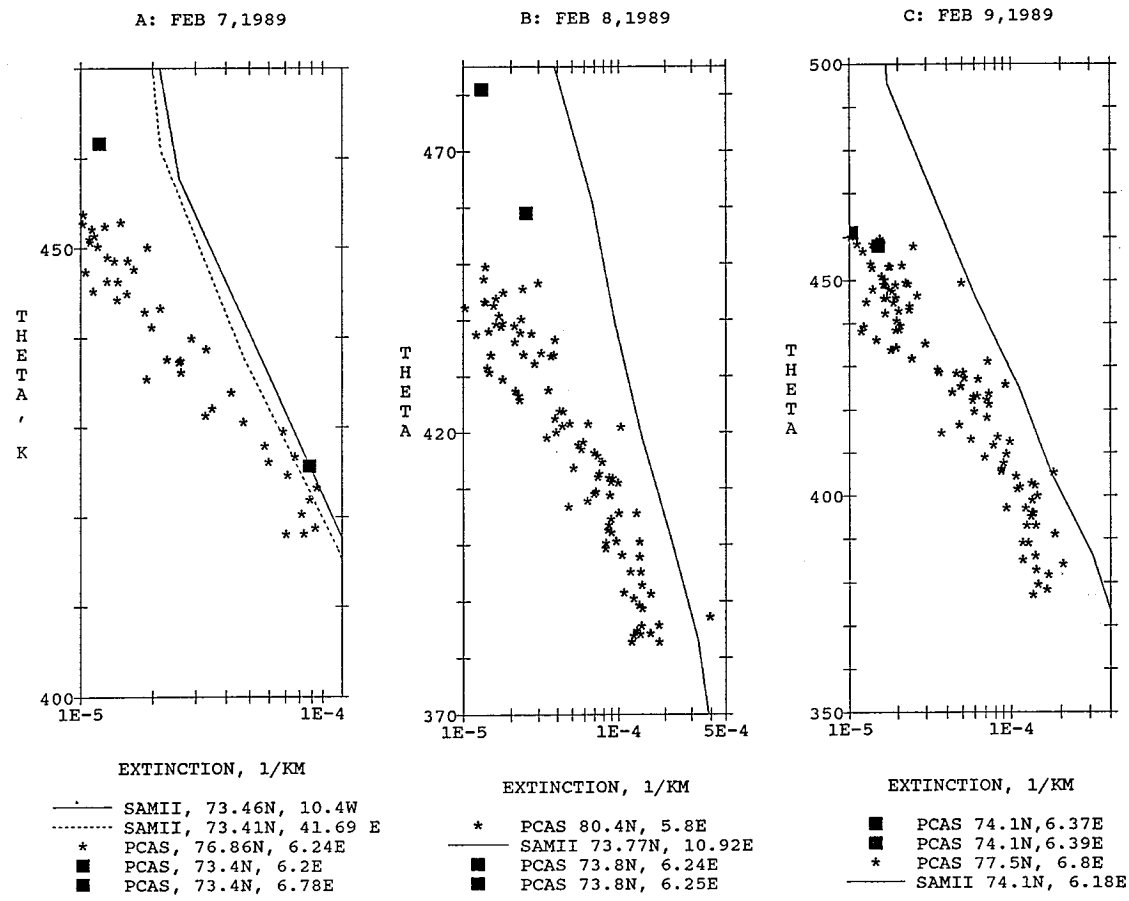

Fig. 6. Comparison of extinction at λ=1μm calculated from PCAS data with SAM II values. The extinction profiles were measured north of the vortex boundary.

the water from the frozen particles, then the reconstructed ambient size distributions are likely to underestimate the size of the actual ambient particles. Since the number distribution is decreasing strongly at diameters near 0.4μm, such underestimation would increase the ratio of FSSP to PCAS concentrations.

If effects of this type were operating, then the extinction calculated from PCAS data might also underestimate actual extinctions due to underestimating the size of frozen particles. Such an effect might explain part of the discrepancy between the extinction seen by SAM II and that estimated from the PCAS data. The compared extinctions were measured inside the vortex.

Errors in reconstructing the ambient size distribution do not present particular difficulties for the analysis presented here. The PCAS is clearly quite effective in removing volatile material from the particles. Therefore the characterization of the amount of sulfuric acid on the particles when they reached the PCAS laser is likely to be robust. The conclusions drawn in the following analysis deal with the amount and distribution of sulfate in the aerosol or could be stated in those terms. If the reconstruction of the ambient aerosol size distribution is wrong due to failure of the assumption of supercooled sulfuric acid and water particles, the conclusions presented in the following analysis still stand.

The PCAS data will not be used in the discussion of PSCs in this paper. Those data which are presented were taken in clear air where the conditions for the formation of PSCs did not exist.

Occasionally large particles occur in the PCAS data record but are not detected by the FSSP–300. These are thought to be artifacts, perhaps caused by photodiode break down and are not permitted to influence conclusions. Medians are usually used to describe combined data and this reduces the influence of suspected outliers.

The ER–2 Condensation Nucleus Counter (ER–2 CNC)

The ER-2 CNC detects particles larger than about 0.008μm in diameter by subjecting the sample to a saturated vapor of butyl alcohol and counting the particles which grow to sizes permitting optical detection. The precise lower size limit at which particles are efficiently counted depends upon pressure and has been determined in laboratory tests [Wilson et al., 1983b]. Particles are lost in transport to the growth chamber by diffusion or impaction and this limits the range of diameters which is accurately counted. At 21 km pressure altitude, 50% of the 0.01μm particles, 72% of the 0.02μm particles and 87% of the 0.04μm particles will be counted. At 13.5 km pressure altitude, 50% of the 0.007μm particles, 86% of 0.02μm particles and 91% of the 0.04μm particles are counted. The upper limit has never been characterized but is estimated to be approximately 1μm. The ER-2 CNC heats the particles to 28 C before detecting them so only particles having a core which is nonvolatile at this temperature and larger than the

minimum size are detected. The abbreviation CN refers to the particles detected and counted by the ER–2 CNC.

Other Measurements Used in this Analysis

Measurements of reactive nitrogen species, principally HNO_3+NO+NO_2+NO_3+$ClONO_2$+NO +$2N_2O_5$+HO_2NO_2, referred to here as NOy [Kawa et al., 1990] are used to determine when the air being sampled has been denitrified. N_2O measurements [Lowenstein et al., 1990a] are also required for this determination. Fahey et al.[1990] have determined that the amount of NOy found in an air parcel can be predicted from the amount of N_2O in cases where the amounts of NOy have not been disturbed by cloud processes. The expected amount of NOy calculated from N_2O is referred to as NOy*. When NOy in an air parcel is less NOy*, then it is assumed that the air has experienced a cloud process involving condensation of HNO_3 on particles and the removal of the particles and HNO_3 by gravitational sedimentation. This process is referred to as denitrification.

NOy, water vapor [Kelly et al., 1990] and temperature measurements [Chan et al., 1990] were used to determine when thermodynamic conditions precluded the formation of nitric acid trihydrate and, for all practical purposes, PSCs. The equilibrium vapor pressure of nitric acid over nitric acid trihydrate was calculated assuming that all the NOy was nitric acid. The vapor pressure relations of Hanson and Mauersberger [1988] were used. The present paper describes sulfate aerosol and therefore events involving PSCs were excluded. When these measurements were unavailable, the FSSP data were used to exclude PSC events from the data set.

N_2O is also used as a tracer for tropospheric air and as a dynamical tracer in this analysis. Low values of N_2O indicate that the air has been in the stratosphere for a long time and gradients of N_2O on constant theta surfaces indicate that subsidence has occurred [Loewenstein et al., 1990b].

Temperature, and pressure measured with the Meteorological Measurement System [Chan et al., 1990] were used to calculate potential temperature, referred to here as theta. Theta is used for the vertical coordinate in most of the analysis which follows. Surfaces of constant theta define isentropic surfaces. Adiabatic air motion occurs along surfaces of constant theta.

Flights and the Vortex Edge

Data presented here were acquired on 17 of the flights of the NASA ER-2 Aircraft in the Airborne Arctic Stratospheric Experiment of 1988-89. The first flight occurred on December 31, 1988 and was from Moffett Field, California to Wallops Island, Virginia. The second flight was to Stavanger, Norway. Thirteen flights were made out of Stavanger, Norway between January 3, 1989 and February 10, 1989. Return flights to Moffett Field occurred on February 20 and 21, 1989. Flights out of Stavanger generally went in a northern direction, included one or more changes of altitude permitting vertical profiles to be measured over a certain extent, and involved sampling on one or more potential temperature surfaces.

On all northern flights, the edge of the polar vortex was penetrated by the aircraft. The vortex is a cold pool of air circled by a strong jet [Schoeberl and Hartmann, 1991]. The edge of the vortex is defined in this paper as the point of highest wind velocity and is that used by Kawa et al. [1990]. At and north of the edge, N_2O decreases during northern motion on isentropic surfaces and shows the results of subsidence of air in the polar winter [Loewenstein et al., 1990b]. The air inside the vortex is often chemically perturbed. The population of chlorine radicals is often enhanced [Brune et al., 1990], reactive nitrogen species have often been removed [Kawa et al., 1990] and clouds containing nitrogen species and water are often observed [Pueschel et al., 1990]. These changes are involved in ozone destruction and have antecedents in and consequences for aerosol processes.

Stratospheric Sulfate Layer as Seen by the PCAS and the ER-2 CNC

Morphology of the Sulfate Layer

Plate 1 summarizes the sulfate mass mixing ratio calculated from the PCAS measurements made on ten flights north from Stavanger on January 3,12,16,20,24 and 30 and February 7,8,9, and 10. Data taken in PCSs have been removed from this record. All available data were sorted into theta bins having increments of 10K and latitude bins having increments of 1 degree. The median of the data in each bin is plotted. Positive latitudes are north of the vortex edge. Figure 7 shows the relationship between geometric altitude and theta for two radiosonde soundings on February 8. One sounding was made 12 degrees latitude south of the vortex edge and the other was made 7 degrees north. The height of the tropopause is marked. Geometric altitudes reached by the ER–2 ranged from about 13 km to 18 km deep in the vortex and reached nearly 20 km outside of the vortex. Sulfate mixing ratios in ppbm, parts per billion by mass, measured on February 8 are plotted on Figure 8. Altitudes were determined from Figure 7. The southern profile was measured over Stavanger.

In the region north of the vortex edge, gradients in sulfate mixing ratio are observed. Plate 1 shows that sulfate mass mixing ratio tends to decrease at the higher values of theta deeper into the vortex. The sulfate gradients on surfaces of constant potential temperature near the vortex edge are consistent with the observation of gradients in other species at that location. Figure 8 shows a clear decrease of sulfate mixing ratio with altitude north of the vortex edge.

In mid-latitudes in summer 1989, the sulfate mixing ratio increased with altitude from 14 to 20 km. The maximum in sulfate mixing ratio occurred between 20 and 24 km geometric altitude and mixing ratio decreased with altitude above 24 km [Hofmann, 1990].

South of the vortex edge on February 8, the increase in sulfate is seen between 9 and 13 km geometric altitude. A broad, nearly flat maximum in the profile extends from 13 to 19 km. The decrease in sulfate mixing ratio with altitude is not reached by the ER–2 south of the vortex edge, but must occur somewhere above 19 km altitude.

Inside the vortex, the decrease of sulfate with altitude and theta is seen clearly in Plate 1 and Figure 8. On February 8, the decrease occurs above 14 km altitude. The sulfate profile inside the vortex is displaced downward with respect to that seen outside the vortex and at mid-latitudes. The downward displacement of the sulfate layer appears to be largely due to subsidence. Loewenstein et al. [1990a] argue that the distribution of N_2O shows that the air in the vortex above 17 km altitude has subsided 4 to 6 kilometers relative to summer arctic profiles. Kent et al. [1985] have reported subsidence of air from 18 km to 12.5 km during the first three months of winter in the northern polar vortex. They used aerosol extinction and optical depth as a tracer for atmospheric motion and showed that the

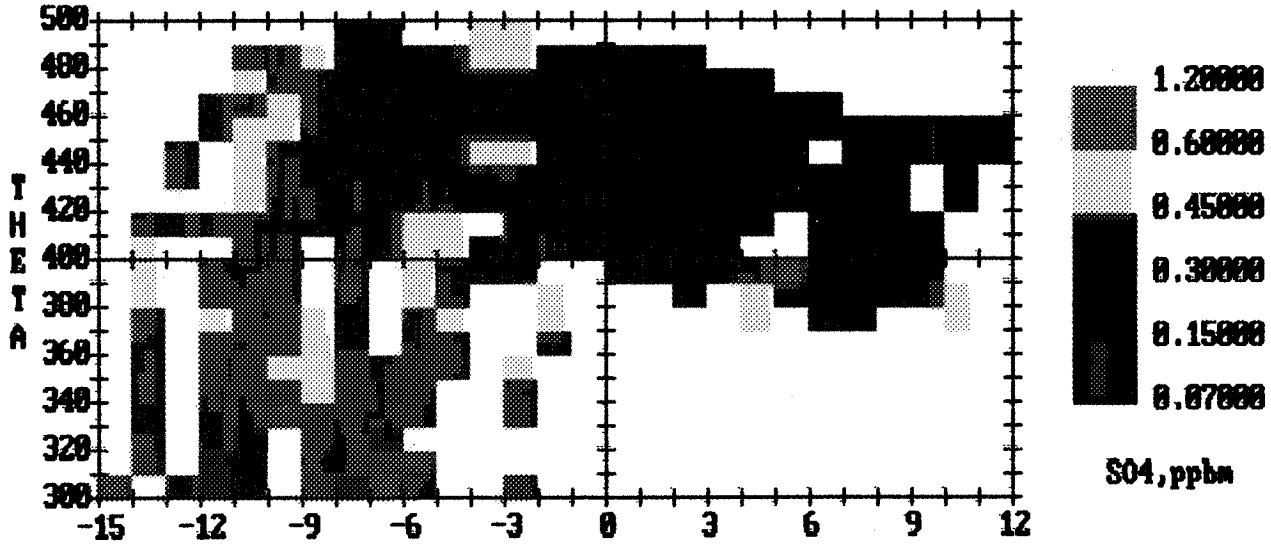

Plate 1. Sulfate mixing ratio, ppbm, as a function of latitude from the vortex edge and theta.

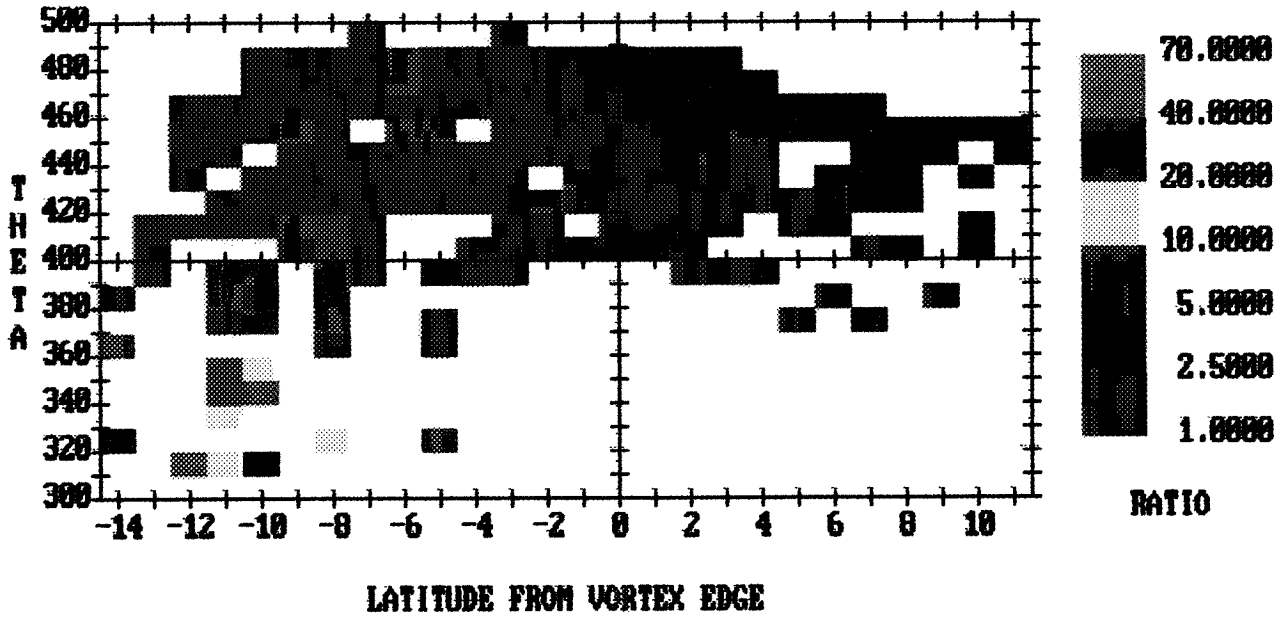

Plate 2. Ratio of CN to N_t from lognormal fits to PCAS data as a function of latitude from the vortex wall and theta. Ratios in excess of 2.5 suggest presence of a nuclei mode.

distances moved by these markers were much larger than could be explained by sedimentation.

Figure 9 shows CN mixing ratios for the same profiles plotted in Figure 8. Outside of the vortex, CN mixing ratios decrease above the tropopause by a factor of twenty and reach a broad minimum which starts above 360 K and extends to the top of the ER-2 profile. In this region, the CN mixing ratio varies by a factor of two. This broad minimum in the CN mixing ratio aligns with the broad maximum in the sulfate mixing ratio profile. Inside the vortex, the CN mixing ratio increases with theta and this increase occurs as the sulfate mixing ratio is decreasing. The CN minimum aligns with the sulfate maximum both in and out of the vortex. These features of the aerosol layer have been illustrated in many balloon soundings [Hofmann et al., 1989].

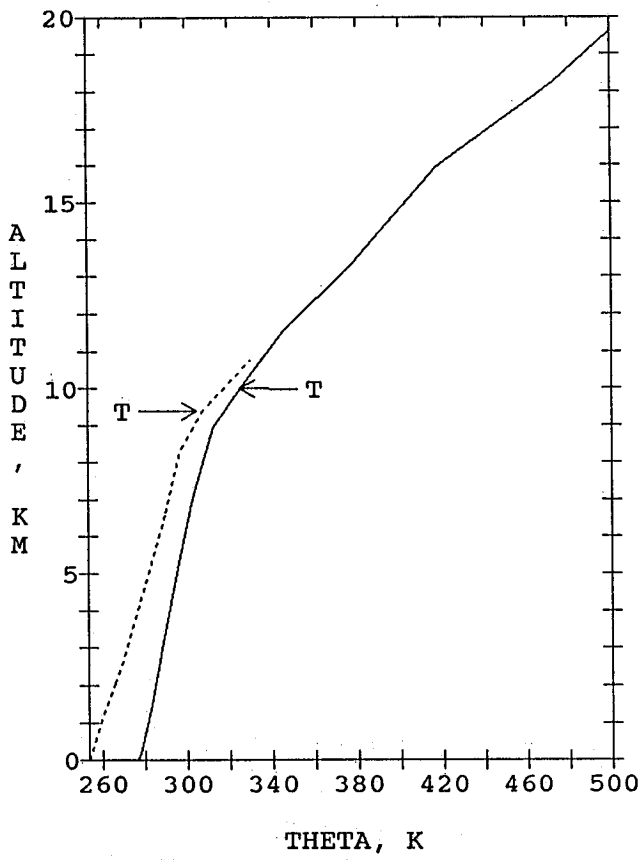

Fig. 7. Altitude versus theta from two radiosondes. Launch 12 degrees latitude south of the vortex edge (solid line). Launch 7 degrees latitude north of the vortex edge (dotted line).

Figure 10 shows sulfate mixing ratios plotted as a function of N_2O in and out of the vortex. All the clear air flight data were grouped for this plot. The curves show the locations of the tenth and ninetieth percentiles for the grouped data. The data exclude measurements made just inside the the vortex edge to avoid the effects of the transition from outside to inside [Loewenstein et al., 1990a]. The smallest sulfate mixing ratios were observed at low N_2O values in the vortex. Values of N_2O this low were not reached out of the vortex. Although there are few data in the overlap regions, sulfate seems to increase with N_2O both in and out of the vortex as N_2O increases from 140 to 180 ppbv. This suggests that the top of the sulfate layer occurs at the same value of N_2O inside and outside the vortex and that the difference in altitude of the sulfate layer between these locations is due to subsidence. For a given value of N_2O, there is less sulfate in the vortex than out of it.

Sulfate Size Distribution

Figures 11, 12 and 13 show four number, surface and volume distributions selected to show features of the sulfate size distribution at various locations with respect to the edge of the vortex and the sulfate layer. Figures 8 and 9 permit the measurement sites to be located with respect to important features of the sulfate layer. These distributions are typical of distributions measured in these regions on most of the flights. Size distribution A was measured outside the vortex at a theta of 335 K. This is above the tropopause and below the minimum in the CN profile (Figure 9) and below the maximum in the sulfate profile (Figure 8). Size distribution B was measured near the top of the ER-2 altitude profile over Stavanger out of the vortex. This location is in the broad region of the sulfate layer where the aerosol number

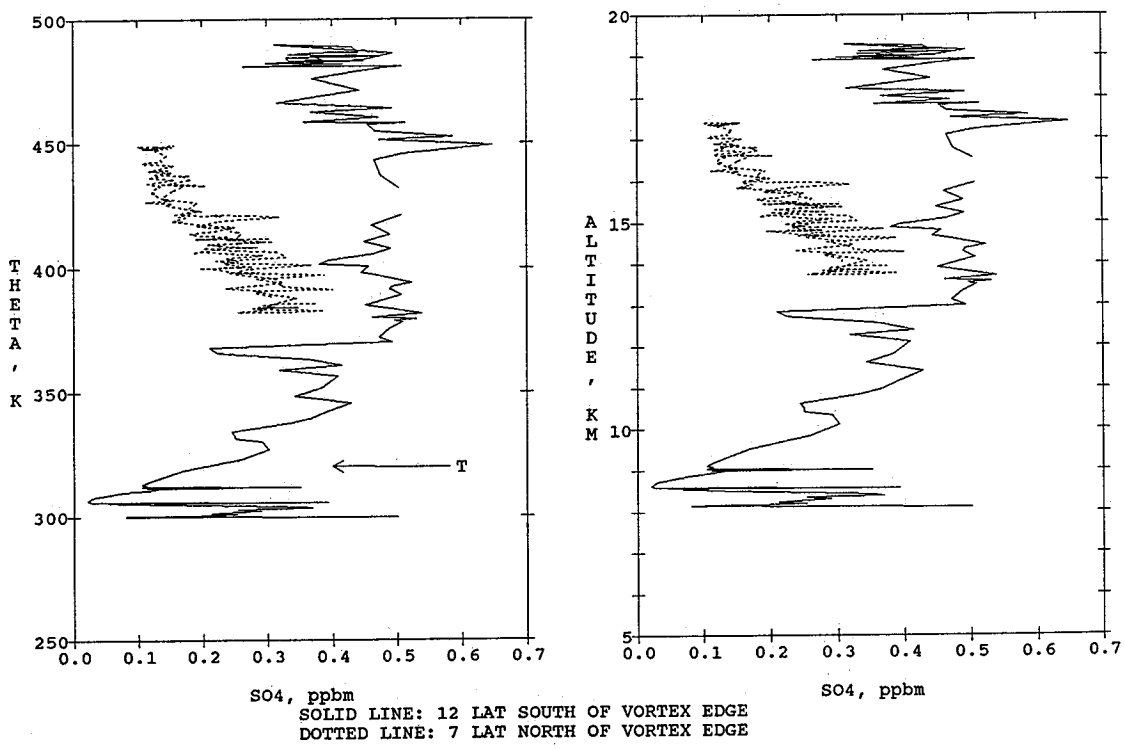

Fig. 8. Sulfate profiles, ppbm, in and out of the vortex on February 8, 1989, as a function of theta and altitude. The vortex edge was at 71N.

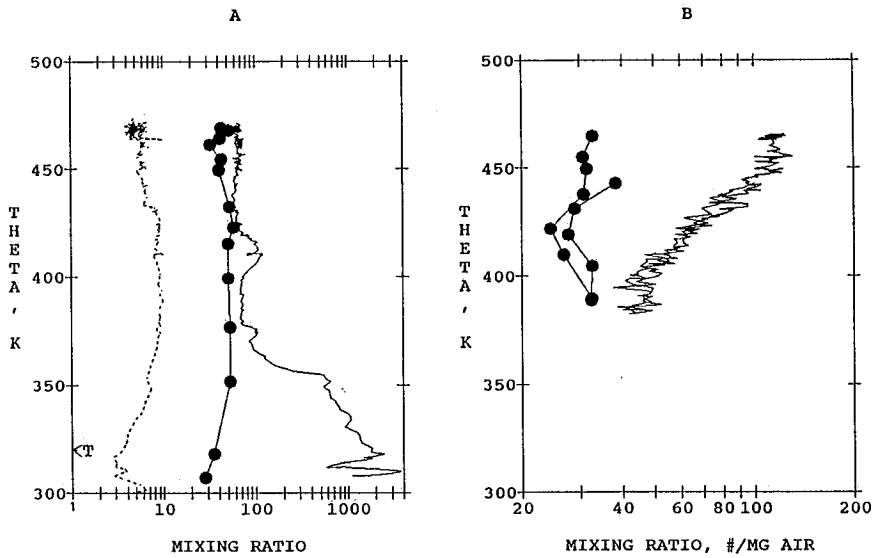

Fig. 9. Profiles of CN mixing ratios, particles/mg air (solid line). Profiles of N_t, the total number determined from fits to PCAS size distributions, particles/mg air (solid circles). Profile of surface mixing ratio, μm^2/mg air (dotted line). Measurements made at (a) 59N and (b) 78N on February 8.

mixing ratio, indicated by CN, is near its minimum, and the sulfate mixing ratio is near its maximum.

Size distribution C was measured near the bottom of the ER-2 profile in the vortex. This location appears to be above, but near, the broad maximum in the sulfate mixing ratio and the CN minimum. Size distribution D was measured 7 degrees inside the vortex near the top of the ER-2 altitude profile. Subsidence had brought the top of the aerosol layer within the reach of the ER-2 here

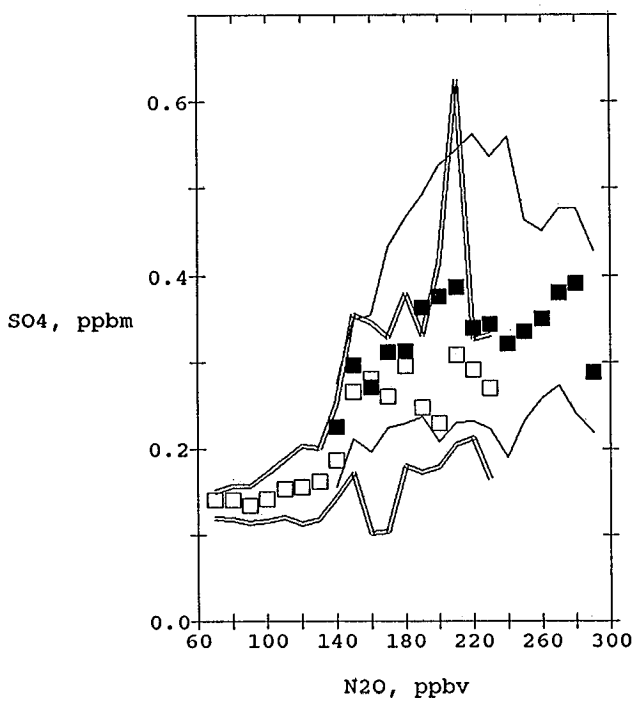

Fig. 10. SO_4, ppbm, as a function of N_2O, ppbv, in (open squares) and out (solid squares) of the vortex. Ten to ninety percentile range indicated by curves. In vortex (double line). Out of vortex (solid line).

and the sulfate mixing ratio is decreasing with altitude in this region. The total aerosol number mixing ratio, CN, is increasing with altitude in this region of particle production [Wilson et al., 1990].

The PCAS distributions plotted in Figure 11 have been fit with lognormal size distributions. These distributions are characterized by three modal parameters, a geometric mean number diameter, d_{gnm}, a geometric standard deviation, σ_g, and a total number, N_t [Fuchs, 1964, p. 12 ff.]. The modal parameters were determined with a function fitting routine which minimized the discrepancy between the lognormal distribution and the measured distribution. These lognormal functions are primarily useful as summaries of the data. The three modal parameters replace the many channels recorded for each size distribution. Since a number of criteria for goodness of fit may be employed, such fits are not unique, and the final determination of the adequacy of the fit is visual inspection. Table 1 lists the modal parameters and the simultaneously determined CN mixing ratio. In each case, the fit distribution passes through many of the measured points and captures major features of the number distribution as measured by the PCAS.

The lognormal fits to the number distributions measured by the PCAS were transformed to surface distributions by use of the Hatch–Choate relations [Hinds, 1982, p. 91 ff.]. These lognormal surface distributions are plotted in Figure 12 along with the surface distributions derived from the PCAS measurements. Note that the lognormal parameters resulting from the fits to the number distribution are successful in describing the first twelve or so size bins of the distribution. The modal parameter N_t describes a lognormal distribution which accurately describes the lower twelve size bins even though about half the particles in the mode are not seen by the PCAS.

In two of the size distributions, A and D, the total number derived from the fits, N_t, is more than a factor of two less than the measured CN values. This fact has been represented graphically in Figure 11. When dN/d(log(Dp)) is plotted against the log of the diameter, Dp, the area under the curve between any two diameters

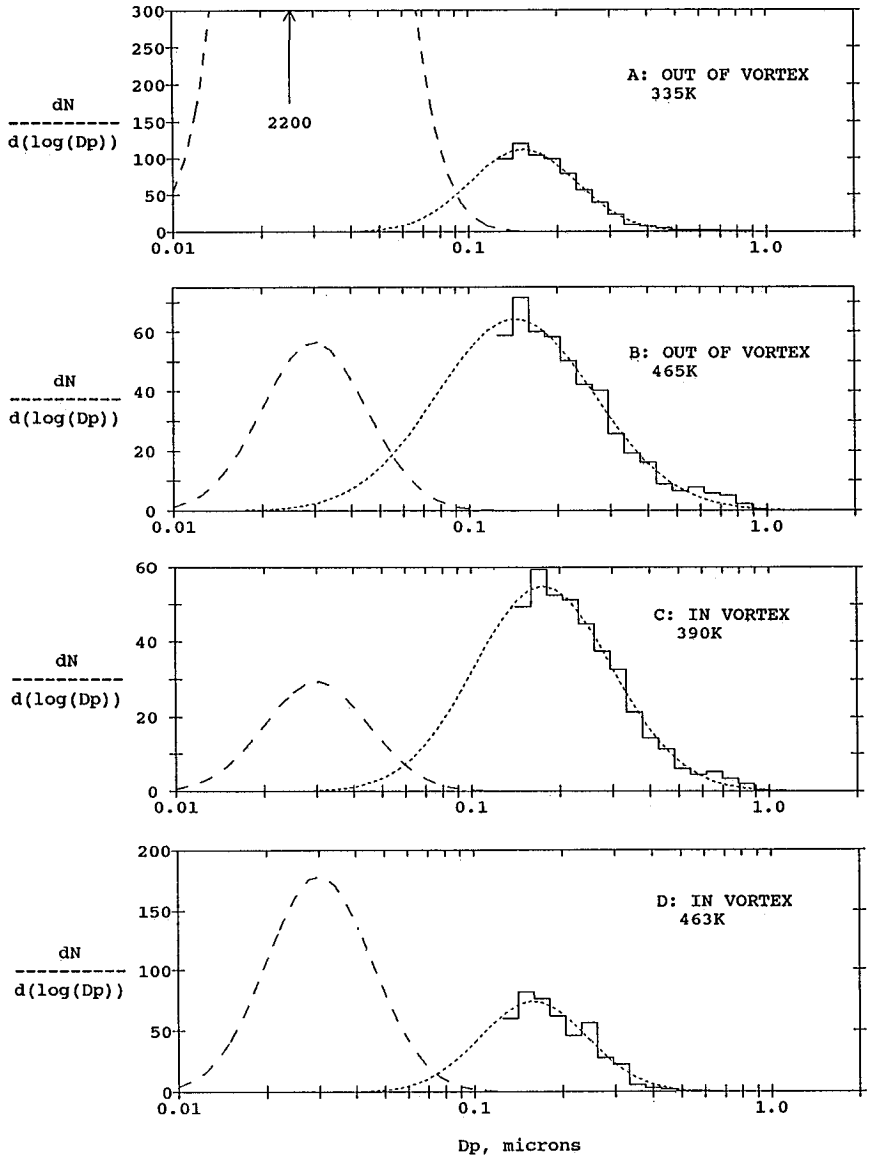

Fig. 11. Number distributions: dN/d(log(Dp)), particles/mg air, for representative distributions. PCAS Measurement (solid line). Lognormal fit to PCAS data (dotted line). Heuristic mode for excess CN (dashed line). (a) Twelve degrees south of vortex at pressure altitude of 11.2 km, (b) 8 degrees south of the vortex at pressure altitude of 17.3 km, (c) 9 degrees north of vortex edge at a pressure altitude of 16.2 km, (d) 6 degrees north of vortex edge at pressure altitude of 19.9 km.

is proportional to the number of particles found between those two diameters. Thus the area under the fine dotted lines is proportional to N_t. The area under the dashed line is proportional to CN–N_t, the number of particles counted by the ER-2 CNC but not accounted for in the lognormal fit to the PCAS measurement. Since the ER-2 CNC can detect particles as small as 0.008μm in diameter, it is assumed that these particles are in the diameter range from about 0.01μm to 0.1μm. The actual d_{gnm}, and σ_g of these modes are unknown, but the area under the curves does represent the number of CN which are unaccounted for by the lognormal fit to the PCAS.

A lognormal distribution can be fit to the PCAS measurements in Figure 11 with the constraint that N_t equal CN. In the case of distribution A, the resulting distribution has a d_{gnm} approximately equal to the lower detection limit of the ER–2 CNC. This distribution is not physically reasonable since it places about half the particles out of the range of the instrument that counted them. Fitting a lognormal with N_t constrained to equal CN for distribution D in Figure 11 does not result in any such major contradiction. However, the lognormal distribution resulting from the unconstrained fit shown in Figure 11 passes closer to more of the measured values than the constrained fit. Thus it is not possible to describe the measurements shown in Figures 11a and 11d as monomodal lognormal distributions without ignoring significant features of the measurements.

In distributions B and C, the CN mixing ratio does exceed N_t, but by less than a factor of two. Given the measurement uncertainties cited above, we will say that these CN and PCAS measurements are not inconsistent with the hypothesis of a monomodal, lognormal size distribution.

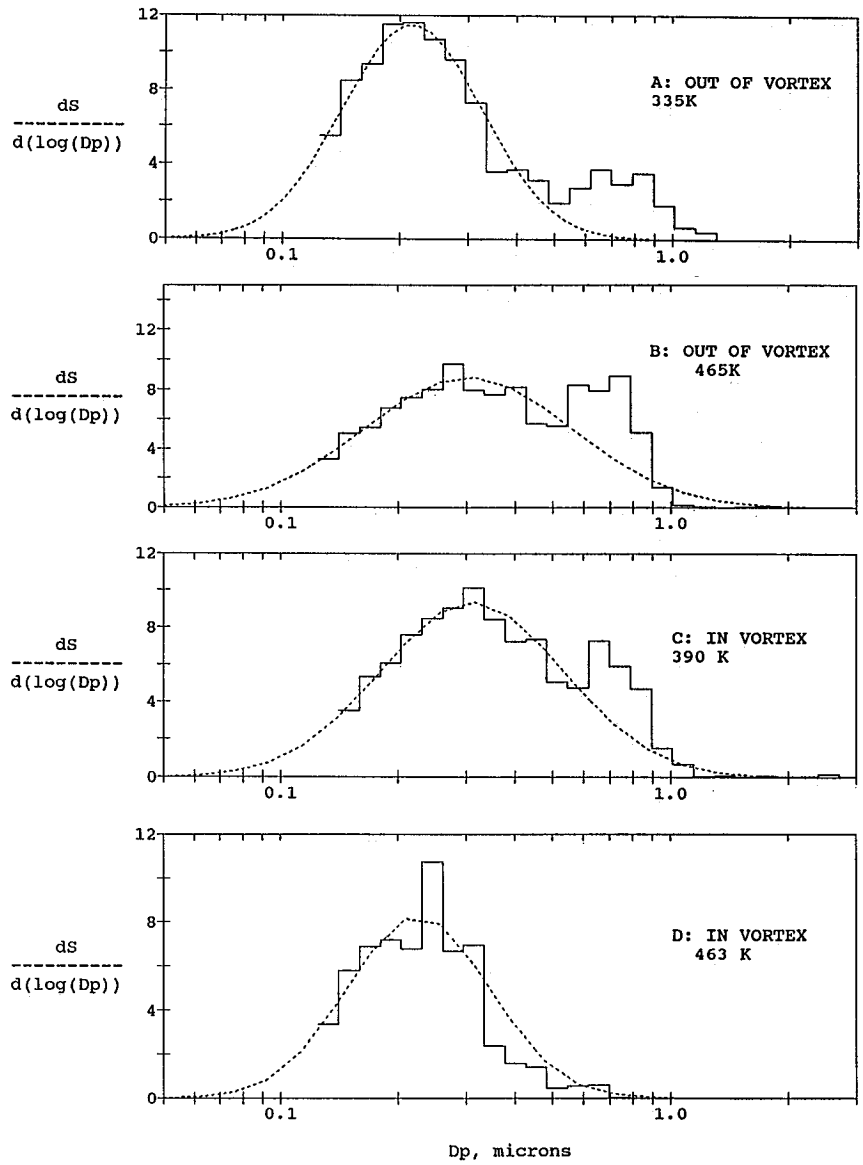

Fig. 12. Surface distributions: dS/d(log(Dp)), μm^2/mg air, for representative distributions. PCAS measurement (solid line). Lognormal fit to PCAS number data (dotted line). (a) Twelve degrees south of vortex at pressure altitude of 11.2 km, (b) 8 degrees south of the vortex at pressure altitude of 17.3 km, (c) 9 degrees north of vortex edge at a pressure altitude of 16.2 km, (d) 6 degrees north of vortex edge at pressure altitude of 19.9 km.

The Nuclei Mode and Regions of New Particle Formation

The presence of a mode with a median diameter in the 0.01 to 0.1 μm diameter range is often associated with new particle formation and is referred to as a nuclei mode [Whitby, 1978]. Figure 9 and Plate 2 show locations where CN exceeds N_t by so much as to strongly suggest a significant population of particles in the 0.01 to 0.1 μm diameter range. It is likely that there is a nuclei mode in this region of the aerosol size distribution. Figure 9 shows profiles of N_t and CN. Plate 2 shows the ratio of CN to N_t as a function of theta and latitude from the vortex.

Figure 9 and Plate 2 clearly show that at potential temperatures below 360 K over Stavanger, CN exceeds N_t by factors of several to factors of 30 to 70. Similar excesses of CN were encountered in every ascent out of Stavanger and in every descent into Stavanger. This type of profile was also observed on all ascents and all descents at mid-latitudes on the ferry flights. Thus, they were seen at latitudes of 38N in December and February as well as at 59N in between. Profiles of this type have also been observed in Darwin Australia in the winter of 1987 and over Moffett Field in summer of 1991. The size distributions in the region around the tropopause strongly resembles distribution A in Figure 11.

The surface mixing ratio profile determined from the PCAS measurements are also plotted on on Figure 9. For theta less than 360 K, this profile correlates negatively with CN. This observation is consistent with new particle formation in this region. For a given concentration of condensable molecules, the number of new particles formed will increase as preexisting surface area decreases [McMurry, 1983].

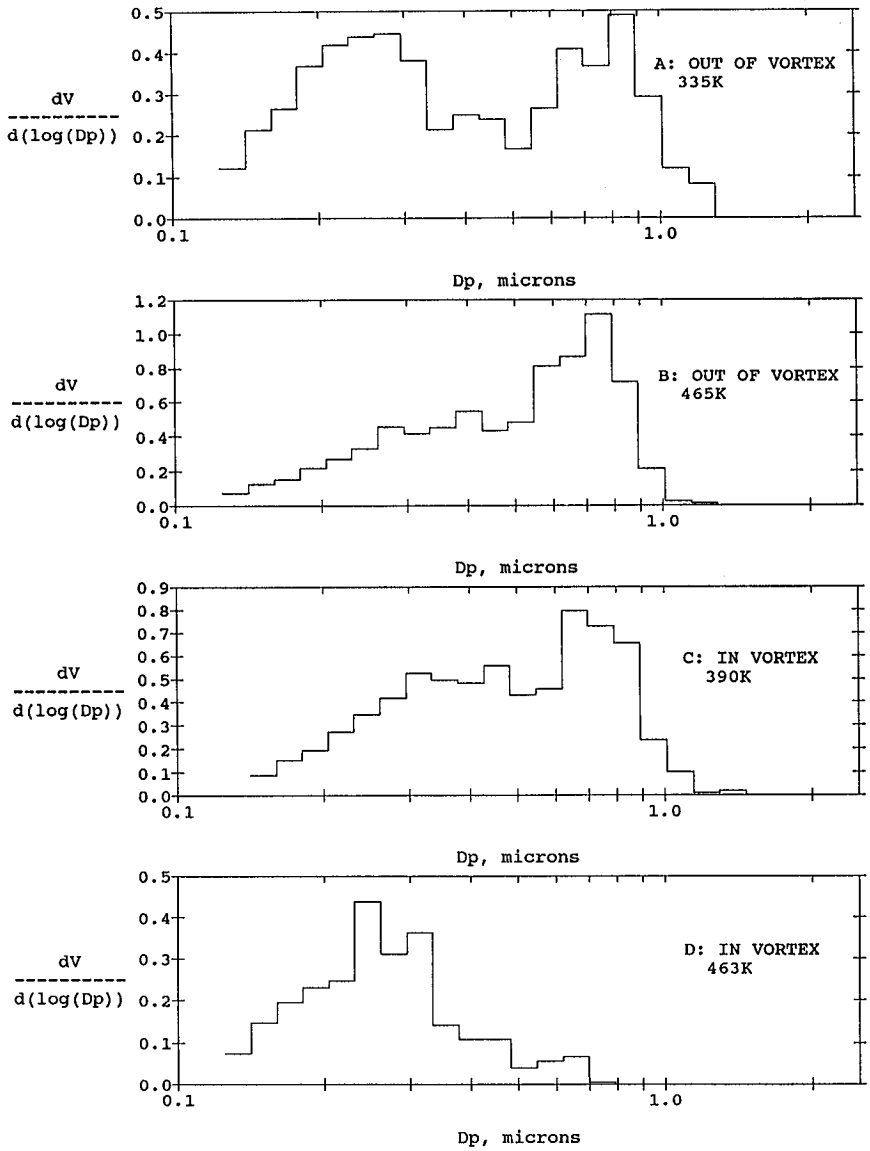

Fig. 13. Volume distributions: dV/d(log(Dp)), μm^3/mg air, for representative distributions. PCAS measurement (solid line). (a) Twelve degrees south of vortex at pressure altitude of 11.2 km, (b) 8 degrees south of the vortex at pressure altitude of 17.3 km, (c) 9 degrees north of vortex edge at a pressure altitude of 16.2 km, (d) 6 degrees north of vortex edge at pressure altitude of 19.9 km.

Other investigators have argued that new particle formation occurs in the upper troposphere. Tony Clarke (personal communication, 1991) reports observations of new particle formation in the remote marine troposphere at altitudes from 8 to 12 km. Hamill et al. [1982] predict that sulfuric acid particles should form on precursor particles in the upper troposphere. These precursor particles are smaller than the detection limit of the CNC. The observations reported here suggest that new particles are formed in the upper troposphere and in the lower stratosphere. It is likely that the aerosol in the few kilometers above and below the tropopause has a nuclei mode present at all latitudes and in all seasons.

TABLE 1. Lognormal Parameters From Fits to Size Distributions Shown in Figures 11, 12, and 13

Dist.	N_t, particles / mg Air	σ_g	D_{gnm}, μm	CN, particles / mg Air
A	49.9	1.51	0.153	983
B	42.8	1.84	0.144	67
C	32.0	1.71	0.175	45
D	33.5	1.52	0.159	112

The profiles of CN and N_t in the vortex, Figure 9b, show increasing divergence between CN and N_t with altitude above the minimum in the CN mixing ratio. This region is also shown clearly in Plate 2. Ratios of CN to N_t in excess of 2.5 are found north of the vortex edge and at theta above 440K. In this region, CN was found to negatively correlate with N_2O [Wilson et al., 1990], indicating a region of new particle formation where one expects a nuclei mode. The presence of a significant

population of particles with diameters between 0.01μm and 0.1μm is implied by size distribution D which was measured in this region and by the relationship between CN and N_t. Hamill et al. [1990] find that the cold conditions in this region of the vortex are conducive for homogeneous nucleation of sulfuric acid–water particles. The formation of these particles would lead to a nuclei mode in this region of the stratosphere as well.

The volume distributions shown in Figure 14 have a mode with modal diameter between 0.5μm and 1.0μm. In order to accurately describe these distributions, a distribution more complicated than a monomodal lognormal would be required. The origin of these modes is uncertain.

Effects of Denitrification on the Size Distribution of the Sulfate Aerosol

Observations in both the northern and southern polar vortices have shown that reactive nitrogen species are removed from the polar stratosphere in winter and early spring [Fahey et al., 1990]. The availability of reactive nitrogen affects the partitioning of chlorine among ozone–destroying forms and those that do not destroy ozone. The removal of reactive nitrogen enhances the potential for ozone depletion [Solomon, 1990]. It is likely that the reactive nitrogen is removed on particles which grow to large sizes due to the condensation of nitric acid and water. These large particles then settle from the stratosphere. A number of mechanisms for removal of reactive nitrogen have been proposed and discussed [Poole and McCormick, 1988; Toon et al., 1990; Salawitch et al., 1989; Wofsy et al., 1990].

Measurements in the Antarctic suggested that only a small fraction of preexisting particles were removed with the reactive nitrogen species in denitrification. Although polar stratospheric clouds were observed in which a large fraction of CN served as nuclei for the formation of larger nitrogen–containing particles, the sedimentation of these particles was not responsible for the denitrification. Rather denitrification seemed to proceed by placing the removed nitrogen species on large particles while involving only a small fraction of the sulfate aerosols [Hofmann et al., 1989; Wilson et al., 1989].

In AASE it was possible to compare the sulfate size distributions in denitrified air with those observed in air that had not been denitrified. Figure 14 shows measurements of N_2O and NOy/NOy* on February 7. The horizontal axis is universal time (UT) in seconds. NOy is total reactive nitrogen and NOy* is the amount of reactive nitrogen is expected in the air parcel [Fahey et al., 1990]. When the ratio NOy/NOy* is near one, the air has not been denitrified. Observations made from 34000 to 35500 UT and from 41000 to 42000 UT were made in nondenitrified air. When the ratio is much less than one, the air has been denitrified as is seen between 36000 and 38500 UT where the ratio is less than 0.4 and more than 60% of the reactive nitrogen has been removed. Between 39000 and 40500 UT the ratio is less than 0.65 and around 35% of the expected NOy is missing.

Figure 15 shows size distributions measured during these intervals in denitrified air and in air that has not been denitrified. Since the number and volume of sulfate particles varies with N_2O, the compared size distributions were measured at similar values of N_2O. The distributions shown in Figure 15a were measured when N_2O equaled approximately 150 ppbm and approximately 70% of the reactive nitrogen had been removed from the denitrified air. The distributions shown in Figure 15b were measured when N_2O equaled about 100 ppbv and about 35% of the NOy had been removed from the denitrified air. Three distributions are shown for each class. The lowest line of each represents the first quartile of the grouped values of dN/d(Log(Dp)) for each size. The middle line of each represents the median and the upper curve represents the third quartile. Since the particle sizes are affected by relative humidity, the size distributions measured in the denitrified air were corrected to the relative humidity of the nondenitrified air. The plotted distributions then have the same mass fraction of sulfuric acid.

In Figure 15a, the third quartile of denitrified air has fewer particles than the first quartile of nondenitrified air for diameters larger than about 0.5 μm. In Figure 15b,

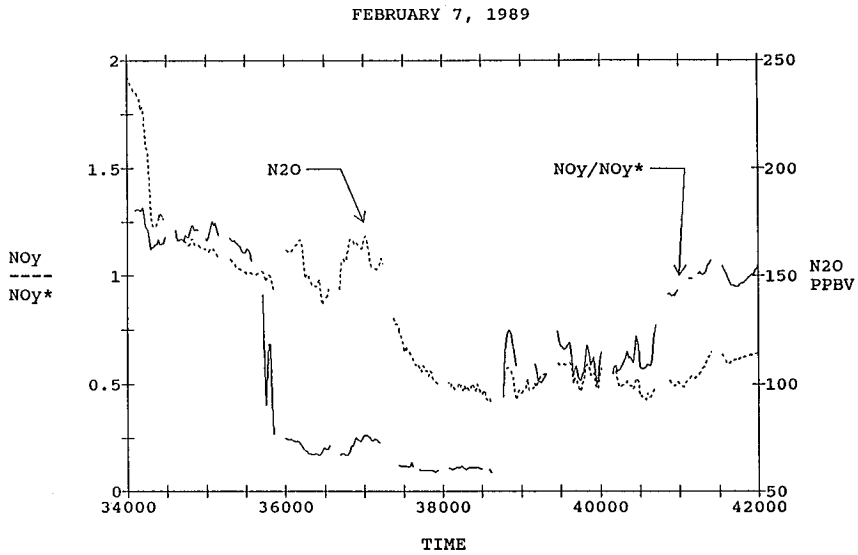

Fig. 14. NOy/NOy* (solid line) and N_2O (dotted line) versus time on February 7, 1989. NOy/NOy*< 1 implies that the air is denitrified.

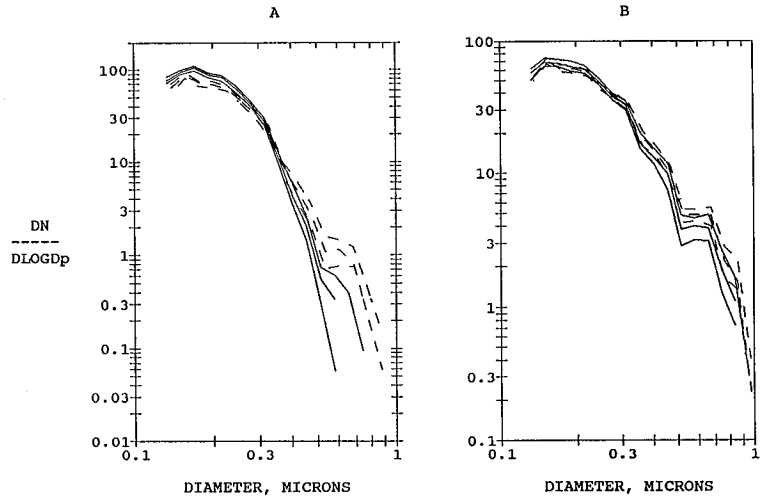

Fig. 15. Number distributions in denitrified (solid line) and nondenitrified air (broken line). Units are particles/mg air. Middle line in each group connects the median value for the grouped channels. Top line is the third quartile, and bottom line is first quartile. Measurements made on February 7.

the median in denitrified air has fewer particles than the first quartile of nondenitrified air for particles larger than about 0.5μm. This suggests that denitrification removes particles from the large end of the sulfate size spectrum. There are more particles in the small end of the distribution in the denitrified case but this effect is not understood.

A similar analysis was performed for the interval between 39000 and 39500 UT on February 8 when approximately 70% of the expected NOy was missing from the air parcel. The distribution resembled that shown in Figure 15b. Denitrified air parcels were observed on January 16, 20, and 30 as well, but in those parcels, NOy was sufficiently elevated with respect to saturation over nitric acid trihydrate to suggest the presence of PSCs and they were not analyzed. The deficit of large particles was observed in each of the three, cloud–free denitrified episodes encountered in AASE.

Mixing ratios for CN, and aerosol sulfate were sorted into denitrified and nondenitrified groups and plotted against N_2O for February 7 and 8. Within the scatter, the CN and aerosol sulfate mixing ratios were the same for the denitrified and nondenitrified air. However, the geometric standard deviations calculated for the volume weighting of the size distributions group around smaller values for size distributions measured in denitrified air than for size distributions measured in nondenitrified air. It appears that the removal of the large particles has reduced the width of the size distributions enough to be seen in a scatter plot.

Conclusions

Measurements of sulfate aerosol were made with a Passive Cavity Aerosol Spectrometer flown on the NASA ER-2 aircraft. Efforts were made to understand and compensate for the effects of anisokinetic sampling, evaporation of particles in sampling and transport, and dependence of refractive index on composition.

Measurements made with the PCAS and ER-2 CNC permitted the size distribution and morphology of the sulfate aerosol layer to be mapped in the region of the north polar vortex. Features of the sulfate layer which were observed included the broad maximum in the sulfate mass mixing ratio, the corresponding minimum in the CN mixing ratio and the top of the aerosol layer. The effect of subsidence on these structures was inferred from simultaneous measurements of N_2O.

Comparison of CN measurements to lognormal fits of PCAS size distributions permitted the hypothesis of a monomodal aerosol to be tested. It was found that monomodal descriptions of the aerosol were likely to be wrong in the region around the tropopause where a nuclei mode is probably needed for an accurate description of the aerosol. The presence of a nuclei mode is also implied by measurements made in the polar vortex where the sulfate mixing ratio is decreasing rapidly with altitude. In both locations, the nuclei mode is likely to be the result of new particle formation.

Some evidence was found for additional structure in the aerosol distribution between 0.5μm and 1μm in diameter. The meaning of this structure is not clear at this time.

Comparison of denitrified air with that which was not denitrified suggests that denitrification removes particles from the large end of the sulfate size distribution. It is tempting to connect that observation with the observation that there is less sulfate at a given value of N_2O in the vortex than out of it. However, sorting measurements made in the vortex into denitrified and nondenitrified cases does not reveal systematic differences in sulfate mass mixing ratio or in CN mixing ratio.

Acknowledgments. This work was supported by R. T. Watson and M. T. Kurylo at the NASA Upper Atmosphere Program through NASA Ames under grant NAG–458 and cooperative agreement NCC 2–470.

References

Belyaev, S. P. and Levin, L. M., Techniques for collection of representative aerosol samples, *J. Aerosol Sci., 5,* 325–338, 1974.

Brune, W. H., D. W. Toohey, J. G. Anderson, and K. R. Chan, In situ observations of ClO in the arctic stratosphere: ER–2 aircraft results from 59N to 80N latitude, *Geophys. Res. Lett., 17,* 505–509, 1990.

Chan, K. R., S. W. Bowen, T. P. Bui,S. G. Scott, and J. Dean–Day, Temperature and wind measurements and model atmospheres of the 1989 airborne arctic stratospheric expedition, *Geophys. Res. Lett., 17,* 341, 1990.

Dye, J. E., B. W. Gandrud, D. Baumgardner, K. R. Chan, G. V. Ferry, M. Loewenstein, K. K. Kelly, and J. C. Wilson, Observed particle evolution in the polar stratospheric cloud of January 24, 1989, *Geophys. Res. Lett., 17,* 413–416, 1990a.

Dye, J. E., B. W. Gandrud, D. Baumgardner, L. Sanford, and G. V. Ferry, A survey of particle measurements in the arctic from the forward scattering spectrometer probe model 300, *Geophys. Res. Lett., 17,* 409, 1990b.

Fahey, D. W., K. K. Kelly, S. R. Kawa, A. F. Tuck, M. Loewenstein, K. R. Chan, and L. E. Heidt, Observations of denitrification and dehydration in the winter polar stratospheres, *Nature, 344,* 321–324, 1990.

Fuchs, N. A., *The Mechanics of Aerosols*, 408 pp., Dover, New York, 1964.

Fuchs, N. A. and A. G. Sutugin, *Highly Dispersed Aerosols*, Ann Arbor Science, Ann Arbor, Mich., 1970.

Gmitro, J. I. and T. Vermeulen, Vapor–liquid equilibria for aqueous sulfuric acid, *Rep. URCL–10886*, Lawrence Radiation Laboratory University of California, Berkeley, 1963.

Gmitro, J. I. and T. Vermeulen, Vapor–liquid equilibria for aqueous sulfuric acid, *AIChE J., 10,* 740–746, 1964.

Hamill, P., R. P. Turco, C. S. Kiang, O. B. Toon, and R. C. Whitten, An analysis of various nucleation mechanisms for sulfate particles in the stratosphere, *J. Aerosol Sci., 13,* 561–585, 1982.

Hamill, P., O. B. Toon, and R. P. Turco, Aerosol nucleation in the winter arctic and antarctic stratospheres, *Geophys. Res. Lett., 17,* 417–420, 1990.

Hanson, D. R., and K. Mauersberger, Laboratory studies of the nitric acid trihydrate: implications for the south polar stratosphere, *Geophys. Res. Lett., 15,* 855–858, 1988.

Hinds, W. C., *Aerosol Technology*, 424 pp., John Wiley, New York, 1982.

Hofmann, D. J., Increase in the stratospheric background sulfuric acid aerosol in the past 10 years, *Science, 248,* 998–1000, 1990.

Hofmann, D. J., and J. M. Rosen, Stratospheric aerosol and condensation nuclei enhancements following the eruption of Alaid in April 1981, *Geophys. Res. Lett., 8,* 1231–1234, 1981.

Hofmann, D. J., J. M. Rosen, and W. Gringel, Delayed production of sulfuric acid condensation nuclei in the polar stratosphere from El Chichom volcanic vapors, *J. Geophys. Res., 90,* 2341, 1985.

Hofmann, D. J., J. M. Rosen, and J. W. Harder, Aerosol measurements in the winter/spring Antarctic stratosphere,1, correlative measurements with ozone, *J. Geophys. Res, 93.,* 665, 1988.

Hofmann, D. J., J. M. Rosen, J. W. Harder,and J. V. Hereford, Balloon borne measurements of aerosol, condensation nuclei, and cloud particles in the stratosphere at McMurdo station Antarctica during the spring of 1987, *J. Geophys. Res., 94,* 11,253, 1989.

Junge, C. E., C. W. Changnon, and J. E. Mason, Stratospheric aerosols, *J. Meteorol., 18,* 81–108, 1961.

Kawa, S. R., D. W. Fahey, L. C. Anderson, M. Loewenstein, and K. R. Chan, Measurement of total reactive nitrogen during the Airborne Arctic Stratospheric Expedition, *Geophys. Res. Lett., 17,* 485, 1990.

Kelly K. K., A. F. Tuck, L.E. Heidt, M. Loewenstein, J. R. Podolske, S. E. Strahan, and J. F. Vedder, A comparison of ER–2 measurements of stratospheric water vapor between the 1987 antarctic and 1989 arctic airborne missions,*Geophys. Res. Lett, 17,* 465, 1990.

Kent, G. S., C. R. Trepte, U. O. Farrukh, and M. P. McCormick, Variation in the stratospheric aerosol associated with the north cyclonic polar vortex as measured by the SAM II satellite sensor, *J. Atmos. Sci., 42,* 1536–1551, 1985.

Loewenstein, M., J. R. Podolske, K. R. Chan, and S. E. Strahan, N2O as a dynamical tracer in the arctic vortex, *Geophys. Res. Lett., 17,* 477, 1990a.

Loewenstein, M., J. R. Podolske, and S. E. Strahan, Atlas instrument characterization: accuracy of the AASE and AAOE data sets, *Geophys. Res. Lett., 17,* 481, 1990b.

McCormick, M. P., W. P. Chu, G. W. Grams, P. Hamill, B. M. Herman, L.R. McMaster, T. J. Pepin, P. B. Russell, H. M. Steele, and T. J. Swissler, High–latitude stratospheric aerosols measured by the SAM II Satellite System in 1978 and 1979, *Science, 214,* 328–331, 1981.

McMurry, P. H., New particle formation in the presence of an aerosol: rates, time scales and sub–0.01 μm size distributions, *J. Colloid Interface Sci., 95,* 72–80, 1983.

Oberbeck, V. R., E. F. Danielsen, K. G. Snetsinger, G. V. Ferry, W. Fong, and D. M. Hayes, Effect of the eruption of El Chichon on stratospheric aerosol size and composition, *Geophys. Res. Lett., 10,* 1021–1024, 1983.

Osborn, M. T., M. C. Pitts, K.A. Powell, and M. P. McCormick, SAM II aerosol measurements during the 1989 AASE, *Geophys. Res. Lett., 17,* 397, 1990.

Pinnick, R. G., J. M. Rosen, and D. J. Hofmann, Stratospheric aerosol measurements III: optical model calculations, *J. Atmos. Sci., 33,* 304–314, 1976.

Poole, L. R., and M. P. McCormick, Polar stratospheric clouds and the Antarctic ozone hole,*J. Geophys. Res., 93,* 8423–8430, 1988.

Pueschel, R. F., K. G. Snetsinger, P. Hamill, J. K. Goodman, and M. P. McCormick, Nitric acid in polar stratospheric clouds: similar temperatures of nitric acid condensation and cloud formation, *Geophys. Res. Lett., 17,* 429, 1990.

Rader, D. J., and V. A. Marple, A study of the effects of anisokinetic sampling, *Aerosol Sci. Technol., 8,* 283–300, 1988.

Rood, R. B., P. A. Newman, L. R. Lait, D. J. Lamich, and K. R. Chan, Stratospheric temperatures during AASE: results from Stratan, *Geophys. Res. Lett., 17,* 337, 1990.

Rosen, J. M., and D. J. Hofmann, Unusual behavior on the condensation nuclei concentration at 30 km, *J. Geophys. Res., 88,* 3725–3731, 1983.

Salawitch, R. J., G. P. Gobbi, S. C. Wofsy, and M. B. McElroy, Denitrification in the antarctic stratosphere, *Nature, 339,* 525–527, 1989.

Schoeberl, M. R. and D. L. Hartmann, The dynamics of the stratospheric polar vortex and its relation to springtime ozone depletions, *Science, 251,* 46–52, 1991.

Solomon, S., Progress towards a quantitative understanding of Antarctic ozone depletion, *Nature, 347,* 347–354, 1990.

Steele, H. M., and P. Hamill, Effects of temperature and humidity on the growth and optical properties of sulfuric acid–water droplets in the stratosphere, *J. Aerosol Sci., 12,* 517–528, 1981.

Steele, H. M., P. Hamill, M. P. McCormick, and T. J. Swissler, The formation of polar stratospheric clouds, *J. Atmos. Sci., 40,* 2055–2067, 1983.

Toon, O. B., R. P. Turco, and P. Hamill, Denitrification mechanisms in the polar stratosphere, *Geophys. Res. Lett., 17,* 445–448, 1990.

Tsai, C. J. and D. Y. H. Pui, Numerical study of particle deposition in bends of a circular cross–section–laminar flow regime, *Aerosol Sci. Technol., 12,* 813–831, 1990.

Turco, R. P., R. C. Whitten and O. B. Toon, Stratospheric aerosols: observation and theory, *Rev. Geophys., 20,* 233–279, 1982.

Whitby, K. T., The physical characteristics of sulfur aerosols, *Atmos. Environ., 12,* 135–159, 1978.

Wilson, J. C., E. D. Blackshear, and J. H. Hyun, Changes in the sub 2.5 micron diameter aerosol observed at 20 km altitude after the eruption of El Chichon, *Geophys. Res. Lett., 10,* 1029–1032, 1983*a*.

Wilson, J. C., J. H. Hyun and E. D. Blackshear, The function and response of an improved stratospheric condensation nucleus counter, *J. Geophys. Res., 88,* 6781, 1983*b*.

Wilson, J. C., M. Loewenstein, D. W. Fahey, B. Gary, S. D. Smith, K. K. Kelly, G. V. Ferry, and K. R. Chan, Observations of condensation nuclei in the Airborne Antarctic Ozone Experiment: implications for new particle formation and polar stratospheric cloud formation, *J. Geophys. Res., 94,* 16,437–16,448, 1989.

Wilson, J. C., M. R. Stolzenberg, W. E. Clark, M. Loewenstein, G. V. Ferry, and K. R. Chan, Measurements of condensation nuclei in the airborne arctic stratospheric expedition: observations of particle production in the polar vortex, *Geophys. Res. Lett., 17,* 361, 1990.

Wofsy, S. C., R. J. Salawitch, J. H. Yatteau, M. B. McElroy, B. W. Gandrud, J. E. Dye, and D. Baumgardner, Condensation of HNO3 on falling ice particles: mechanism for denitrification of the polar stratosphere, *Geophys. Res. Lett, 17,* 449, 1990.

K. R. Chan, G. V. Ferry, and M. Loewenstein, NASA Ames Research Center, Moffett Field, CA 94035.

W. E. Clark, Department of Mechanical Engineering, California Polytechnic State University, San Luis Obispo, CA 93407.

K. K. Kelly, NOAA Aeronomy Laboratory, 325 Broadway, Boulder, CO, 80303.

M. R. Stolzenburg, Aerosol Dynamics Inc., 2329 Fourth St., Berkeley, CA 94710.

J. C. Wilson, Department of Engineering, University of Denver, Denver CO, 80202.

(Received March 6, 1991;
revised December 31, 1991;
accepted December 31, 1991.)